TÉCNICO LISBOA

Thermal characterisation of compressed earth blocks stabilised with recycled cement

Bruno Filipe Oliveira Acúrcio

Thesis to obtain the Master of Science Degree in

Civil Engineering

Supervisors: Prof. José Alexandre de Brito Aleixo Bogas
Prof. Maria da Glória de Almeida Gomes

Examination Committee

Chairperson: Prof. Nuno Gonçalo Cordeiro Marques de Almeida
Supervisor: Prof. José Alexandre de Brito Aleixo Bogas
Member of the Committee: Prof. Maria Paulina Santos Forte de Faria Rodrigues

September 2025

DECLARATION

I hereby declare that this document is my original work and that it fulfils all the requirements of the University of Lisbon's Code of Conduct and Good Practices.

Thermal characterisation of compressed earth blocks stabilised with recycled cement

Bruno Filipe Oliveira Acúrcio

Dissertação para obtenção do Grau de Mestre em

Engenharia Civil

Dissertação elaborada no âmbito do Projecto FCT Eco⁺RCEB

Eco-efficient recycled cement compressed earth blocks

Task 4 – Thermal performance of CSEB

Projeto PTDC/ECI-CON/0704/2021

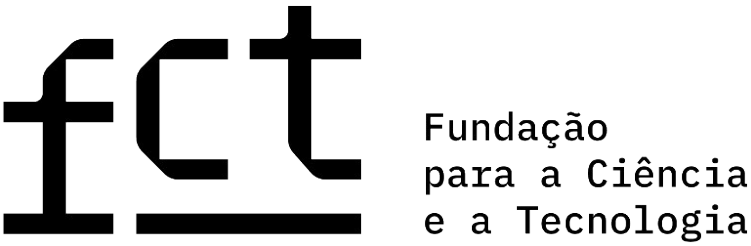

Resumo

Com as preocupações ambientais atuais, existe um esforço crescente por encontrar soluções ecologicamente mais viáveis e sustentáveis. A construção, sendo representante de um dos setores com uma maior contribuição de emissões de CO_2 para a atmosfera não foge à regra. Desta forma, a utilização de materiais como a terra, neste caso e mais especificamente os blocos de terra comprimida (CEB) estabilizados com cimento reciclado, têm surgido como uma alternativa mais ecológica em detrimento de outras soluções praticadas atualmente.

Com o objetivo de analisar o comportamento térmico destas soluções, realizou-se uma campanha experimental com 18 composições diferentes, desde composições não estabilizadas (UCEB) a composições estabilizadas com Cimento Portland (CP e PLC) e Cimento Reciclado (RCP e RCC). Começou-se pela caracterização em diferentes estados (seco, saturado e ambiente de laboratório) das propriedades mecânicas das diferentes composições produzidas, seguindo-se da caracterização térmica das diferentes composições pelo método transiente e estacionário. Tendo em consideração os diferentes métodos, foi possível observar uma corelação da massa volúmica e porosidade total com a condutibilidade térmica. Dependendo da quantidade de CDW e tipo de ligante utilizado na sua estabilização foi possível obter valores de condutibilidade térmica compreendidos entre 0.67 e 1.14 W/(m$\times$K).

Em geral, verificou-se que os CEB estabilizados com RCP foram termicamente mais eficientes comparativamente às restantes composições, especialmente em relação às não estabilizadas.

Palavras-Chave

Cimento reciclado; Propriedades térmicas; Sustentabilidade; Resíduos de construção e demolição (RCD); Construção em terra.

Abstract

With current environmental concerns, there is a growing effort to find more ecologically viable and sustainable solutions for the practice of any activity in society. The construction sector, as one of the major contributors to CO_2 emissions into the atmosphere, is no exception. In this context, the use of materials such as earth, more specifically, compressed earth blocks (CEB) stabilised with recycled cement, has emerged as a more environmentally friendly alternative to conventional construction solutions.

To analyse the thermal behaviour of these solutions, an experimental campaign was carried out involving 18 different compositions, ranging from unstabilised blocks (UCEB) to blocks stabilised with Portland Cement (OPC and PLC) and Recycled Cement (RCP and RCC). The study began with the characterisation of mechanical properties under different conditions (dry, saturated, and laboratory environment), followed by thermal characterisation using both the transient and steady-state methods. Considering the different methods, a correlation between bulk density and total porosity with thermal conductivity was observed. Depending on the amount of CDW and the type of binder used for stabilisation, thermal conductivity values between 0.67 and 1.14 W/(m·K) were recorded.

Overall, CEB stabilised with RCP were found to be thermally more efficient than the other compositions, particularly when compared to the unstabilised ones.

Keywords

Recycled cement; Thermal properties; Sustainability; Construction and demolition waste (CDW); Earth construction.

Table of Contents

1 Introduction 1
1.1 General considerations 1
1.2 Objectives 2
1.3 Methodology 2
1.4 Thesis Structure 3
2 State of the Art 5
2.1 History of earthen construction 5
2.2 Compressed Earth Blocks 6
2.2.1 Composition 6
2.2.2 Stabilisation 7
2.2.2.1 Mechanical stabilisation 7
2.2.2.2 Physical stabilisation 8
2.2.2.3 Chemical stabilisation 8
2.3 Recycled cement 9
2.4 Thermal properties of Compressed Earth Blocks 10
2.4.1 Theoretical framework 10
2.4.2 Methods for evaluating thermal conductivity 12
2.4.2.1 Transient methods 12
2.4.2.2 Stationary methods 13
2.4.3 Previous studies on CEB thermal properties 14
3 Experimental Campaign 17
3.1 Experimental program 17
3.2 Materials 18
3.2.1 Earth 18
3.2.2 CDW 20
3.2.3 Stabilisers 21
3.2.3.1 Portland cement 21
3.2.3.2 Recycled cement 21
3.3 CEB production 24
3.3.1 Composition 24
3.3.2 Earth preparation 25

3.3.3 Mixing and moulding 26
3.4 Mortar production 26
3.5 CEB characterisation 27
3.5.1 Density 28
3.5.2 Compressive strength 28
3.5.3 Thermal properties - Modified Transient Method 28
3.5.4 Thermal properties - Adapted Steady-State Method in a climate chamber 29
3.5.4.1 Experimental setup 30
3.5.4.2 Experimental characterisation 32
4 Results and Discussion 35
4.1 Density and total porosity 35
4.2 Compressive strength 39
4.3 Thermal characterisation - Transient Method 42
4.3.1 Thermal conductivity 44
4.3.1.1 Influence of the type and content of stabiliser 47
4.3.1.2 Influence of CDW 49
4.3.2 Other thermal properties 50
4.4 Thermal characterisation - Adapted Steady-State Method (climate chamber) 53
4.4.1 Temperature profiles 53
4.4.2 Thermal conductivity 58
4.4.3 Building envelope solutions 60
5 Conclusions 65
5.1 General conclusions 65
5.2 Future research directions 66
References 69
Appendices 77
Appendix 1 - Stationary test 77
Appendix 2 – ISODUR thermal plaster – Technical datasheet 84

List of Figures

FIGURE 1 - A) GREAT WALL OF CHINA BUILT IN RAMMED EARTH (JORGE, 2006); B) TEMPLE OF RAMSES II BUILT IN ADOBE (MINKE, 2005); C) CITY OF SHIBAM (YEMEN) BUILT IN ADOBE (F. PACHECO-TORGAL, 2011). 5
FIGURE 2 - GRAPHICAL DISTRIBUTION EARTH CONSTRUCTION IN PORTUGAL: A) RAMMED EARTH; B) ADOBE; C) WATTLE AND DAUB (JORGE, 2006). 6
FIGURE 3 - GRANULOMETRIC CURVE FOR CEB PRODUCTION. ADAPTED FROM XP P13-901 (2001). 7
FIGURE 4 - PLASTICITY DIAGRAM FOR CEB PRODUCTION. ADAPTED FROM XP P13-901 (2001). 7
FIGURE 5 - LIFECYCLE DIAGRAM OF RECYCLED CEMENT AND PORTLAND CEMENT (BANDEIRA, 2020) 10
FIGURE 6 - TRANSIENT PLANE SOURCE METHOD (TPS) (SILVA, 2017). 13
FIGURE 7 - TRANSIENT LINE SOURCE METHOD (TLS) (SILVA, 2017). 13
FIGURE 8 - MODIFIED TRANSIENT PLANE SOURCE (MTPS) (SILVA, 2017). 13
FIGURE 9 - GUARDED HOT PLATE DIAGRAM (FRANCO, 2007). 13
FIGURE 10 - HEAT FLOW METER DIAGRAM (FRANCO, 2007). 13
FIGURE 11 - FA SOIL 18
FIGURE 12 - TV CLAYEY RESIDUE. 18
FIGURE 13 - DIFFRACTOGRAMS OF FA SOIL AND TV RESIDUE ADAPTED FROM (RODRIGUES, 2024). 19
FIGURE 14 - GRANULOMETRIC CURVE OF FA SOIL, TV RESIDUE, CDW AND THE GRANULOMETRIC RANGE PROPOSED BY THE STANDARD XP P13-901 (2001). 20
FIGURE 15 - CONSTRUCTION AND DEMOLITION WASTE (CDW) 20
FIGURE 16 - A) JAW CRUSHER; B) MEDIUM-SIZED JAW CRUSHER; C) ROLL CRUSHER; D) COARSE AGGREGATE DERIVED FROM PASTE; E) MEDIUM-SIZED AGGREGATE; F) FINE AGGREGATE RESULTING FROM CRUSHING. 23
FIGURE 17 - A) BALL MILL; B) METAL BALLS; C) DEFLOCCULATING ADDITIVE; D) PARTICLES WITH A DIAMETER OF LESS THAN 150 MM 23
FIGURE 18 - GRANULOMETRIC CURVE OF OPC AND RCP. 23
FIGURE 19 – KERN DBL HIGH PRECISION THERMOBALANCE. 25
FIGURE 20 - PREPARATION OF FA SOIL: A) PULVERISING; B) PULVERISED SOIL; C) SIEVING; D) SIEVED SOIL. 26
FIGURE 21 - CEB PRODUCTION: A) VERTICAL MIXER; B) OSKAM V/F SEMI-AUTOMATIC HYDRAULIC PRESS; C) WET CURING. 26
FIGURE 22 – COMPRESSIVE STRENGTH TEST. 28
FIGURE 23 - ISOMET 2114 FROM APPLIED PRECISION LTD. 29
FIGURE 24 - TESTS CONDUCTED IN THREE CONDITIONS: A) SATURATED; B) DRY; C) LABORATORY ENVIRONMENT. 29
FIGURE 25 - A) DRILLING SCHEME FOR STABILISED BLOCKS; B) STABILISED BLOCK; C) DRILLING SCHEME FOR UNSTABILISED BLOCKS; D) UNSTABILISED BLOCK. 30
FIGURE 26 - A) FITOCLIMA CLIMATIC CHAMBER FROM ARALAB; B) POSITION OF SMALL CEB-WALLS IN THE CHAMBER. 31

FIGURE 27 - A) CEB PLACEMENT; B) INSULATION; C) ROUGHCAST APPLICATION (FIRST LAYER); D) RENDERING (SECOND LAYER). 31
FIGURE 28 - CALIBRATION OF HEAT FLUX METERS ON A SINGLE-PANE WINDOW. 32
FIGURE 29 - DATATAKER 85 CONNECTED TO THERMOCOUPLES. 32
FIGURE 30 - TRANSIENT METHOD PLANE PROBE APPLIED TO A WALL. 33
FIGURE 31 – RELATIONSHIP BETWEEN FRESH DENSITY (P_F) AND LONG-TERM TOTAL POROSITY (TP). 37
FIGURE 32 - RELATIONSHIP BETWEEN DRY DENSITY (PD, 28D) AND LONG-TERM TOTAL POROSITY (TP). 37
FIGURE 33 – RELATIONSHIP BETWEEN DRY DENSITY AT 28 DAYS ($P_{D,28D}$) AND LONG-TERM TOTAL POROSITY (TP), FOR DIFFERENT PERCENTAGE OF RC BINDER. 38
FIGURE 34 – DRY DENSITY ($P_{D,28D}$, BARS) AND LONG-TERM TOTAL POROSITY (TP, DASHED LINE) AS A FUNCTION OF THE PERCENTAGE OF CDW. 39
FIGURE 35 – RELATIONSHIP BETWEEN UNCONFINED COMPRESSIVE STRENGTH ($F_{C,UN,LAB}$) AND LONG-TERM TOTAL POROSITY (TP) FOR DIFFERENT STABILISER CONTENTS. 41
FIGURE 36 – RELATIONSHIP BETWEEN UNCONFINED COMPRESSIVE STRENGTH ($F_{C,UN,LAB}$) AND PERCENTAGE OF SOIL REPLACEMENT BY CDW. 42
FIGURE 37 - THERMAL CONDUCTIVITY (Λ) FOR THE ANALYSED CEB COMPOSITIONS UNDER DIFFERENT CONDITIONS. 45
FIGURE 38 - THERMAL CONDUCTIVITY INCREASE FACTOR (KS) AS A FUNCTION OF TOTAL POROSITY (TP). 46
FIGURE 39 - THERMAL CONDUCTIVITY (Λ) OF THE DRY CEB AS A FUNCTION OF THEIR DRY DENSITY IN THIS STUDY AND REPORTED BY OTHER AUTHORS. 46
FIGURE 40 - THERMAL CONDUCTIVITY (Λ) FOR THE ANALYSED CEB AS A FUNCTION OF THEIR DRY DENSITY 47
FIGURE 41 - THERMAL CONDUCTIVITY (Λ) OF THE DRY CEB AS A FUNCTION OF STABILISER PERCENTAGE AND TOTAL POROSITY (TP). 48
FIGURE 42 - THERMAL CONDUCTIVITY IN THE DRY STATE (Λ) FOR THE ANALYSED CEB AS A FUNCTION OF THEIR TOTAL POROSITY. 49
FIGURE 43 - THERMAL CONDUCTIVITY (Λ) IN LABORATORY ENVIRONMENT FOR THE ANALYSED CEB AS A FUNCTION OF THEIR TOTAL POROSITY 49
FIGURE 44 - THERMAL CONDUCTIVITY (Λ) OF THE DRY CEB AS A FUNCTION OF CDW PERCENTAGE AND TOTAL POROSITY (TP). 50
FIGURE 45 - SPECIFIC HEAT CAPACITY OF THE DRY CEB, C_{DRY}, AS A FUNCTION OF TOTAL POROSITY, TP. 51
FIGURE 46 - THERMAL DIFFUSIVITY OF THE DRY CEB AS A FUNCTION OF DRY DENSITY. 51
FIGURE 47 - THERMAL INERTIA OF DRY CEB WITH 25% CDW. 52
FIGURE 48 - THERMAL INERTIA OF DRY PC CEB WITH 0-40% CDW. 52
FIGURE 49 - INTERNAL (CONTINUOUS LINE) AND EXTERNAL (DASHED LINE) SURFACE TEMPERATURES OF THE DIFFERENT CEB PROTOTYPES WALLS. 53
FIGURE 50 - HEAT FLOW OF DIFFERENT CEB WALLS PROTOTYPES. 54
FIGURE 51 - WALL TEMPERATURES STABILISED WITH RCP FROM INSIDE TO OUTSIDE. 56
FIGURE 52 - WALL TEMPERATURES STABILISED WITH OPC FROM INSIDE TO OUTSIDE. 57
FIGURE 53 - WALL TEMPERATURES UNSTABILISED FROM INSIDE TO OUTSIDE. 57
FIGURE 54 - AVERAGE WALL TEMPERATURES OF THE DIFFERENT MIXTURES FROM INSIDE TO OUTSIDE. 58

FIGURE 55 - THERMAL CONDUCTIVITY AS A FUNCTION OF CEB DRY BULK DENSITY BY TRANSIENT AND STATIONARY METHOD.....60
FIGURE 56 - LAYER ARRANGEMENT OF THE SINGLE-WALL CONSTRUCTION.....62
FIGURE 57 - LAYER ARRANGEMENT OF THE DOUBLE-WALL CONSTRUCTION (REFERENCE). 63

List of Tables

TABLE 1 - THERMAL CONDUCTIVITY OF CEB BY DIFFERENT AUTHORS (UPDATED FROM SILVA, 2015).....16
TABLE 2 - STANDARDS ADOPTED FOR SOIL CHARACTERISATION.....18
TABLE 3 - CHARACTERISTICS OF FA AND TV SOILS ADAPTED FROM (RODRIGUES, 2024).....19
TABLE 4 - STANDARDS ADOPTED FOR CDW CHARACTERISATION.....20
TABLE 5 - CHARACTERISTICS OF CDW ADAPTED FROM (RODRIGUES, 2024).....21
TABLE 6 - CHARACTERISTICS OF CEM I 42.5 R AND CEM II/B-L 32,5.....21
TABLE 7 - CHARACTERISTICS OF RCP AND RCC.....24
TABLE 8 - COMPOSITION OF CEB MIXES USED IN THE MODIFIED TRANSIENT METHOD.....25
TABLE 9 - COMPOSITION OF MORTAR MIXES USED IN THE ADAPTED STEADY-STATE METHOD.....27
TABLE 10 – CHARACTERISTICS OF COMPOSITIONS CONSIDERED ON TRANSIENT METHOD.....35
TABLE 11 – FRESH DENSITY (P_F), VOLUME OF VOIDS AFTER COMPACTION (V_V), HARDENED DENSITY (P_{28D}) AND LONG-TERM TOTAL POROSITY (TP) FOR THE STUDIED COMPOSITIONS.....36
TABLE 12 – AVERAGE UNCONFINED COMPRESSIVE STRENGTH AT 28 DAYS FOR LABORATORY CONDITIONS ($F_{C,UN,LAB}$), SATURATED CONDITIONS ($F_{C,UN,SAT}$) AND DRIED CONDITIONS ($F_{C,UN,DRY}$).....40
TABLE 13 - THERMAL PROPERTIES OF CEB IN DRY STATE, AVERAGE VALUES (AV) AND STANDARD DEVIATIONS (SD).....43
TABLE 14 - THERMAL PROPERTIES OF CEB IN EQUILIBRIUM WITH LAB ENVIRONMENT, AVERAGE VALUES (AV) AND STANDARD DEVIATIONS (SD).....43
TABLE 15 - THERMAL PROPERTIES OF CEB SATURATED, AVERAGE VALUES (AV) AND STANDARD DEVIATIONS (SD).....44
TABLE 16 - THERMAL CONDUCTIVITY OF THE COMPOSITIONS.....59
TABLE 17 - THERMAL RESISTANCE AND THERMAL TRANSMITTANCE COEFFICIENT OF RCP, OPC AND UCEB.61
TABLE 18 - COMPOSITION AND THERMAL PERFORMANCE OF A SIMPLIFIED EXTERIOR WALL.....62
TABLE 19 - CURRENT ZONE CHARACTERISTICS.....63
TABLE 20 - MINIMUM THICKNESS OF THERMAL INSULATION REQUIRED TO MEET REGULATORY LIMITS.....63
TABLE 21 - CONCRETE THICKNESS FOR U-VALUE EQUIVALENT TO CEB COMPOSITIONS.....64

Abbreviations and Symbols

IST	Instituto Superior Técnico;
CEL	Civil Engineering Laboratory;
CEB	Stabilised compacted earth blocks;
CDW	Construction and demolition waste;
PC	Portland cement;
RC	Recycled cement;
HQRS	High-quality recycled sand;
GeoLab-IST	IST Geosciences and Geotechnologies Laboratory;
PL	Plastic Limit;
LL	Liquid Limit;
PI	Plasticity Index;
XRD	X-ray diffraction;
OWC	Optimum Water Content;
TV	Soil from Torres Vedras;
FA	Soil from Air Force;
PLC	CEM II/B-L 32,5;
RCC	Recycled cement from concrete;
OPC	CEM I 42.5 R;
RCP	Recycled cement from paste;
SI	System of Unit;
TP	Total Porosity;
GHP	Guarded Hot Plate;
HFM	Heat Flow Meter;
TPS	Transient Plane Source;
TLS	Transient Line Source;
MPTS	Modified Transient Plane Source;
$\mathbf{r_f}$	Fresh density (Kg/m^3);
c	Specific heat (J/(Kg$\times$ºC));
cρ	Volumetric heat capacity (J/m$^3\times$ºC);
α	Thermal diffusivity (m^2/s);
Tm	Average temperature (ºC);
l	Thermal Conductivity (W/(m$\times$K)).
Vv	Volume of voids (%)
$\mathbf{f_{c,un}}$	Unconfined compressive strength (MPa)
$\mathbf{f_c}$	Compressive strength (MPa)

Description of the CEB compositions

UCEB	Unstabilised CEB with 25% of CDW1;
UCEBCDW0	Unstabilised CEB with 0% of CDW1;
OPC4	Stabilised CEB with 4% of OPC and 25% of CDW1;
OPC8	Stabilised CEB with 8% of OPC and 25% of CDW1;
OPC8TH	Stabilised CEB with 8% of OPC and 25% of CDW1;
OPC8CDW0	Stabilised CEB with 8% of OPC and 0% of CDW1;
OPC8CDW15	Stabilised CEB with 8% of OPC and 15% of CDW1;
OPC8CDW25	Stabilised CEB with 8% of OPC and 25% of CDW1;
OPC8CDW40	Stabilised CEB with 8% of OPC and 40% of CDW1;
OPC80RCP20	Stabilised CEB with 8% of binder (80% of OPC and 20% of RCP) and 25% of CDW1;
OPC50RCP50	Stabilised CEB with 8% of binder (50% of OPC and 50% of RCP) and 25% of CDW1;
OPC80RCC20	Stabilised CEB with 8.8% of binder (80% of OPC and 20% of RCC) and 25% of CDW1;
OPC50RCC50	Stabilised CEB with 10% of binder (50% of OPC and 50% of RCC) and 25% of CDW1;
PLC8	Stabilised CEB with 8% PLC and 25% of CDW1;
RCP8	Stabilised CEB with 8% RCP and 25% of CDW1;
RCP8CDW0	Stabilised CEB with 8% RCP and 0% of CDW1;
RCP4	Stabilised CEB with 4% RCP and 25% of CDW1;
RCC8	Stabilised CEB with 12% RCC and 25% of CDW1.

1 Introduction

1.1 General considerations

Earth has been one of the oldest and most ecologically sustainable materials used in construction, with records dating back to 10,000 BC in ancient Mesopotamia (Azevedo, 2021). Currently, around 8 - 10% of the global population still lives in earthen dwellings (Marsh and Kulshreshtha, 2022), highlighting its continued relevance and adaptability to modern sustainable construction practices (Azevedo, 2021). In Portugal, traditional techniques such as rammed earth, adobe, and wattle and daub make up a significant part of the built heritage, reflecting a rich cultural legacy and the adaptation of ancient methods to contemporary needs (Nabais, 2023; Silva, 2005).

With the growing focus on sustainability and energy efficiency, earthen construction faces significant challenges, particularly due to its durability limitations, such as water resistance and applicability in high-rise structures. However, recent advances in stabilisation techniques, such as the use of recycled cementitious materials, have helped to overcome some of these barriers. The use of recycled cement not only improves the durability and mechanical strength of Compressed Earth Blocks (CEB) (Bogas et al., 2023; Cruz et al., 2024; Cruz and Bogas, 2024a) but also aligns with the urgent need to reduce the environmental impact associated with conventional cement production. This focus not only addresses the responsibility of the construction sector as one of the largest global CO_2 emitters, with cement production being a major contributor (UNEP, 2021), but also tackles the intensive material consumption and high energy demands of the industry. Additionally, it promotes the use of construction and demolition waste as valuable resources for producing new construction materials, fostering a circular economy, and reducing the sector's carbon footprint (F. Pacheco-Torgal, 2011).

In this context, this dissertation focuses on the thermal evaluation of earth blocks stabilised with recycled cement derived from both cement paste and concrete. This innovative approach not only proposes a more sustainable use of resources but also aligns with global carbon emission reduction goals. Given that buildings in the European Union are responsible for approximately 40% of total energy consumption and 35% of greenhouse gas emissions, over half of which is due to heating and cooling systems, improving the thermal insulation properties of construction materials becomes crucial (L. Fernandes and Leitão, 2023). This research significantly contributes to advancing the understanding of the mechanical properties and durability of CEB while also promoting considerable progress in the knowledge of their thermal capabilities. This improvement is essential for enhancing energy efficiency in buildings, directly addressing the guidelines set by the European Union Directive on the Energy Performance of Buildings, which mandates that all new buildings be nearly zero-energy. Furthermore, integrating recycled cement into CEB can facilitate meeting carbon neutrality targets set for 2030 and 2050, contributing to a significant reduction in CO_2 emissions in the construction sector.

1.2 Objectives

By addressing sustainability, material recycling, and the improvement of the energy performance of construction materials, this work aims at assessing the thermal behaviour of CEB unstabilised and stabilised with recycled and non-recycled cementitious binders, making a significant contribution to environmental sustainability and the promotion of a circular economy in construction. It also aspires to be a catalyst for a paradigm shift in how earth materials can be used in civil engineering.

Based on these premises, the main objectives of the study were defined as follows:

- Experimentally characterise the physical and thermal properties of CEB stabilised and unstabilised with different binders, including recycled cement (RCP and RCC), OPC, and PLC.
- Evaluate the influence of composition and types of stabilisation on the thermal performance of CEB, considering variations in bulk density, porosity, and CDW content.
- Assess the relationship between mechanical properties and thermal behaviour, linking density and strength to thermal conductivity.
- Compare two experimental methods (the transient and the adapted steady-state method) for determining thermal properties under conditions close to real use.
- Identify the most thermally efficient CEB compositions and demonstrate the potential of recycled binders to support more sustainable construction practices.

This study stands out by demonstrating that the conscious integration of sustainable practices and innovative technologies in construction is not merely a necessity but a real opportunity to reshape the foundations of the construction industry. In doing so, it seeks not only to meet current demands for energy efficiency and environmental impact reduction but also to anticipate and shape future practices, ensuring that future generations inherit a legacy of resilient, efficient, and environmentally responsible infrastructure. Ultimately, this work proposes a new horizon for civil construction, where sustainability and innovation intertwine to create environments truly adapted to the demands of our time and aligned with global environmental imperatives.

1.3 Methodology

The present subchapter describes the methodology adopted in this dissertation, outlining the different stages of the work, from the initial characterisation of materials to the thermal evaluation of the CEB. This process was divided into several phases to ensure a systematic and rigorous approach.

Initially, the characterisation of the materials used was carried out, including the characterisation of the different soils and the construction and demolition waste (CDW), followed by the characterisation of the various types of chemical stabilisers used, such as Portland cement and recycled cement derived from cement paste and concrete. This phase involved a detailed analysis of the different materials to determine their physical and chemical properties, which are essential for the production of compressed earth blocks.

After the characterisation phase, the production of the blocks started. This process included the production of different compositions, varying the proportions of their constituents to explore different formulations and identify those that exhibit the best performance. After their production, the blocks were

tested to characterise their physical and mechanical properties, such as density, porosity, and mechanical strength.

Finally, the thermal evaluation of the blocks was conducted using two distinct methods: the transient method and the stationary method. In the transient method, a wider range of compositions was analysed, varying the amount of recycled cement (RC), CDW, and ordinary Portland cement (OPC). This method allowed for a quicker and more diversified assessment of the thermal properties of different formulations. Conversely, the stationary method focused on three pre-selected compositions, providing a more in-depth and detailed analysis of their thermal properties in a context that closely resembles real-life applications.

1.4 Thesis Structure

This dissertation is structured into five chapters: the introduction and the conclusions are presented in the first and fifth chapters, respectively; a detailed review of the state of the art is explored in the second chapter; the experimental methodology and the analysis of results are addressed in chapters three and four. The content of each chapter is detailed as follows:

- **Chapter 1:** Addresses the general considerations underpinning this dissertation, including the objectives and adopted methodology, as well as describing the organisation of the document.
- **Chapter 2:** Presents a review of the existing literature in the field of earth construction, highlighting the environmental impact of civil engineering, stabilisation techniques for earth mixtures, the production process of recycled cement (RC), different techniques for evaluating thermal conductivity, as well as results from various previous works with the same purpose and techniques used in this study.
- **Chapter 3:** Describes in detail the experimental campaign conducted, from the characterisation of the fresh and hardened states of the blocks, through the production of paste to the thermal characterisation tests of the blocks.
- **Chapter 4:** Discusses the results obtained, both from the preliminary study and the tests detailed in the previous chapter, analysing the implications of the findings and their relevance to the field of study.
- **Chapter 5:** Summarises the main conclusions drawn from the discussion of the results chapter and suggests future developments of this research.

Additionally, at the end of the document, a list is presented containing all the bibliographic references, standards used, and appendices that document the results of the tests mentioned in chapter three.

2 State of the Art

This chapter aims to thoroughly review the state of the art and research gaps related to earth construction and the application of CEB stabilised with recycled cement. First, earth construction techniques and CEB features will be examined. Next, the stabilisation strategies, emphasising the use of recycled cement, will be analysed. The thermal characterisation of CEB will be finally approached, in order to provide the context needed to comprehend the research done in this thesis. Specifically, the thermal conductivity and thermal performance of the stabilised CEB will be addressed.

2.1 History of earthen construction

Earth has been employed as a construction material from the beginning of time. The first signs of earth construction date back to around 10,000 BC in ancient Mesopotamia (Minke, 2005). For instance, the Egyptians built temples and fortifications such as the temple of Ramses II using adobe blocks (Figure 1b). Other examples of earth construction include the Great Wall of China, which dates back to the 7th century BC and was built using rammed earth (Figure 1a), and the city of Shibam in Yemen, built in the 16th century AC using adobe blocks (Figure 1c).

Figure 1 - a) Great Wall of China built in rammed earth (Jorge, 2006); b) Temple of Ramses II built in adobe (Minke, 2005); c) City of Shibam (Yemen) built in adobe (F. Pacheco-Torgal, 2011).

Nowadays, earthen construction still accounts for 8 – 10% of global housing (Marsh and and Kulshreshtha, 2022). This type of construction has a greater emphasis in low and medium HDI countries located in Africa, Central America, the Middle East, and some Asian regions (Silva, 2015) and is commonly associated with the use of local resources, that results in an economical construction with low environmental impact apart from its technical advantages such as the high thermal inertia of massive earthen walls and the passive moisture control of any earthen building material (Ranesi et al., 2021) Moreover, the waste generated can be effectively recycled and reused, supporting modern efforts to maintain ecological and sustainable balance (Zhang et al., 2024).

The use of earth as a building material in Portugal dates to around 5000 BC (Silva et al., 2013), with three different techniques standing out: rammed earth, adobe, and wattle and daub (Silva et al., 2013) (Figure 2). Rammed earth is more prevalent in the centre and south of the Country due to favourable weather conditions, low availability and consequent high cost of stones in the region (Silva, 2015). On the central coast, construction with adobe blocks is more common. In this region, clayey soils and coarse sands stand out. This lime adobe block technique accounts for around 40% of buildings in the Aveiro district (Silveira et al., 2012). In the north of the country, traditional construction uses stone, with wattle and daub being frequently employed in the internal partition walls (Silva et al., 2013).

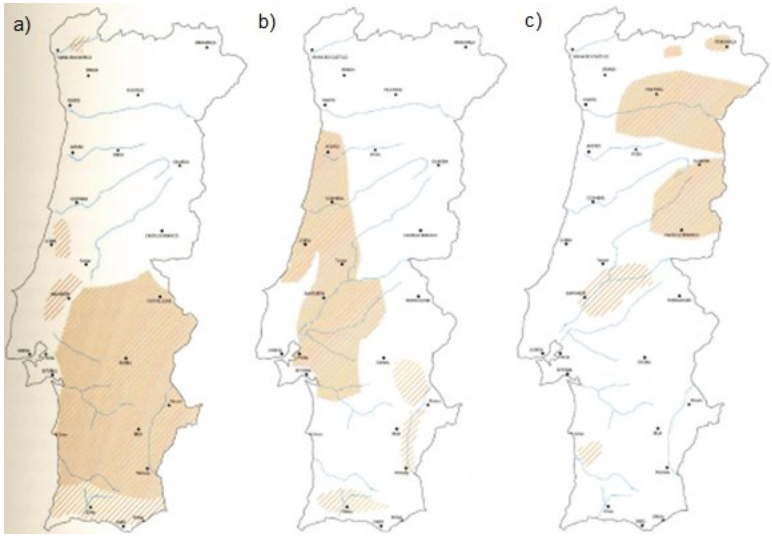

Figure 2 - Graphical distribution earth construction in Portugal: a) Rammed earth; b) Adobe; c) Wattle and daub (Jorge, 2006).

2.2 Compressed Earth Blocks

Compressed earth blocks (CEB) emerged as an innovative technique at Colombia in 1952, representing an effort to improve the performance of adobe construction (Lourenço et al., 2002). Initially, developed by engineer Raul Ramirez at the Cinval Centre in Bogotá, CEB are blocks commonly made of earth and clay compacted and shaped with a semi-automatic hydraulic press, differing from traditional earthen building materials for their dimensional regularity and higher density that gives them greater mechanical strength (Lourenço et al., 2002). In addition, CEB can be stacked immediately after production, which eliminates the need for large storage spaces (Little and Morton, 2001). However, unstabilised CEB as well as other unstabilised earthen material, have low water resistance (Cruz et al. 2024). To address this shortcoming, it can be required to stabilise CEB increasing their mechanical properties in addition to their water resistance.

Moreover, to further increase their sustainable nature, these blocks can include in their composition construction and demolition waste (CDW) as a partial replacement of earth.

2.2.1 Composition

The formulation of stabilised CEB is a process that directly influences their mechanical properties, durability, and performance. This process begins with the selection and characterisation of the soil, which typically represents 80-90% of the composition, followed by the setting of the optimal amount of water and stabilisers, factors that ensure the final quality and strength of the blocks (Rodrigues, 2024).

The particle size distribution of earth and the determination of consistency (Atterberg's) limits are key parameters for designing the compactness and cohesion of the final material. Namely, a poor particle distribution or improper water content can compromise the structural integrity of the block (Malkanthi et al., 2021). In fact, soil granulometry directly affects the compactness and mechanical strength of the blocks. An extensive granulometric range is necessary to ensure good complementarity between coarse and fine particles, reducing void volume and increasing block density. The Association Française de Normalization (XP P13 - 901 (2001)) recommends that the granulometric curve fall within

a specific range as illustrated in Figure 3. Uzoegbo (2020) suggests that clay and silt content should range between 10% and 40%, because lower values impair workability and higher values hinder cement stabilisation. Furthermore, expansive clays such as montmorillonite should be avoided, as they are unstable during wetting and drying cycles, compromising durability (Ouedraogo et al., 2020).

Atterberg's limits define earth plasticity at different moisture contents and help assessing the earth behaviour for moulding and drying, ensuring that the material achieves suitable plasticity without excessive shrinkage (Azevedo, 2021). The XP P13 - 901 (2001) standard provides reference values for consistency limits, recommending their evaluation during soil selection and preparation (Figure 4).

The optimal water content (OWC) represents the moisture content that maximises earth compactness and block bulk density, without compromising the workability on fresh state. Rigassi (1985) suggests an optimal range between 9% and 17%, while Riza et al. (2011), using more recent techniques to determine OWC, recommend values between 10% and 13% to ensure proper moulding and good mechanical strength. Tests such as the Proctor test in a laboratory setting or the drop test, conducted on-site, help determine the OWC, ensuring that the mixture has the plasticity and moisture necessary for moulding and drying (Lourenço et al., 2002).

Organic matter in the soil should be minimised, as its decomposition over time creates voids, reducing block strength and durability (Rodrigues, 2024).

Adding stabilisers, such as ordinary Portland cement (OPC) or recycled cement (RC), plays a critical role in enhancing block strength and durability. Typically, stabiliser contents range between 4% and 10%. Values exceeding this range become economically unfeasible, while lower percentages fail to provide significant improvements over unstabilised blocks (Azevedo, 2021).

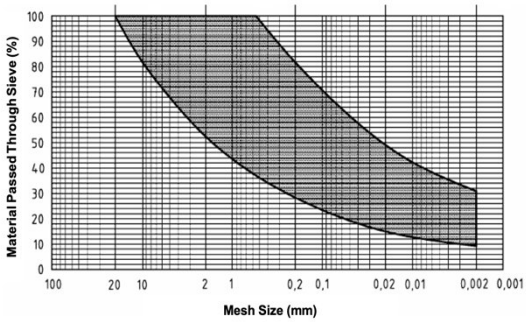

Figure 3 - Granulometric curve for CEB production. Adapted from XP P13-901 (2001).

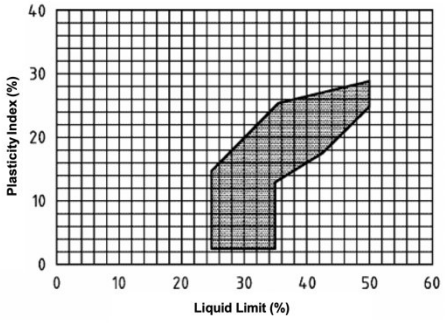

Figure 4 - Plasticity diagram for CEB production. Adapted from XP P13-901 (2001).

2.2.2 Stabilisation

2.2.2.1 Mechanical stabilisation

Mechanical stabilisation involves soil compaction through manual or hydraulic presses to reduce the void volume between soil particles and increase the compactness of the blocks, increasing the block bulk density (Nabais, 2023). However, the compaction leads to higher density and lower porosity with a reduction of efficiency for thermal insulation. This makes bulk density an important control parameter in block production, as it influences mechanical strength, thermal conductivity, and material durability (Mansour et al., 2016).

For this type of stabilisation, it is common to use the hydraulic press capable of exerting compaction pressures of around 10 MPa. The manual press, on the other hand, rely on the operator's physical strength (higher variability) and achieves pressures between 4 MPa and 6 MPa. As expected, hydraulic presses produce blocks with better and more similar mechanical properties due to their higher compaction and the lower variability in the production process (Uzoegbo, 2020).

2.2.2.2 Physical stabilisation

Physical stabilisation involves the addition or removal of different products in formulation to optimise soil particle cohesion, thereby increasing its mechanical strength. Traditionally, natural fibres of animal and vegetal origins such as dry straw, animal hair, bamboo, and sisal have been used (Turco et al., 2021). The addition of these fibres is a practice in the reinforcement of the soil matrix in earth materials, redistributing shrinkage stresses throughout the block to reduce surface cracking during the curing and drying process (Turco et al., 2021; Uzoegbo, 2020). This technique is also generally employed to enhance the tensile strength of the blocks. For instance, in a study conducted by Turco et al. (2021), adding natural fibres demonstrated improvements in the physical, mechanical, thermal, and acoustic insulation, fire resistance, and overall durability properties.

Another approach involves the addition of aggregates, typically fine aggregates, such as sand and fly ash. Their addition aims to improve the soil's particle size distribution, increasing the mixture’s compactness through a filler effect. This process reduces the porosity of the blocks, making them less prone to cracking, and improves their water resistance, thereby increasing durability (Uzoegbo, 2020). Nevertheless, an optimal amount of filler needs to be set, as in a recent study by Malkanthi et al. (2021) is highlighted that the optimal particle size distribution for soil used in CEB production should contain no more than 15% fine material.

Furthermore, Malkanthi et al. (2021) investigated the incorporation of CDW to partially substitute the sand concluding that a replacement rate up to 24% by CDW can significantly enhance the mechanical strength and durability of CEB. The results underline the effectiveness of physical stabilisation to improve the mechanical properties of CEB and also a contribution to environmental sustainability and circular economy is expected.

2.2.2.3 Chemical stabilisation

Chemical stabilisation involves adding chemical substances to the soil to enhance its physical and chemical properties. The introduction of chemical binders, such as cement, air lime or hydraulic lime, promotes the formation of new compounds, which strengthen the internal cohesion between particles (Ávila et al., 2022; Silva, 2015). This process significantly enhances the CEB mechanical strength and water resistance, making the material more durable (Uzoegbo, 2020; Venkatarama Reddy, 2012).

Cement stabilisation creates an insoluble cementitious gel, composed of hydrated calcium silicates and aluminates, which disperses into the porous regions of the earthen material. The interaction between earth and cement is pivotal in enhancing the structural integrity and reducing water susceptibility of construction materials. This process primarily increases strength through the creation of chemical bonds between the cementitious materials and the clay fractions within the soil. These

bonds are formed via pozzolanic reactions, where the silica and alumina from the clay react with the calcium hydroxide released by the hydration of cement. This reaction results in the formation of calcium silicate hydrates and other cementitious compounds that are integral to the material's enhanced durability and mechanical properties. Furthermore, these pozzolanic reactions contribute to a denser microstructure, significantly improving the material's resistance to water penetration and environmental degradation (Adam and Jones, 1995; Exelbirt, 2011; Hall et al., 2012; Kerali, 2001).

Despite its effectiveness as a stabiliser, cement raises significant environmental concerns. Its production is associated with high levels of CO_2 emissions, raw material consumption, and high energy usage (WBCSD & IEA, 2009). As a result, recent studies have sought sustainable stabilisers, such as silica fume, fly ash, biopolymers, geopolymers, pozzolana, cow dung and ground granulated blast-furnace slag (Abdulsalam et al., 2018; C. Sekhar and Nayak, 2018; Egenti et al., 2013; Mendonça et al., 2021; Kamwa et al., 2022; Ma et al., 2024). Although some of these options are environmentally promising, their technical and economic viability remains limited (Nabais, 2023). Furthermore, materials like silica fume are increasingly scarce and economically unviable, which hinders their long-term applicability (Azevedo, 2021).

2.3 Recycled cement

More recently, the need for consuming fewer raw materials and boosting circular economy in construction gave impulse to the research on new recycling methods of cementitious materials to obtain recycled binders (Carriço et al., 2021; Carriço et al., 2020). According to the CEMBUREAU Activity Report (2023), global cement production reached 4.1 billion tons in 2022. This high production volume entails significant environmental impacts, including intensive raw material consumption, high CO_2 emissions, and energy demands. The recycled cement (RC) production seeks to mitigate these issues by reusing CDW, enabling a 60% reduction in greenhouse gas emissions and lowering landfill waste deposition (Bandeira, 2020; Carriço et al., 2020).

The production of RC involves multiple stages (Figure 5), starting with the collection of CDW, followed by the crushing, the removal of dust from particles and separation of concrete components, the grinding to reduce particle size and, finally, the thermoactivation, which restores the material's hydration capacity (Carriço et al., 2021; Sousa et al., 2023). This last step is conducted at temperatures between 600°C and 800°C and is essential for reactivating the binding properties of hydrated cement. The process is divided into three stages: 1) gradual heating; 2) maintaining the temperature at a predefined target value; 3) controlled cooling. The cooling stage is critical for forming a stable cementitious microstructure (Shui et al., 2009; Yu and Shui, 2014). Studies indicate that RC can develop properties comparable to OPC classes 32.5, 42.5, and 52.5 cements after thermoactivation, depending on the percentage of RC incorporated into the cementitious mixture (Carriço et al., 2020).

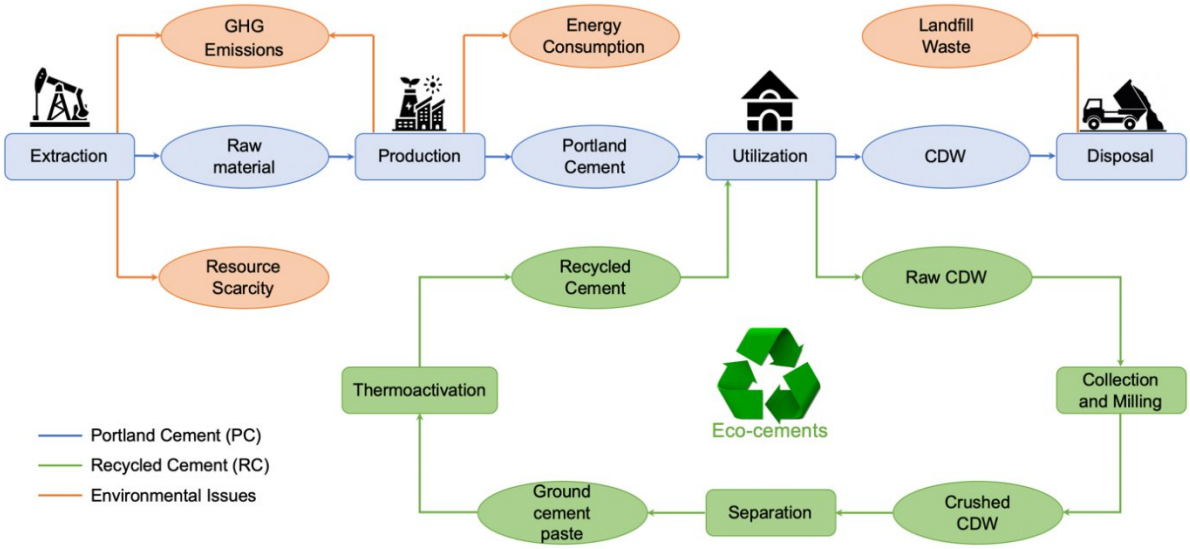

Figure 5 - Lifecycle diagram of Recycled Cement and Portland Cement (Bandeira, 2020)

According to Bogas et al. (2020), RC presents greater water demand than OPC, due to its higher porosity, specific surface area and free lime content. Due to the greater amount of water added, the porosity of the cementitious materials increases, which in turn negatively affects their mechanical strength and durability. However, RC showed the same binding capacity of OPC (Bogas *et al*., 2023). Studies conducted by the Department of Civil Engineering, Architecture and Environment at Instituto Superior Técnico have shown that RC production from old concrete can achieve purity levels exceeding 75% with particle sizes below 150 µm using the method patented by Bogas et al. (2019). This approach optimises RC reactivity, ensuring higher hydration efficiency and recovery of cementitious properties (Carriço et al., 2021).

In addition to promoting waste reuse and reducing CO_2 emissions, CEB stabilised with RC showed a significant improvement over unstabilised blocks (UCEB), particularly in mechanical strength and durability against external elements (Bogas et al., 2023; Real, 2019, Cruz et al., 2024). The RC CEB mechanical performance was still found slightly lower than for OPC CEB despite the similar binder capacity of the stabilisers, due to the higher porosity of RC CEB produced with higher water content. Nevertheless, it is not excluded that RC CEB can be produced with similar porosity than OPC CEB with the addition of natural additives (decreasing the water demand) and, consequently, with a more similar mechanical strength (Bogas et al., 2023).

2.4 Thermal properties of Compressed Earth Blocks

2.4.1 Theoretical framework

As mentioned, the present work analyses the thermal behaviour of CEB, for the assessment of their suitability and effectiveness in different environmental contexts. To achieve this goal, it was necessary to understand the concepts of thermal conductivity, specific heat, and diffusivity.

Thermal conductivity (λ) is a property of materials that quantifies its ability to conduct heat through a homogeneous material (FIP, 1983). It is defined as the average heat flow through a cubic volume with edges of one meter, per unit time, under a temperature gradient of 1°C between opposite faces. In the International System of Units, thermal conductivity is expressed in Watts per meter per

Kelvin (W/(m·K)). In this work, degrees Celsius (°C) (W/(m·ºC)) were used, assuming equivalent values (FIP, 1983). Materials with high thermal conductivity efficiently conduct heat and are commonly used as heat dissipators, while those with low conductivity are employed as thermal insulators due to their ability to slow down heat transfer (Silva, 2015).

Specific heat capacity (*c*), typically expressed in Joules per kilogram per degree Celsius (J/(kg·°C)), defines the amount of thermal energy required to raise the temperature of a unit mass by one degree Celsius. This property directly influences the ability of a material to moderate internal temperature fluctuations, providing more stable and comfortable environments (Holm and Bremner, 2000). Volumetric heat capacity (c_ρ) is given by the product of the specific heat capacity and density ($c_\rho = c \cdot \rho$) and is expressed in Joules per meter cubic per degree Celsius (J/(m^3·°C)). It refers to the required amount of heat energy to raise the temperature of a unit volume of a substance by one degree Celsius (or Kelvin). Thus, volumetric heat capacity is a measure of how much thermal energy a material can store in a given volume, whereas specific heat capacity is in a given unit mass.

Finally, thermal diffusivity, is a property that describes the ability of a material to conduct heat relative to its capacity to store thermal energy. Thermal diffusivity, α (m²/s), is determined by dividing the thermal conductivity, λ (W(m·ºC), of the material by the product of its specific heat, *c* (J/(kg·°C), and bulk density ρ (kg/m^3), as reported in equation 2.1. It provides a measure of how quickly a material can respond to temperature changes in its environment (Fernandes, 2014; Holm and Bremner, 2000; Neville, 1995). Materials with low thermal diffusivity are effective in slowing down heat transfer, which contributes to the thermal insulation of buildings and the maintenance of a more controlled internal climate.

$$\propto = \frac{\lambda}{c \cdot \rho} \quad [m^2/s] \tag{2.1}$$

Thermal resistance (R_T) is a measurement of material's ability to resist conducting heat flow. The thermal resistance of a building element can be determined using equation (2.2) for layers arranged in serie. In this expression, d_i represents the thickness and λ_i the thermal conductivity of each material. When a structure, such as a wall, consists of several uniform layers of different materials in direct contact or separated by air gaps of constant thickness, the total thermal resistance of the element is the sum of the resistance of each layer, including the air gaps, as described by Cavanaugh (2002).

$$R_T = \sum_{i=1}^{n} \frac{d_i}{\lambda_i} \quad \left[(m^2 \cdot ^\circ C)/W\right] \tag{2.2}$$

The thermal insulation capacity of a building element is often assessed using the thermal transmittance coefficient, *U*, determined from equation (2.3). This coefficient corresponds to the sum of the inverse of the thermal resistances of the various layers, along with the interior (R_{si}) and exterior (R_{se}) surface resistances of the building element.

$$U = \frac{1}{\sum \frac{d_i}{\lambda_i} + R_{si} + R_{se}} \quad \left[W/m^2 \cdot ^\circ C\right] \tag{2.3}$$

Heat transfer in materials can occur through three distinct mechanisms: conduction, convection, and radiation. The thermal conductivity coefficient is a metric that quantifies how easily heat is

transmitted through materials by conduction. For the development of this work, the focus was specifically on conduction mechanisms, excluding the analysis of heat transfer through convection and radiation. This coefficient depends on various factors, including the material's density, pore size distribution, and microstructure (Silva, 2017).

2.4.2 Methods for evaluating thermal conductivity

Understanding the thermal performance of construction materials is dependent on assessing their thermal conductivity. This property is directly influenced by various physical characteristics of the material such as bulk density, moisture content, temperature, and internal structure. The internal structure encompasses aspects like porosity, anisotropy, and potential structural defects. Additionally, external factors like the age of the sample, storage conditions, and production methods also play significant roles on the thermal conductivity of a material (Fernandes, 2014; Franco, 2007).

The ISO 10456 (2007) standard defines two methods for evaluating the thermal conductivity of a building material/ constructive element: transient and stationary methods.

2.4.2.1 Transient methods

Transient methods are a dynamic and efficient approach to measure the thermal properties of materials. These methods use heat pulses instead of continuous heat flow (as stationary methods), enabling a rapid analysis without bringing the sample to thermal equilibrium. Only when the test is started the sample reaches thermal equilibrium with the environment to ensure consistent results. Subsequently, a heat pulse is applied via a probe in direct contact with the sample, and temperature variations are monitored in real time, and thermal conductivity registered on the receptor (Fernandes, 2014; Franco, 2007).

Among transient methods, the most common are the Transient Plane Source (TPS) method, the Transient Line Source (TLS) method, and the Modified Transient Plane Source (MTPS) method.

In the TPS method, a double-sided plane probe is used, inserted into the interior of the prepared sample, as illustrated in Figure 6. The TLS method, on the other hand, employs a needle-shaped probe that penetrates through the body of the sample, as shown in Figure 7. Finally, the MTPS method uses a single-sided probe, which must be in full contact with a flat and smooth surface of the sample to ensure accurate measurements, as represented in Figure 8.

Figure 6 - Transient Plane Source Method (TPS) (Silva, 2017).

Figure 7 - Transient Line Source Method (TLS) (Silva, 2017).

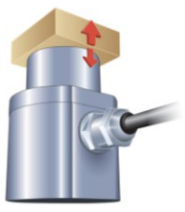

Figure 8 - Modified Transient Plane Source (MTPS) (Silva, 2017).

The choice of the appropriate method depends on the specific characteristics of the sample and the precise measurement requirements, considering the advantages and limitations of each transient technique.

2.4.2.2 Stationary methods

Stationary methods for assessing thermal conductivity are based on applying a constant temperature gradient across a sample of known thickness. These methods are primarily divided into two types: the Guarded Hot Plate (GHP) method and the Heat Flow Meter (HFM) method, both regulated by specific standards such as ISO 8301 (2010), NP EN 12667 (2012), and ASTM C518-21 (2021) for HFM, and ISO 8302 (1991) and ASTM C177-19 (2019) for GHP (Fernandes, 2014; Franco, 2007).

The GHP method employs a setup where the sample is placed between two isothermal plates, one hot and two cold, allowing for precise measurement of heat flow through the sample as illustrated in Figure 9 in one direction and the other. The HFM method, represented in Figure 10, configures the sample in a single direction, from hot to cold, simplifying assembly and reducing preparation time.

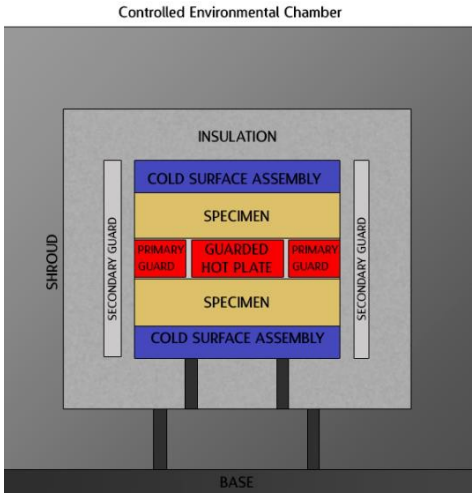

Figure 9 - Guarded Hot Plate Diagram (Franco, 2007).

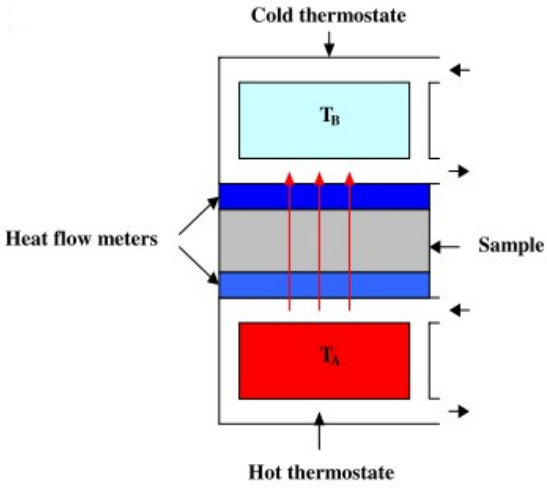

Figure 10 - Heat Flow Meter Diagram (Franco, 2007).

Both methods apply Fourier's law to determine thermal conductivity, where the amount of energy transferred is proportional to the material's conductivity (Fernandes, 2014; Franco, 2007). Fourier's Law is represented in Equation 2.4 where "Qc" is the steady-state heat flow through the element (W), "K_p" the thermal conductance of the element (W/(m²·°C)) "A" the cross-sectional area of the element (m²) and "T_k" the temperatures on the faces of the element (°C). Despite their high precision and reliability, these methods require specific equipment and are energy and water-intensive, as well as needing long periods to achieve thermal equilibrium, which can pose challenges in terms of efficiency and cost.

$$Q_c = K_p \times A \times (T_1 - T_2) \tag{2.4}$$

In addition, there is a less conventional method, known as the Lee Disk method, which also uses stationary conditions to determine thermal conductivity. First described by Lee and Charlton in 1896, this method involves two distinct phases: heating until reaching stationary conditions and subsequent cooling, with temperature measurements taken over time (Fidalgo et al., 2013).

2.4.3 Previous studies on CEB thermal properties

Table 1 presents a synthesis of results (adapted from Silva (2015)) from laboratory tests and in-situ tests run on CEB unstabilised or stabilised with cement, lime or both, to better understand the thermal performance of these materials in various application contexts. CEB stabilised with cement are generally associated with higher thermal conductivity compared to those stabilised with hydraulic lime, as observed by Real et al. (2024) and Turco et al. (2024). Additionally, the amount of stabiliser added is crucial, as demonstrated by Gomes (2015). For instance, increasing the amount of hydraulic lime typically leads to a reduction in thermal conductivity. The moisture conditions further affect thermal properties: CEB tested in a dry state, exhibit lower thermal conductivity compared to those with a 5% moisture content (Adam and Jones, 1995). Moreover, the compaction pressure can improve pore uniformity and distribution, potentially decreasing thermal conductivity by minimising the void spaces within the material.

Indeed, the high heterogeneity in composition, production and compaction of CEB leads to significant variations in their thermal properties. These variations are particularly observed in older constructions, due to differences of the materials incorporated, as referred by Sampaio *et al.*, (2014). Moreover, the same authors observed that the moisture content of the analysed CEB influenced directly the thermal results, with higher conductivity at higher moisture content (Sampaio et al., 2014).

Real et al. (2024) found that the incorporation of CDW led to a slight reduction of thermal conductivity due to the more refined porosity introduced by CDW over the earth matrix, for the same total porosity. Depending on the type of earth, the unstabilised CEB of the same study exhibited a similar to higher total porosity compared to OPC stabilised CEB, ranging 30.4-34.4%, and a dry density varying between 1754 kg/m³ and 1835 kg/m³. This increased porosity generally indicates a greater amount of air trapped within the soil matrix. Moreover, unstabilised blocks tended to have a coarser microstructure characterised by fewer and larger pores. Therefore, the thermal conductivity, within the range of 0.53 W/(m·K) to 0.75 W/(m·K) for UCEB produced with different types of earth, was slightly higher than that of CEB produced with OPC and the same type of earth. Indeed, the CEB stabilisation has the effect of reducing the thermal conductivity (even in cases with lower total porosity). This reduction is mainly due to changes in the distribution of porosity: in CEB with coarser porosity, the contact between the solids facilitates the heat flow, resulting in higher conductivity, whereas a more refined porosity (introduced by cement stabilisation) hinders heat transfer (Real et al., 2024). Thus, although stabilisers contribute to particle bonding and increased mechanical strength, their direct impact on thermal properties is primarily determined by the changes introduced in the microstructure (Real et al., 2024).

The inclusion of porous components in CEB composition, such as straw, cork or mineral aggregates (i.e., pumice and expanded perlite) also alters the thermal properties of CEB. This approach has been shown to decrease the thermal conductivity of earth construction, as also highlighted in the research by Meneses et al. (2011), Soebarto (2009), Allinson and Hall (2010), Taylor and Luther (2004), and Goodhew et al. (2000). It's noted that the thermal conductivity expected of earthen building elements lies in the range of 0.60–1.20 W/(m·K) (Table 1), with corresponding bulk density values typically between 1700 and 2000 kg/m^3 (Turco et al., 2024).

Studies from N. Gomes (2015) and Real et al. (2024) indicate that the addition of CDW in CEB may reduce the thermal conductivity, compared to blocks made solely of earth without any CDW incorporation. Therefore, the partial earth substitution with CDW was found to improve CEB insulation properties by changing the total porosity and microstructure of the blocks. Note that the addition of CDW to CEB composition also contributes to produce a more environmentally sustainable material and, by recycling materials that would otherwise be discarded, to implement circular economy in construction.

Table 1 - Thermal conductivity of CEB by different authors (updated from Silva, 2015).

Document Consulted	Stabiliser		Thermal Conductivity λ (W/m.K)	Observations	
	Type	Proportion (% by mass)		State	Content
Lourenço (2002)	None		0,81-0,93	No soil characterisation	
	Cement	8	0,81-0,93	-	-
	Hydraulic Lime	12 a 19	0,93-1,04	CP of 30 MPa	
Kerali (2001)	-	-	0,23-1,04	General Values	
Adam and Jones (1995)*	Cement	5	0,41-0,51	Dry State	-
			0,71-0,88	5% Moisture Content	-
	Hydraulic Lime	6	0,25-0,46	Dry State	-
			0,44-0,80	5% Moisture Content	-
Sampaio et al. (2014)	None		0,5	Dry State	-
			0,6-0,7	Laboratory Ambient Condition	-
N. Gomes (2015)	Hydraulic Lime	6,25	0,519	-	CDW inclusion
	Hydraulic Lime + Cement	5 + 1,7	0,999	-	-
Real et al. (2024)	None		0,53	-	No CDW inclusion
			0,75	-	25% CDW inclusion
	Cement	8	0,80	-	No CDW inclusion
	Cement	8	0,69	-	25% CDW inclusion
	Recycled Cement	8	0,63	-	25% CDW inclusion
Turco et al. (2024)	Hydraulic Lime	5	0,65	-	-
			0,653-0,636	-	5% to 15% of Wheat Straw
			0,653-0,523	-	1% to 5% of Cork Agglomerate
			0,506-0,479	-	10% to 15% Olive Pits

Legend: CP – Compaction Pressure; * CP of 10 MPa

Real et al (2014) were the first to study the influence of RC on the thermal conductivity of CEB. The authors found that incorporating RC increased the total porosity of CEB, resulting in a slight reduction in thermal conductivity (Table 1). In addition, for the same total porosity, more refined microstructure is obtained with RC, which also helps to reduce thermal conductivity (Real et al 2014).

However, despite the increasing research and the growing interest in this area, there is a noticeable gap in studies regarding the thermal performance of CEB stabilised with RC retrieved from

concrete waste. This deficiency is significant given the potential environmental and economic benefits of utilising recycled materials in construction. Further exploration into this area could not only bridge this knowledge gap but also lead to more sustainable building practices, optimising the use of waste materials, while enhancing the energy efficiency of the resulting structures.

3 Experimental Campaign

This chapter describes the experimental campaign carried out to characterise and analyse the thermal properties of compressed earth blocks (CEB) stabilised with recycled cement (RC), and to compare them with reference blocks that are either unstabilised (UCEB) or stabilised with Portland cement (OPC). The study involved 4 main phases, including the production of RC, the manufacture of CEB, and the preparation and calibration of the equipment and materials required for their development, as well the respective characterisation of CEB. The characterisation of the blocks' thermal properties was aligned with a series of standardised procedures and specific test methods to provide a solid basis for validating the results obtained.

The production of RC and CEB took place in different phases and locations, beginning at the IST Geosciences and Geotechnologies Laboratory (GeoLab-IST) and at the Montemor-o-Novo Convent Workshops (ACOC), where RC was produced and the blocks were manufactured, respectively. Subsequently, the thermal properties of the blocks were tested at IST's Civil Engineering Construction Laboratory (CEL), using two methodologies, considering previously calibrated equipment to guarantee the accuracy and consistency of the results. In this thesis, the term “thermal properties” refers specifically to the thermal conductivity, specific heat, and thermal diffusivity.

3.1 Experimental program

The experimental program was divided into four main phases:

- Production of recycled cement.
- Production of CEB.
- CEB thermal characterisation using the modified transient method (Isomet 2114).
- CEB thermal characterisation using the adapted steady-state method (climate chamber).

The first phase of the program focused on the production of RC. This process involved mechanical crushing and grinding techniques to reduce the size of the cementitious fraction, which had previously been obtained from concrete waste or lab-made cement pastes. Afterwards, the resulting material underwent a high-temperature thermal treatment, yielding the RC.

In the second phase, the production of CEB was carried out. During this stage, different compositions were considered, varying the quantity and type of materials in the mixtures, specifically the amount of CDW used as a partial substitute of soil and the type and amount of binder (OPC or RC). The production followed a strict methodology, ensuring the homogeneity and quality of the manufactured blocks, maximising material reuse, and reducing the environmental impact associated with their development.

The third phase focused on testing the different mixtures produced in the second phase. First, tests were conducted using the modified transient method (Isomet 2114), with the main aim of experimentally characterising the thermal conductivity of the CEB described. Finally, in the fourth phase, three reference compositions of CEB (UCEB and CEB with 8%RC or 8% OPC) were tested on a prototype wall built in a climate chamber at the Civil Engineering Laboratory. This test provided a thorough analysis of the blocks’ thermal behaviour under controlled conditions.

3.2 Materials

3.2.1 Earth

In the present subsection, the soil designated as FA (Figure 11) was extracted from the Portuguese Air Force and it was collected at a depth greater than one meter to minimise the presence of organic matter. To adjust the particle size distribution of this soil, which was found to be sandy, a fine material rich in clay was added. This material, sourced from the by-products of the Cobert tiles factory in Torres Vedras, is referred to as TV (Figure 12).

Figure 11 - FA soil.

Figure 12 - TV clayey residue.

These materials were part of an extensive characterisation carried out within the framework of the Eco+RCEB project, as documented by Rodrigues (2024). Throughout the author's study, the products were fully characterised: the granulometric curve was determined by dry sieving and the clay content by X-ray adsorption spectroscopy; the consistency limits, optimum water content, organic matter content, and bulk density of particles were determined following the standards reported in Table 2. The same author also determined the mineralogical composition of FA soil and TV using X-ray diffraction (XRD) analyses (Figure 13). FA soil and TV residue were predominantly composed of non-expansive clay minerals, such as kaolinite and illite, in addition to quartz and microcline. These clay minerals are considered ideal for producing CEB due to their non-expansive nature (Sampaio et al., 2014). FA soil additionally contained albite and orthoclase. The results of the tests carried out have been compiled in Table 3 providing a comprehensive overview of the earth properties.

Table 2 - Standards adopted for soil characterisation.

Parameter	Standard
Granulometry	LNEC E-195 (1966)
Bulk density	NP EN 1097-7 (2012), NP-143 (1969)
Water absorption	NP EN 1097-6 (2016)
Consistency limits	NP-143 (1969)
Organic matter content	XP P94-047 (1998)
Compaction test (Proctor)	ASTM D 698 - 12 (2021)

Table 3 - Characteristics of FA and TV soils adapted from (Rodrigues, 2024).

Parameter		FA	TV
Granulometry (%)	Gravel (>4.75 mm)	1.4	0.0
	Sand (0.075< d <4.75 mm)	85.6	8.5
	Silt + Clay (d <75 µm)	13.0	49.3
	Clay (%)[a]	10.7	42.2
Consistency Limits (%)	Liquid Limit	23.7	47.0
	Plastic Limit	18.4	25.7
	Plasticity Index	5.4	21.3
Bulk Density of Particles (kg/m³)		2633	2630
Water Absorption (%)		1.4	-
Organic Matter (%)		0.8	1.5
Optimum Water Content (%)		12.8	-

a: determined from X-ray adsorption spectroscopy

The results indicate that the FA soil is weakly clayey, displaying low plasticity index values that justify the addition of TV. Indeed, Figure 14 clearly illustrates the need of incorporating TV for the FA granulometric curve to comply with XP P13-901 (2001), as recommended for the production of stabilised CEB. Nevertheless, FA alone fits within the consistency limits recommended in the literature for the production of both unstabilised and cement-stabilised CEB, with a liquid limit between 25% and 40% and a plasticity index between 2% and 18%, as suggested by standards NBR 10833 (1989), WD-ARS 1333 (2018), and HB 195 (2002). The organic matter of both FA and TV were below the maximum threshold of 4% for CEB production, according to WD-ARS 1333 (2018). Finally, the optimum water content of FA was found to be in the range of 10-13%, as recommended by Riza et al. (2011).

Additionally, according to the ASTM D2497-11 (2011), the FA soil is classified as SC-SM (silty clayey sand), the TV as SCL (sandy lean clay), and the combination of the two as SC (clayey sand).

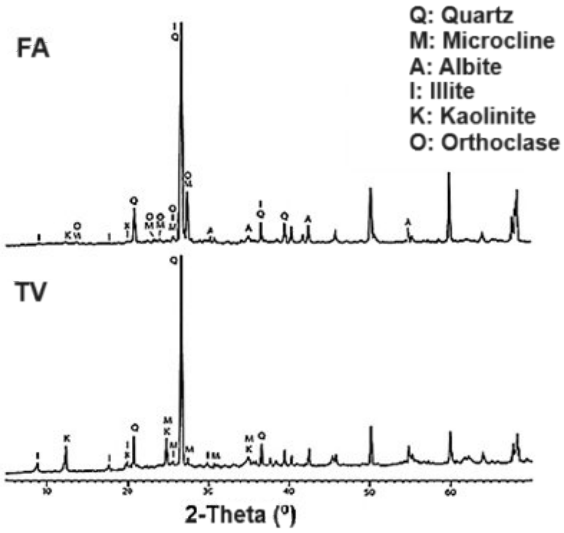

Figure 13 - Diffractograms of FA soil and TV residue adapted from (Rodrigues, 2024).

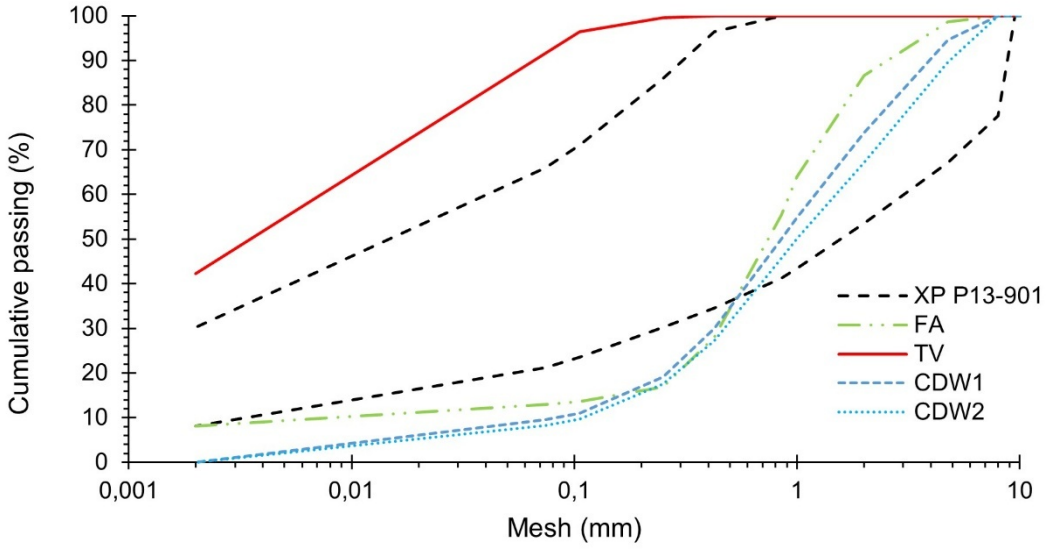

Figure 14 - Granulometric curve of FA soil, TV residue, CDW and the granulometric range proposed by the standard XP P13-901 (2001).

3.2.2 CDW

One type of CDW, supplied by the waste management company Vimajas, was used in this study as a partial substitute for soil (Figure 15). The standards adopted for its characterisation are summarised in Table 4. The CDW had a maximum particle size of less than 8 mm, ideal for the use in soil-mixtures to produce CEB (Cruz and Bogas, 2024b).

Figure 15 - Construction and demolition waste (CDW)

Table 4 - Standards adopted for CDW characterisation.

Parameter	Standard
Granulometry	NP EN 933-11 (2011)
Bulk density and water absorption	NP EN 1097-6 (2016)
Mineralogical composition and organic matter content	NP EN 933-1 (2012)

The characterisation of CDW, which includes granulometry, bulk density, water absorption, and composition analyses, was detailed in a previous study of the Eco+RCEB project (Rodrigues, 2024). The results are summarised in Table 5. Construction waste has high variability, which leads to differences in its characteristics between different supply batches. In the present study, the CDW used for the production of blocks and mortars came from two distinct supplies. For this reason, Table 5 presents the characteristics of CDW1 and CDW2, employed in the production of CEB and in the production of earth mortars used for laying and rendering CEB, respectively. The granulometric curve, presented in Figure 14, shows a similarity between the granulometric curve of CDW1 and FA. This

eases the direct partial substitution of FA without significant changes on the CEB compactness. The main difference between CDW1 and CDW2 lies in the higher proportion of bituminous material of the latter.

Table 5 - Characteristics of CDW adapted from (Rodrigues, 2024).

Parameter		CDW1	CDW2
Granulometry (%)	Gravel (>4.75 mm)	5.5	10.4
	Sand (0.075< d <4.75 mm)	85.0	81.4
	Silt + Clay (d <75 µm)	9.5	8.2
Composition (%)	Concrete and mortar	45.3	31.8
	Natural aggregate and stone	27.9	35.2
	Ceramic material	16.4	10.5
	Bituminous material	2.2	18.8
	Others	8.3	3.7
Bulk Density of Particles (kg/m³)		2300	2266
Water Absorption (%)		4.3	3.9

3.2.3 Stabilisers

3.2.3.1 Portland cement

Portland Cement type I 42,5 R (CEM I 42,5 R) was used for CEB stabilisation, in the production of earth mortar used for the joints and rendering of the CEB walls, as well as on the production of the cement paste and concrete that originated recycled cement paste (RCP) and recycled cement concrete (RCC), respectively. In one mixture, a low-grade cement type II/B-L 32,5 (Portland limestone cement, PLC) was also used as a more economical and environmentally friendly alternative to OPC. Table 6 shows the physical, chemical, and mechanical properties of OPC and PLC supplied by SECIL.

Table 6 - Characteristics of CEM I 42.5 R and CEM II/B-L 32,5.

Specifications		CEM I 42.5 R (OPC)	CEM II/B-L 32.5 (PLC)
Density (g/cm³)		3.03	3.0
BET specific surface area (m²/g)		1.97	9.81
Compressive strength of paste (MPa)	2 day	29.3	20.8
	7 days	43.3	32.2
	28 days	56.3	40.8
$SiO_2 + Al_2O_3 + Fe_2O_3$ (%)		19.45 + 4.98 + 2.91	15.88 + 4.12 + 2.44
CaO + MgO (%)		63.0 + 1.63	59.67 + 1.43
Free CaO (%)		2.73	2.15
Normal consistency		0.30	0.27
Setting time (min)	Initial	158	151
	Final	236	219

3.2.3.2 Recycled cement

Recycled cement was produced from the cementitious fraction of lab-made OPC pastes with a water/ cement (w/c) ratio of 0.55, as well as from concrete with the same paste composition, but with also the incorporation of siliceous sand and coarse limestone aggregates. Both paste and concrete were wet-cured for 7 days, followed by at least 3 months in natural environment. These residues are

representative of old hydrated cement waste. Note that the composition of the waste paste, namely the w/c, has little influence on final RC properties (Carriço et al., 2022).

The process of producing recycled cement involved three crushing stages and one milling stage, in order to reduce the particle size and increase the specific surface area to favour the hydration reaction, followed by the thermoactivation of the resulting residue.

In the first crushing stage, the IST CEL jaw crusher (Figure 16a) was used to reduce 15 cm edged specimens to particle size below 70 mm. This was followed by a new crushing process using a jaw crusher with a smaller opening (Figure 16b), resulting in a medium-sized aggregate. In the last crushing process, the medium-sized aggregate was exposed to a roller mill, reducing the material to fine dimensions, as illustrated in Figure 16.

For concrete specimens, the final stage included the process of separating the concrete constituents. Indeed, there was the additional challenge of separating the cementitious matrix from the remaining concrete components (aggregate) to obtain poorly contaminated RC. This procedure was based on a method developed and patented at IST (Carriço et al., 2021; Hu, 2019). In an initial stage of successive sieving and milling in the roller mill, particles sizes were reduced below 1 mm. Subsequently, the material was separated into fractions of 0–150 μm, 150–250 μm, 250–500 μm, and 500–1000 μm, with the intermediate fractions (150–500 μm) undergoing magnetic separation (Carriço et al. 2021; Hu 2019). Thus, by exploiting the paramagnetic characteristics of the cement paste, it was possible to isolate a cementitious product with reduced aggregate contamination, making it more suitable for recycled cement production.

a) b) c)

d) e) f)

Figure 16 - a) Jaw Crusher; b) Medium-sized Jaw Crusher; c) Roll Crusher; d) Coarse aggregate derived from paste; e) Medium-sized aggregate; f) Fine aggregate resulting from crushing.

The resulting material was milled at GeoLab-IST in a horizontal ball mill for 2 hours, where 10 kg of material were joined to 515 balls with diameters between 20 and 30 mm. To make the process more effective, the material was previously dried at 100 ºC for 24 hours, and a deflocculating additive (Figure 17) was added at a rate of 0.2% of the weight to reduce particle agglomeration.

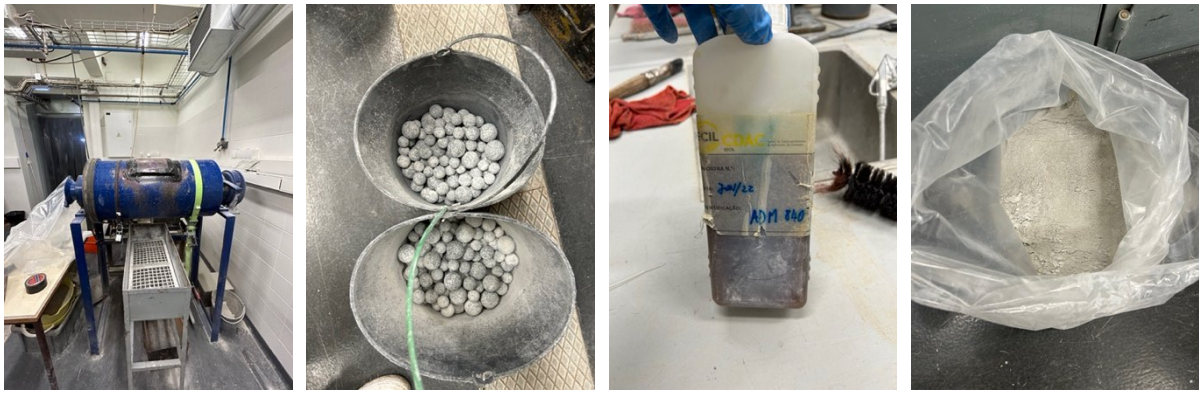

a) b) c) d)

Figure 17 - a) Ball mill; b) Metal balls; c) Deflocculating additive; d) Particles with a diameter of less than 150 µm

Finally, thermoactivation was carried out in an horizontal furnace at CEL - IST. The material, laid out on metal trays, was subjected to a heating rate of 10 ºC/min. Once the temperature levels of 250 ºC and 550 ºC were reached, it was stabilised at these levels for 1 hour. Finally, maintaining the same heating rate, the temperature was raised to 750 ºC and kept at this level for 3 hours.

RC was characterised in another study integrated into the Eco+RCEB project (Rodrigues, 2024). The main characteristics of these materials are presented in Table 7. The particle size distribution of RCP and OPC, performed by laser granulometry (Mastersizer 3000, Malvern), are illustrated in Figure 18. It was observed that the granularity of the RCP is marginally coarser than that of the OPC. Additionally, the RCP showed a higher water demand and a higher free lime content than the OPC, as indicated in Table 6 and Table 7.

Figure 18 - Granulometric curve of OPC and RCP.

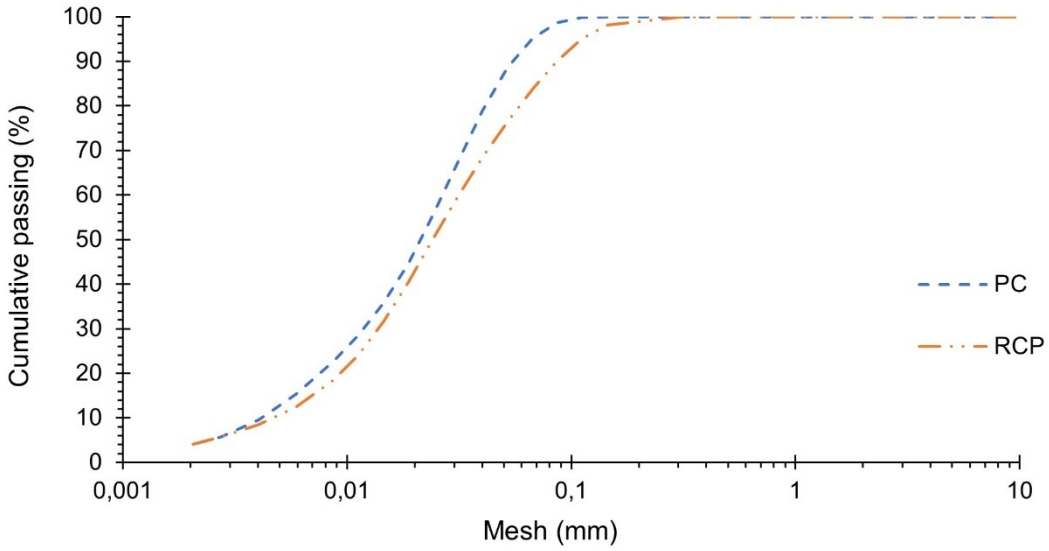

As RCC was derived from pre-separated concrete waste, it exhibited some degree of aggregate contamination. In the work of Rodrigues (2024) the average amount of aggregates in RC was estimated as 32.8%.

Table 7 - Characteristics of RCP and RCC.

Specifications		RCP	RCC
Density (g/cm³)		3.00	2.96
BET specific surface area (m²/g)		7.86	-
$SiO_2 + Al_2O_3 + Fe_2O_3$ (%)		19.1 + 5.1 + 3.0	-
CaO + MgO (%)		60.8 + 1.8	-
Free CaO (%)		17.9	-
Normal consistency		0.74	0.54
Setting time (min)	Initial	170	>720
	Final	460	<1440

3.3 CEB production

This chapter presents the compositions and describes the production process of the CEB, including the mixing, moulding, and curing stages. The blocks were produced with dimensions of 295x140x90 mm^3. The production was supported by the Cultural Association of Art and Communication "Oficinas do Convento" in Montemor-o-Novo, which provided the space needed for the production of approximately 120 blocks.

3.3.1 Composition

The mix-design of CEB followed the recommendations of another study conducted as part of the Eco+RCEB project (Rodrigues, 2024). The binder content was based on the recommendations mentioned in the literature (Azevedo, 2021; Nabais, 2023, Rodrigues, 2024), and summarised in Table 8. Regarding the water and TV contents, their determination was based on a preliminary experimental study carried out by Rodrigues (2024). In this study, the author concluded that for unstabilised mixtures, a higher proportion of TV must be introduced, as clay is the only binder. The mix-design was based on fuller reference curves, as well as on the grading limits specified in XP P13-901 (2001).

The CEB were produced with different types (OPC, PLC, RCP, and RCC) and contents (0%, 4% and 8% by weigth) of stabiliser, different percentages of OPC replacement by RCP or RCC (20%, 50% and 100%), of FA replacement by CDW1 (0%, 15%, 25%, 40%) and curing conditions. CDW1 with the same particle size distribution of earth mixtures was used in OPC8CDW0, OPC8CDW15, OPC8CDW25 and OPC8CDW40. In all the other mixtures, the earth was directly replaced with 25% CDW1. In these cases, the term CDW was omitted from the nomenclature. The stabiliser content of RCC CEB was adjusted to account for the aggregate contamination (33%). For comparison purposes, unstabilised blocks (UCEB) and CEB with 8% OPC having the same water content as CEB with 8% RCP (OPC8TH) were produced.

It is important to highlight that the amount of water added to the mixture considered the moisture content of the FA soil, TV, and CDW1 at the time of use, determined using a high precision thermobalance (Kern DBL) (Figure 19). Additionally, the water absorbed by the mixture's components was also considered (Table 3 and Table 5).

Figure 19 – Kern DBL high precision thermobalance.

Table 8 - Composition of CEB mixes used in the Modified Transient Method.

Designation	Binder	Binder (%)[a]	Water (%)[b]	CDW1 (%)[c]	TV (%)[d]	w/b[e]
UCEB	-	-	9	25	18	-
UCEBCDW0	-	-	9	0	18	-
OPC4	OPC	4	9	25	14	2.34
OPC8	OPC	8	9	25	11	1.22
OPC8TH	OPC	8	12	25	11	1.62
OPC8CDW0	OPC	8	9	0	11	1.22
OPC8CDW15	OPC	8	9	15	11	1.22
OPC8CDW25	OPC	8	9	25	11	1.22
OPC8CDW40	OPC	8	9	40	11	1.22
OPC80RCP20	80%OPC+20%RCP	8	9	25	11	1.22
OPC50RCP50	50%OPC+50%RCP	8	10	25	11	1.35
OPC80RCC20	73%OPC+27%RCP	8.8	9	25	11	1.11
OPC50RCC50	40%OPC+60%RCP	10	9	25	11	0.99
PLC8	PLC	8	9	25	11	1.22
RCP8	RCP	8	12	25	11	1.62
RCP8CDW0	RCP	8	12	0	11	1.62
RCP4	RCP	4	10	25	14	2.34
RCC8	RCC	12	12	25	11	1.12

a: % by dry weight of FA + TV + CDW1; b: % by dry weight of all solids; c: % by volume of FA + TV + CDW1; d: % by volume of FA; e: effective water/binder ratio

3.3.2 Earth preparation

FA was initially spread on plastic sheets to dry. This process facilitates the pulverisation and sieving steps. After drying, the soil was transported in wheelbarrows to a mechanical paddle pulveriser (Figure 20a). In this equipment, the earth was pulverised with a single pass. The pulverised soil (Figure 20b) was then sieved using a rotary sieve with an 8 mm square mesh (Figure 20c) to remove stones, clumps, and organic matter, as well as to adjust the granulometry of the earth. After this, the earth was stored ready to be used and protected from moisture (Figure 20d). TV and CDW1 did not need any additional pre-treatment.

a) b) c) d)

Figure 20 - Preparation of FA soil: a) Pulverising; b) Pulverised soil; c) Sieving; d) Sieved soil.

3.3.3 Mixing and moulding

A vertical-mixer (Figure 21a) was used for CEB production. First, the solids were homogenised. Then, the water was gradually added and the mixer activated for 4 min during which it was stopped twice for manual remixing. The wet mixture was then weighed and moved to the OSKAM V/F hydraulic press (Figure 21b) for compaction. This semi-automatic hydraulic press has a production capacity of 720 blocks per hour. A fixed amount of mixture was placed into a downstream compartment and, from there, automatically inserted into the mould. The mixture was then compacted at the pressure of 5-6 MPa and one CEB at the time was produced.

The fresh density of each mixture was evaluated on the average weight of three CEB, whose geometry determined using a metal ruler. At this stage, the blocks were fragile and had low cohesion, so they were carefully (to avoid edge damage and/or cracks) transported to pallets where they were placed always guaranteeing space between them, regularly watered, and covered with a plastic sheet (Figure 21c). After at least seven days of wet curing, the blocks were transported to LC-IST, where were exposed under laboratory environmental conditions for additional 21 days, with temperatures ranging from 19 to 26°C and relative humidity between approximately 55% and 75%.

a) b) c)

Figure 21 - CEB production: a) Vertical mixer; b) OSKAM V/F semi-automatic hydraulic press; c) wet curing.

3.4 Mortar production

In this section, the production process of the mortars used for the execution of the joints between blocks and for the rendering of the CEB walls is described. The development of the mixes was carried

out at the CEL of IST, where they were prepared, applied, and subsequently monitored as part of the thermal testing campaign.

The adopted mortar formulations aimed to be representative of real-world application solutions and were based on compositions used in previous research conducted within the scope of the Eco+RCEB Project. This approach ensured both experimental consistency and comparability of thermal performance results.

Table 9 presents the composition of the mortars used in this study.

Table 9 - Composition of mortar mixes used in the Adapted Steady-State Method.

Position	Designation	Binder type	Binder (%)[a]	CDW2 (%)[b]	FA (%)[c]	Fine Sand (%)[c]	TV (%)[b]	Water (%)[d]	ρ_{28d} (kg/m^3)
3, 5, 7	UPC12	OPC	12	25	45.4	22.7	0	23	1647
2, 4, 8	RCP12	RCP	12	25	45.3	22.6	0	28	1567
6, 9	UM	-	0	25	47.3	18.7	9.0	24	1702

a: dry mass of FA; b: volume of FA; c: volume of FA + Binder; d) dry mass of FA + CDW + Binder

The mortar production was based on the mixing of materials previously characterised in Section 3.2, following a standardised procedure for all mixtures, regardless of their specific compositions. For each wall, a 1-litre mortar batch was prepared for the mortar joints between blocks, and a 1.5-litre batch was prepared for the rendering.

The mortar production process followed the steps outlined below: i) The mixer bowl was cleaned with a damp cloth to prevent water loss during mixing; ii) The liquid components, namely water, were added first; iii) The binders corresponding to each composition were then incorporated; iv) This initial mixture was blended for 30 seconds; v) After this period, the aggregates, fine sand, CDW2 and FA soil were gradually added, starting with the coarser fraction followed by the finer one, over a 30-second interval; vi) Once all aggregates were incorporated, the mixer speed was increased for a further 30 seconds, followed by a pause during which the mortar was manually remixed with a spatula to ensure complete homogenisation; vi) The mixing process then resumed at high speed for an additional 60 seconds; vii) Upon completion of the mixing cycle, the mortar was manually stirred again before application.

3.5 CEB characterisation

In the present study the main physical and mechanical properties, as well as the thermal insulation properties of CEB were evaluated. The blocks were tested at 28 days of age. Regarding the thermal conductivity, two different methods were adopted. The first was a transient method of the MPTS type (flat probe). This procedure, applied to all produced blocks, allowed for fast thermal conductivity measurement without needing the material to reach a steady state. The second method was an adaptation of the stationary Heat Flow Meter method, used on small-scale prototype masonry walls built with CEB laid and rendered with stabilised or unstabilised earth mortar. Following this approach, only reference UCEB and CEB produced with 8% RC or 8% CP were tested.

3.5.1 Density

The bulk density was determined in accordance with the EN 772-13 (2000) for masonry blocks, as the ratio between the mass and the volume of CEB. The volume immediately after CEB production ("fresh density") and for unstabilised CEB was calculated by the geometric method. The volume of stabilised CEB in the hardened state was determined by hydrostatic weighing, following the method specified in EN 772-3 (1998).

3.5.2 Compressive strength

The determination of compressive strength was based on the EN 772-1 (2011) and NBR 8492 (1984) standards. This property was assessed using half-blocks, with their largest face oriented in the direction of load application. A Controls press with a maximum capacity of up to 3000 kN and a minimum loading rate of 0.1 kN/s was used for the test.

Prior to compressive strength testing, plywood boards were placed between the half-block and the upper and lower plates of the press (Figure 22) to ensure uniform load distribution on the specimen and minimise friction. The compressive strength, f_c (MPa) was calculated using Equation 3.1, where F_c (kN) is the maximum force applied to the blocks, obtained from the force-time graph recorded by the Automax Multitest software, and A (mm^2) is the area of the compressed surface of the specimen. Tests were performed on the largest face of the half-blocks, measuring 147.5 × 140 mm.

Figure 22 – Compressive strength test.

$$f_c = \frac{F_c}{A} \ [\text{MPa}] \tag{3.1}$$

3.5.3 Thermal properties - Modified Transient Method

The first method used for the determination of CEB thermal properties, required the use of a portable heat transfer analyser ISOMET 2114 from Applied Precision Ltd (Figure 23). The equipment, with the flat probe, operates within a temperature range of -15 ºC to 50 ºC with an error of 1 ºC. The device is portable and compatible with various probes. A flat contact probe was employed, sensible to values of thermal conductivity from three ranges: 0.04 to 0.3 W/(m·K), 0.3 to 3 W/(m·K), and 3 to 6 W/(m·K.) After selecting the measuring range, the probe was placed on a regular surface area for approximately 20 to 30 minutes.

According to the manufacturer (Applied Precision 2023), the equipment has an associated error for thermal conductivity (λ) of 5% plus 0.001 W/(m·K) for values in the range of 0.015 to 0.7 W/(m·K), and 10% for values in the range of 0.7 to 6 W/(m·K). The contact probe also measures the volumetric specific heat capacity (cp) between 4.0×10^4 and 3.0×10^6 J/(m³·K), with an associated uncertainty of 15% plus 1.0×10^3 J/(m^3·K).

Figure 23 - ISOMET 2114 from Applied Precision Ltd.

For CEB, the test was performed within the thermal conductivity range of 0.3 to 3 W/(m·K) under three different conditions (Figure 24): dry, saturated, and in equilibrium with the laboratory environment. The CEB were placed in the oven at 100 ºC for a minimum of 48 hours to reach dry state and after cooled before starting the test. Only the stabilised CEB were immersed in water for 48 hours, to ensure the saturation. Afterward, the excess surface water was removed, and the blocks were wrapped in plastic film. The saturated condition was not applied to unstabilised CEB as they are disintegrated in contact with water. The CEB left at laboratory conditions were considered in equilibrium with the environment after 5 days. The measurements of the single blocks were made with a thermal conductivity range of 0.3 to 3 W/(m·K).

The CEB blocks integrated in the prototype masonry wall, as described in 3.5.4, were also measured with this method (Figure 24c). Tests were carried out in a laboratory environment, within the thermal conductivity range of 0.04 to 0.3 W/(m·K).

a) b) c)

Figure 24 - Tests conducted in three conditions: a) Saturated; b) Dry; c) Laboratory environment.

3.5.4 Thermal properties - Adapted Steady-State Method in a climate chamber

In a second stage of this work, unstabilised and stabilised CEB, namely UCEB, OPC8 and RCP8, were integrated in a real scale wall of about 2.7x3 m^2 that is part of a controlled climatic chamber

available in the LC of IST. Only reference CEB with 25% CDW and 8% stabiliser were tested due to the limited area of the chamber wall. Nevertheless, the main objective was achieved, namely, to reassess the influence of RC on the thermal insulation properties of CEB. The experimental setup and thermal characterisation conducted in this stage are presented in the following sub-sections.

3.5.4.1 Experimental setup

The experimental setup for this test included the preparation of the blocks, including their drilling for the insertion of pre-welded T-type thermocouples, the construction of small-scale masonry walls and their integration into the climate chamber, as well as the installation of all thermal measurement devices and the calibration of heat flux sensors.

First, T-type thermocouples were inserted in 3 blocks per composition, to record temperature variations across its thickness. The drilling scheme was different for unstabilised and stabilised CEB. All stabilised blocks were drilled alternately, as shown in Figure 25a and 25b, keeping the thermocouple on the same face. In contrast, the unstabilised blocks required drilling on both faces (Figure 25c). This is due to the block being too fragile, causing it to crack by splitting during drilling (Figure 25d).

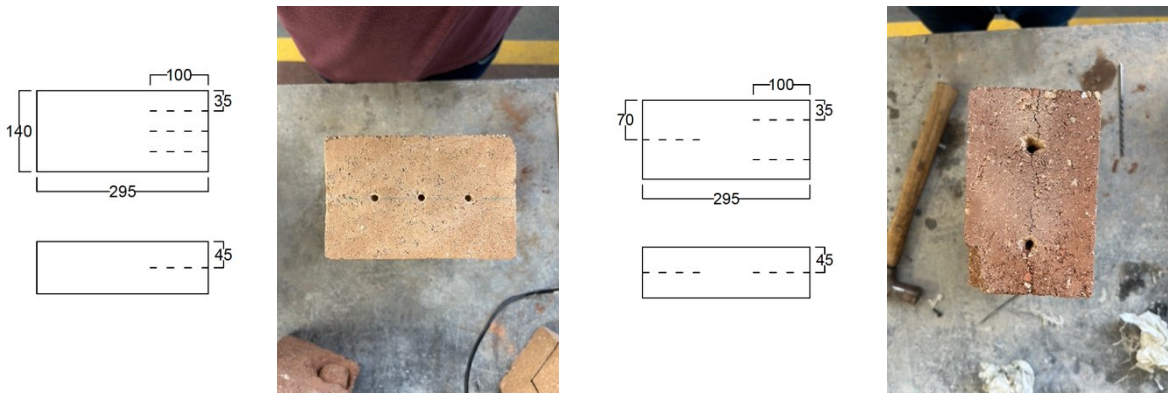

a) b) c) d)

Figure 25 - a) Drilling scheme for stabilised blocks; b) Stabilised block; c) Drilling scheme for unstabilised blocks; d) Unstabilised block.

A Fitoclima climatic chamber from ARALAB (Figure 26), which allowed the temperature to be controlled and fixed indoors, was used to impose a heat flow and, by measuring the heat flow with heat fluxmeters and temperatures with thermocouples, to determine the thermal transmission coefficient and thermal conductivity of small CEB walls. These small walls were inserted in nine windows of one of the external walls of the chamber, which was previously built with a double brick masonry wall with interior insulation between the two layers (Figure 26a).

The setup included 2 small walls of unstabilised CEB, 3 of CEB with OPC, and 3 of CEB with RCP, disposed according to Figure 26b. Additionally, a polyurethane (PUR) specimen was incorporated into the test as a reference (REF) material due to its well-known thermal properties, allowing for more effective control of the test and facilitating the comparison of results (Figure 26b). The UCEB, RCP8 and OPC8 walls were covered with the UM, RCP12 and UPC12 rendering mortars indicated in 3.4, respectively. The distribution of the different CEB across the various openings of the climatic chamber, as well as the airflow interference within the chamber, was based on a previous study using the same method by Real (2019) on concrete samples. The final layout is shown in Figure 26b.

The internal temperature of the chamber was set at 40 ºC (hot side) and the external side was exposed to the ambient temperature of the Civil Engineering Laboratory (cold side), where temperature was monitored and minor fluctuations disregarded. The thermal properties of the CEB-walls were measured resorting to thermocouples and heat flux meters connected to a datataker.

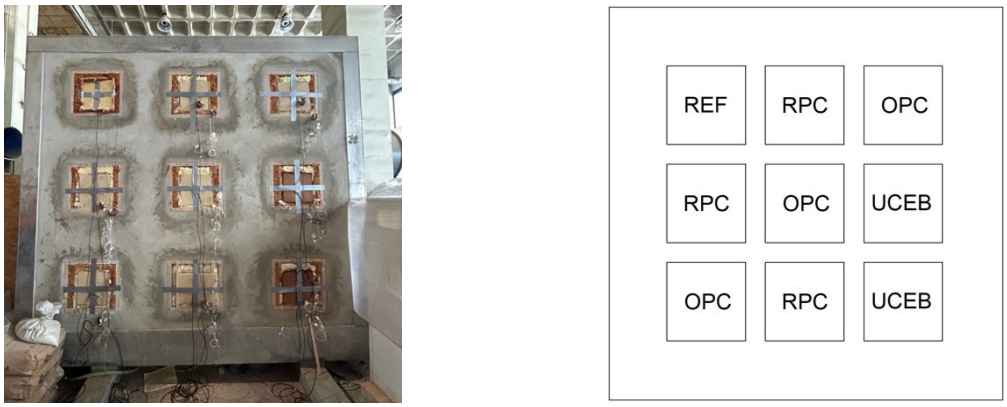

a) b)

Figure 26 - a) Fitoclima climatic chamber from ARALAB; b) Position of small CEB-walls in the chamber.

Three blocks were used in the execution of the small CEB-walls, which were arranged as in real applications, with the blocks laid on their largest face (Figure 27). These small walls were built as following (Figure 27): i) the earth based mortar, produced according to 3.4, was placed in the centre of the climatic chamber opening and one CEB was placed on the top of it and slightly pressed; ii) the CEB position was corrected with the aid of a spirit level; iii) on the top of it two additional layers were built following the same procedure (Figure 27a); iv) to fill gaps and eliminate the exceeding mortar from the joints, the CEB exposed surfaces were cleaned with a sponge; v) the thermocouples were installed in pre-drilled holes (Figure 27a); vi) lateral XPS insulation was applied (Figure 27b) and completed by spraying polyurethane foam to fill all the remaining spaces and prevent any heat loss (Figure 27c); vii) the block's surface was thoroughly wetted and rendered in two layers, using the same mortar applied for the joints. The first mortar layer was applied with 0.2 cm thick (roughcast, Figure 27c). After about 3 days, a second layer of 1.8 cm thickness was applied and roughly finished with a trowel (Figure 27d), for a total thickness of 2 cm. The render was wetted daily over the following 5 days to prevent cracking.

a) b) c) d)

Figure 27 - a) CEB placement; b) Insulation; c) Roughcast application (first layer); d) Rendering (second layer).

As mentioned, thermocouples Type T with 0.2 mm of thickness were installed to capture the temperature distribution across the wall section. Three thermocouples were embedded along the thickness of the central block, positioned at different depths to measure the internal temperature

gradient. Additionally, one thermocouple was placed on the external surface exposed to the climatic chamber, and another on the external surface facing the laboratory environment. One reference wall was also built with only polyurethane (PUR) and two thermocouples: one on the inner face exposed to the climatic chamber and one on the outer face exposed to laboratory conditions. This arrangement of thermocouples allows for capturing significant thermal gradients within the walls.

Before starting the tests, all heat flux sensors were calibrated, using a glazed window as a reference surface. Each sensor was placed on the interior side of the glass, with the exterior side exposed to outdoor environmental conditions, as shown in Figure 28. The assumption was that the thermal transmittance of the glass was known and stable, allowing the recorded heat flux to be compared to theoretical values. To minimise the effect of rapid and unpredictable solar radiation changes, only data collected during night-time hours were considered. This approach ensured better thermal stability and more reliable calibration results, by avoiding temperature spikes caused by direct sunlight exposure.

Figure 28 - Calibration of heat flux meters on a single-pane window.

3.5.4.2 Experimental characterisation

Monitoring and data collection were carried out using a Datataker 85 data acquisition system (Figure 29) and its channel extender. This device was connected to 58 previously prepared thermocouples and 9 Hufseflux heat flux sensors, centred and distributed across each opening (Figure 26a). It is important to emphasise the need to ensure that the heat flux sensors are in direct contact with the wall, preferably positioned on a flat and even surface.

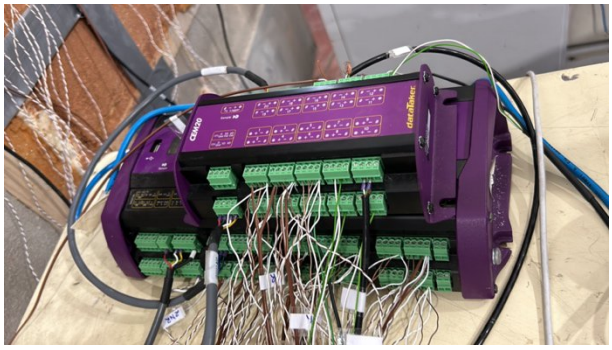

Figure 29 - Datataker 85 connected to thermocouples.

Data was acquired every minute, with average values recorded over ten-minute intervals. The test was conducted for 7 days, allowing the conditions within the chamber and the walls to reach a steady state, yielding more accurate and reliable results.

The thermal conductivity of the walls was determined from the values of heat fluxes and the surface and external temperatures of each block. As the external temperature of the chamber was affected by the ambient temperature of the laboratory, it was not possible to maintain strict control over the stationary regime conditions, which may affect the precision of the obtained results. Indeed, due to the daily variation in exterior temperatures, the values of heat fluxes and surface temperatures did not remain constant over time. Therefore, the Progressive Average method was adopted, as described in the EN ISO 9869:1994 standard, and used in previous studies by Silva (2015) and Real et al. (2016). This method involves calculating the heat flux (q) at each moment, using the average of the values measured at previous times, according to expression 3.2.

$$q_{i+1} = \frac{q_i + q_{i-1} + q_{i-2} + \ldots}{i} \tag{3.2}$$

The calculation of thermal conductivity (λ) was conducted using equation 3.3, where q represents the heat flux across the thickness of the slab, expressed in Watts per square meter (W/m²) e is the thickness of the slab, measured in meters (m); and T_{is} and T_{es} correspond to the interior and exterior surface temperatures of the block, respectively, expressed in degrees Celsius (°C). The value of λ was subsequently adjusted to the reference temperature of 10 ºC based on the average temperature recorded on each wall, following the procedure of the ISO 10456 (2007) standard.

$$\lambda = \frac{q \cdot e}{T_{is} - T_{es}} \quad [W/m^{\circ}C] \tag{3.3}$$

Additionally, each small wall underwent the transient method conducted in two stages, using the Isomet 2114 equipment. Both interior and exterior values of thermal conductivity, volumetric heat capacity, and thermal diffusivity were recorded (Figure 30).

Figure 30 - Transient Method plane probe applied to a wall.

4 Results and Discussion

In the present chapter, the results obtained during the experimental campaign described in Chapter 3, which was planned in accordance with the objectives defined in Chapter 1, are analysed and interpreted. As previously mentioned, the main objective is to assess the thermal performance of compressed earth blocks (CEB) stabilised with recycled cement (RC) and compare it with that of reference UCEB and CEB with PC. To this end, the thermal conductivity of different CEB, with various types (RCP, RCC, PC, PLC) and contents (0%, 4%, 8%) of stabiliser, the partial replacement of PC with RC (20% and 50%) and the partial substitution of earth with CDW (0%, 15%, 25%, 40%) was assessed using an expedite transient method. Table 10 summarises the compositions considered. In addition, the thermal performance of prototype small CEB-walls built in a climatic chamber was also assessed using an adapted stationary method. The small walls were built using UCEB, RCP8 and PC8, and the UM, RCP12 and PC12 mortars indicated in 3.4, respectively.

Table 10 – Characteristics of compositions considered on transient method.

Designation	Binder type	Binder (%)	Water (%)	CDW1 (%)	TV (%)	w/b_{ef}*
UCEB	-	-	9	25	18	0.0
UCEBCDW0	-	-	9	0	18	0.0
OPC4	OPC	4	9	25	14	2.3
OPC8	OPC	8	9	25	11	1.2
OPC8TH	OPC	8	12	25	11	1.6
OPC8CDW0	OPC	8	9	0	11	1.2
OPC8CDW15	OPC	8	9	15	11	1.2
OPC8CDW25	OPC	8	9	25	11	1.2
OPC8CDW40	OPC	8	9	40	11	1.2
OPC80RCP20	80%OPC+20%RCP	8	9	25	11	1.2
OPC50RCP50	50%OPC+50%RCP	8	10	25	11	1.35
OPC80RCC20	73%OPC+27%RCP	8.8	9	25	11	1.1
OPC50RCC50	40%OPC+60%RCP	10	9	25	11	1.0
PLC8	PLC	8	9	25	11	1.2
RCP8	RCP	8	12	25	11	1.62
RCP8CDW0	RCP	8	12	0	11	1.6
RCP4	RCP	4	10	25	14	2.6
RCC8	RCC	12	12	25	11	1.12

*- Effective water to binder ratio

4.1 Density and total porosity

Table 11 summarises the fresh density (ρ_f) and hardened density at 28 days (ρ_{28d}) of CEB. Based on the CEB composition, the densities of each material used in CEB production and the values of ρ_f, it is possible to estimate the volume of air voids after compaction, V_v (Table 11). The long-term total porosity (PT) can also be estimated using Equation 4.1, calculated as the sum of V_v and the volume of mixing water, minus the volume of hydration products formed from the stabiliser. In Equation 4.1, M_w and ρ_w correspond to the mass of mixing water and its density, respectively; M_b is the mass of binder; w_b is the chemically bound water after full hydration, considered to be 0.23 for PC and 0.22 for RC

(Bogas et al. 2022; Carriço et al. 2020); and α_H is the long-term hydration degree, assumed to be 0.8 for both binder types.

$$P_T = Vv + \frac{M_w - \alpha_H \times w_b \times (1 - 0.254) \times M_b}{\rho_w} \quad (4.1)$$

Table 11 – Fresh density (ρ_f), volume of voids after compaction (V_V), hardened density (ρ_{28d}) and long-term total porosity (Tp) for the studied compositions.

Designation	r_f (kg/m³)	V_V (%)	ρ_{28d} (kg/m³)	Tp (%)	$\rho_f - \rho_{28d}$ (kg/m³)
UCEB	2188	4.5	1991	26.2	197
UCEBCDW0	2195	6.4	2031	26.9	164
OPC4	2168	5.9	1994	26.2	174
OPC8	2155	6.9	2007	26.0	148
OPC8TH	2151	3.8	1965	28.1	186
OPC8CDW0	2169	8.2	2056	26.4	113
OPC8CDW15	2153	7.7	2006	26.4	147
OPC8CDW25	2159	6.7	2004	25.8	155
OPC8CDW40	2179	4.6	1993	24.6	186
OPC80RCP20	2137	7.6	1976	26.6	161
OPC50RCP50	2107	7.8	1926	28.2	181
OPC80RCC20	2122	8.3	1968	27.0	154
OPC50RCC50	2117	8.5	1958	27.0	159
PLC8	2157	6.8	2000	26.0	157
RCP8	2097	6.0	1912	29.8	185
RCP8CDW0	2115	7.1	1929	30.0	186
RCP4	2112	7.1	1925	28.7	187
RCC8	2114	5.4	1928	28.5	186

The fresh density values range between 2097 kg/m³ and 2195 kg/m³, within the range recommended by Rigassi (1985). In turn, the long-term total porosity ranged between 25.8% and 30.0%. It was found a linear inverse trend between T_P and ρ_f (Figure 31). However, the correlation was not high, because fresh density includes the total amount of water added to the mix, while T_P only reflects the portion of water that remained unbound after hydration. Therefore, variations in binder type, water/binder ratio, and hydration efficiency affects this correlation. Also, PC8TH had lower V_V when compared to PC8, despite the slightly lower fresh density and greater long-term total porosity. The lower density and higher T_P can be explained by the fact that OPC8TH was produced with greater w/b_{ef} that led to a higher amount of free water in the mix. The lower Vv is related with the CEB production. As documented in (Cruz and Bogas 2024), the PC8TH was produced with a greater water content to OMC ratio (1.32) than PC8 (0.99), which resulted in a better dispersion and compactness of the solid mixture. Indeed, the authors found a more refined porosity of PC8TH compared to PC8.

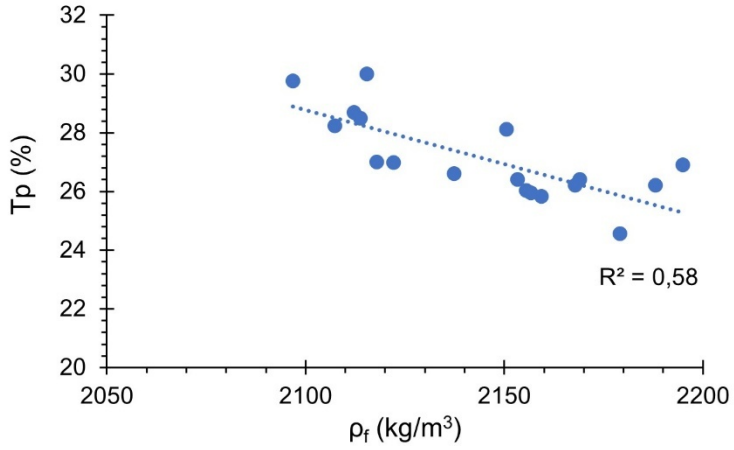

Figure 31 – Relationship between fresh density (ρ_f) and long-term total porosity (Tp).

Stabilisation with RC led to an overall reduction in fresh density and an increase in the long-term total porosity compared to PC CEB or unstabilised CEB. This is mainly due to the higher w/b_{ef} ratio used in RC CEB, resulting from their greater water demand. The compactness achieved during block production played a significant role in porosity. For instance, T_p was 6.0% higher in RCP8 (29.8%) than in OPC8TH (28.1%), despite using the same mixing water, due to the greater compactness of the latter.

The long-term total porosity of RCC8 (28.5%) was lower than that of RCP8, which can be attributed primarily to the lower water demand of RCC. Indeed, RCC was produced with approximately 67% purity, requiring the increase of binder content to ensure the same amount of cementitious material. The same is observed comparing OPC50RCC50 to OPC50RCP50.

Regarding dry density, the results followed the same trend as fresh density (Figure 32), but showing a slightly higher correlation coefficient. Nevertheless, as density is no longer affected by the evaporated water, it would be expected a higher correlation coefficient. This is because density and total porosity are differently affected by CDW, as discussed later. In fact, if only CEB with the same amount of CDW are considered, the coefficient of correlation increases to 0.9 (Figure 32).

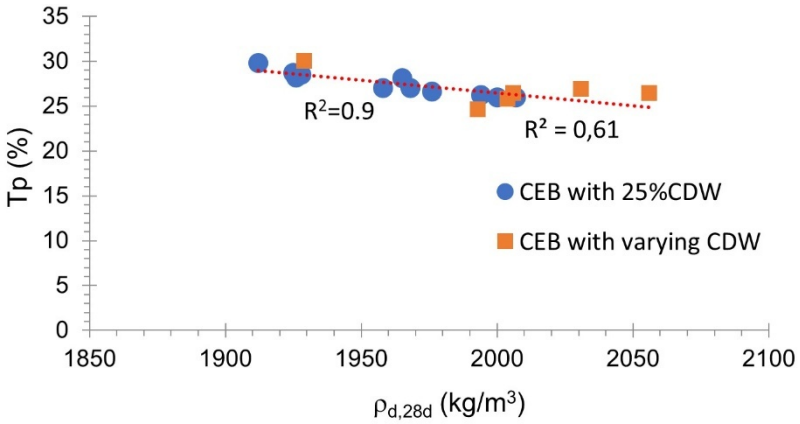

Figure 32 - Relationship between dry density (ρd, 28d) and long-term total porosity (Tp).

These differences in dry density observed among the compositions, highlighted in Figure 32, can be better understood by considering the hydration behaviour of the binders and the water retained during curing. Assuming complete drying, the dry density at 28 days ($\rho_{a,28}d$) depends primarily on the

hydration capacity of the binder. As shown, unstabilised CEB exhibited the most significant reduction in density between the fresh and 28-day states ($\rho f – \rho_{a,28}d$), indicating the highest amount of free water that was not retained after drying. In contrast, higher dry densities were recorded for Portland cement-stabilised CEB, particularly those with OPC, reflecting a more efficient hydration process and better retention of water within the microstructure.

In contrast, RC8, produced with greater w/b_{ef}, had higher variation from fresh to dry density ($\rho_f - \rho_{d,28d}$) than PC8. However, for the same w/b_{ef}, the reduction of density was similar in PC8TH and RCP8. This indicates that both PC and RC develop identical hydration capacity. The same was found in (Cruz and Bogas 2024), although considering 28 days density. It would be expected a greater mass loss in RC CEB, because, as mentioned, the water bound in RC (0.22) is slightly lower than that of PC (0.23) and also because RC is initially more carbonated than PC, reducing the amount of reactive material (Carriço et al. 2021, 2022). However, both phenomena have low significance. As expected, the partial replacement of PC with RC resulted in intermediate dried density and P_T values (Figure 33 and Table 11).

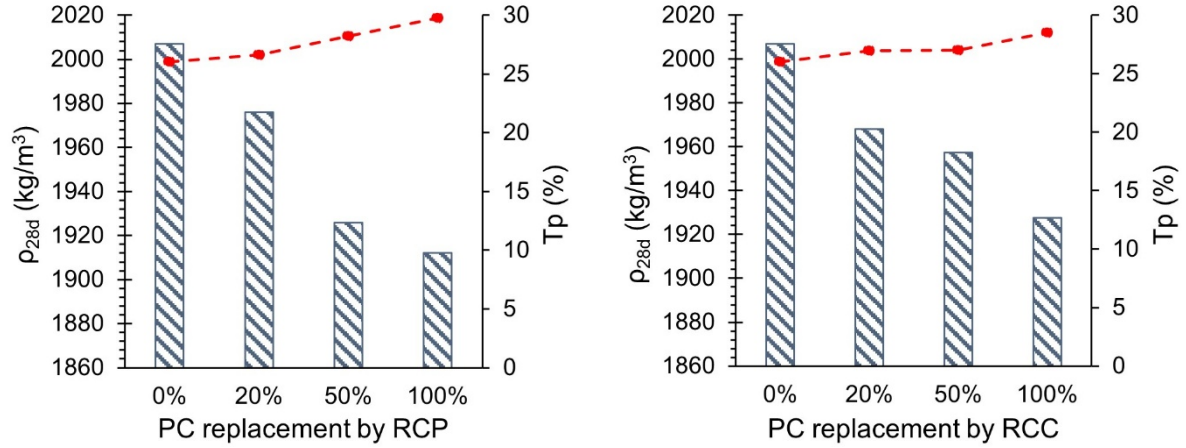

Figure 33 – Relationship between dry density at 28 days ($\rho_{d,28d}$) and long-term total porosity (Tp), for different percentage of RC binder.

As expected, the replacement of PC with PLC had little influence on the dry density and long-term total porosity of CEB. However, $\rho_f - \rho_{d,28d}$ of PLC8 was slightly higher than other PC mixtures, which may be attributed to the formation of lower amount of hydration products. In fact, as indicated in 3.2.3, PLC contains about 30% lime, resulting in 30% higher effective water/clinker ratio.

As detailed in subchapter 3.2, except in reference mixes with 25% CDW, the incorporation of different amounts of CDW involved the partial replacement of soil, maintaining the same particle size distribution. Thus, the main difference between these mixtures results from the substitution of earth with more porous aggregates of lower density. As a result, the dry density decreased with the percentage incorporation of CDW (Figure 34). However, the reduction of density for over 15% CDW was not significant. Moreover, the P_T decreased progressively with increasing CDW content, which goes against the trend of dry density. This is attributed to better granular compactness achieved in RCP with increased amount of CDW, especially above 15% content. Moreover, only the water-accessible voids in the CDW are considered in the estimation of P_T. Finally, OPC8 presented similar dry density (2007 and 2004 kg/m³) and T_P (26 and 25.8%) to OPC8CDW25 (Table 11). This suggests that directly

replacing earth with CDW, without preserving the same particle size distribution, had little impact on the compactness of the CEB. This is consistent with the similar granulometry of FA and CDW, as shown in subchapter 3.2.

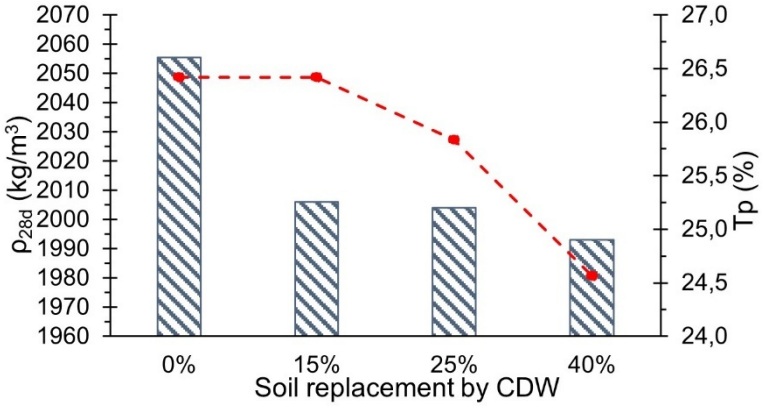

Figure 34 – Dry density ($\rho_{d,28d}$, bars) and long-term total porosity (Tp, dashed line) as a function of the percentage of CDW.

4.2 Compressive strength

Table 12 summarises the average unconfined 28-days compressive strength (fc,un), at different moisture conditions (saturated, dry, laboratory conditions). This property is inherently independent of block geometry. In fact, the compressive strength of CEB is significantly influenced by the aspect ratio of the block, defined as the ratio between height (H) and length (L) (Krosnowski, 2011; Morel et al., 2007; Neves, 2019). Therefore, according to the HB 195 (2002) standard, fc,un, can be determined by affecting the compressive strength values by a correction factor, which depends on the H/L ratio. Given that the blocks were tested with H/L=0.64, a correction factor of 0.58 was applied according to this normative. The compressive strength under saturated conditions and under dry conditions was evaluated only for reference CEB stabilised with 8% of PC, RC or the partial replacement of PC with RC. In UCEB, the fc,un was only determined in dried conditions, because they lost their cohesion within 2 minutes of water immersion.

Table 12 – Average unconfined compressive strength at 28 days for laboratory conditions ($f_{c,un,lab}$), saturated conditions ($f_{c,un,sat}$) and dried conditions ($f_{c,un,dry}$).

Designation	$f_{c,un,lab}$ (MPa)	$f_{c,un,sat}$ (MPa)	$f_{c,un,dry}$ (MPa)
UCEB	2.1	*	4.3
UCEBCDW0	1.8	*	*
OPC4	5.4	*	*
OPC8	7.9	3.7	10.9
OPC8TH	7.3	3.3	10.9
OPC8CDW0	7.9	*	*
OPC8CDW15	6.9	*	*
OPC8CDW25	8.2	*	*
OPC8CDW40	6.2	*	*
OPC80RCP20	7.2	3.6	10.8
OPC50RCP50	6.3	3.1	10.6
OPC80RCC20	7.2	3.5	8.3
OPC50RCC50	6.4	3.2	8.2
PLC8	6.4	*	*
RCP8	5.7	2.8	6.9
RCP8CDW0	4.9	*	*
RCP4	3.5	*	*
RCC8	5.5	2.7	6.7

*: not determined

The mechanical strength of CEB is affected by several factors, such as the composition, the water content, the compaction force applied and the curing conditions, which makes it challenging the direct comparison with results from literature where different stabilisation materials, curing times, and testing protocols were applied (Azevedo 2021; Kerali, 2001). For instance, in the present study, the CEB with 8% OPC under dry conditions presented a compressive strength ($f_{c,un,dry}$) of 10.9 MPa, whereas in previous studies it was found within 2.0 – 8.10 MPa for similar CEB formulation (Bogas et al., 2018; Bogas et al., 2023; Cabrera et al., 2021; Islam et al., 2020; Yogananth et al., 2019). This strength improvement is mainly due to the higher compaction pressure (5-6 MPa), and the mix-design optimisation carried out in the production of CEB in the present work. Therefore, all stabilised compositions largely complied the minimum of 2.0 MPa suggested by HB 195 (2002) for CEB tested in dry conditions, including UCEB. All the tested CEB also complied with the minimum value of 1 MPa in saturated conditions, ranging 2.7-3.8 MPa.

As expected, the compressive strength of CEB increased with the stabiliser content, as observed in previous studies (Azevedo, 2021; Gonçalves, 2023; Nabais, 2023). Indeed, the addition of both PC and RC, starting from 4%, significantly increased the compressive strengths of CEB, with RCP4 and OPC4 showing a compressive strength 1.7 and 2.6 times higher than UCEB, respectively.

Due to its higher water demand and w/bef, RC CEB presented lower compressive strength than PC CEB. In fact, fc,un,lab of RCP CEB was 38% and 57% lower than that of OPC CEB for the same binder content (8% and 4% binder, respectively). However, even comparing compositions of equal w/bef, PC8TH showed 27% higher compressive strength than RCP8. This is attributed to the lower

compactness and higher total porosity achieved in RCP8. Indeed, a strong correlation between compressive strength and T_P is observed when CEB with varying binder and CDW contents are considered separately (Figure 35). The same conclusions were obtained by Gonçalves (2023) and Nabais (2023). Noteworthy is the similar behaviour regardless the type of binder, which indicates that both RC and PC developed similar hydration and binding capacity. In these mixes, the difference in compressive strength is attributed solely to the compactness achieved in the blocks. Therefore, if CEB can be produced with similar porosities, the mechanical strength is not significantly affected by the replacement of PC with RC. The different behaviour of CEB with varying amounts of CDW is discussed later.

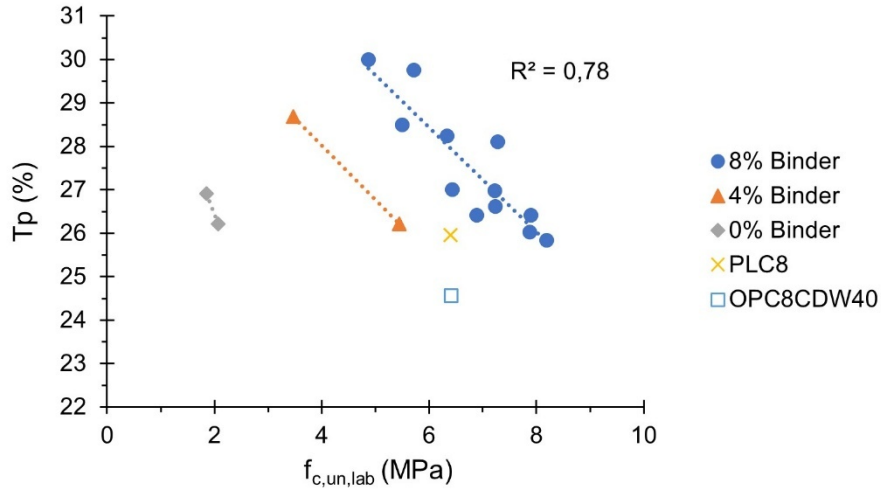

Figure 35 – Relationship between unconfined compressive strength ($f_{c,un,lab}$) and long-term total porosity (Tp) for different stabiliser contents.

As mentioned, the binding properties of unstabilised CEB were ensured only by clay, which explains the much lower $f_{c,un,lab}$ /T_P ratio compared to stabilised CEB (in grey in Figure 35). It is also observed that CEB with 8% PLC, which has a lower binding capacity than PC, led to a compressive strength closer to that of CEB with 4% PC. This is consistent with the 30% content of filler in PLC, which corresponds to an equivalent amount of cement of only 5.6% (subchapter 3.3.1).

As mentioned, the RCC content was adjusted to account for the aggregate contamination, maintaining the same w/b_{ef}. Nevertheless, the $f_{c,un}$ of RCC8 was slightly lower than that of RCP8, under all the moisture conditions, even taking into account that RCP8 was produced with higher T_P. This can be related to the fact that RCC8 was produced with an equivalent w/b_{ef} of 1.67, slightly above the 1.62 of RCP8. Moreover, the hydration reactions could have been slightly hindered by the aggregate contamination that reduced the contact surface area of cement particles. Nevertheless, the performance of RCP8 and RCC8 was similar. In addition, the partial replacement of PC with RC led to similar compressive strength, regardless of the RC type. This shows that the implemented separation method was effective in producing RC from old concrete waste, and the remaining fine aggregates in RCC did not significantly hinder cement reactivity or block compactness.

No clear trend in compressive strength was observed concerning the influence of CDW content (Figure 36). As mentioned in subchapter 3.2.2, CDW was composed mostly by porous aggregates, such as old cement-based materials and ceramics. According to Ren et al. (2024), concrete waste presents micro-cracks and weak aggregate-paste interface due to CDW processing. Therefore, the

addition of this recycled aggregate can hinder the mechanical strength of CEB, despite eventual improvements in compactness. Indeed, when comparing the compressive strength of CEB with 0% and 25% CDW, the improvement in compactness must have prevailed. Moreover, since CEB have significantly lower bearing strength compared to porous aggregates, the quality of the stabiliser matrix plays a dominant role in determining strength, while the influence of CDW becomes less significant. For both unstabilised CEB, RC CEB or PC CEB, the highest strength was obtained for CEB with 25% CDW, being 4-16% higher than that of CEB with 0% CDW. However, for 15% and 40% CDW, the $f_{c,un,lab}$ was reduced by 15% and 24%, respectively. In the first case, the total porosity was similar to that of CEB with 0% CDW. However, for 40% CDW the strength was reduced despite their compactness. On the one hand, the volume of CDW is sufficiently high to potentially affect compressive strength. On the other hand, CEB containing CDW tend to retain higher moisture content under laboratory conditions due to slower drying, which in turn leads to reduced strength. Finally, there was just a small difference in $f_{c,un,lab}$ between OPC8 and OPC8CDW25, the latter presenting a 4% increase. This corroborates the previous findings showing a little influence of the direct replacement of earth with CDW.

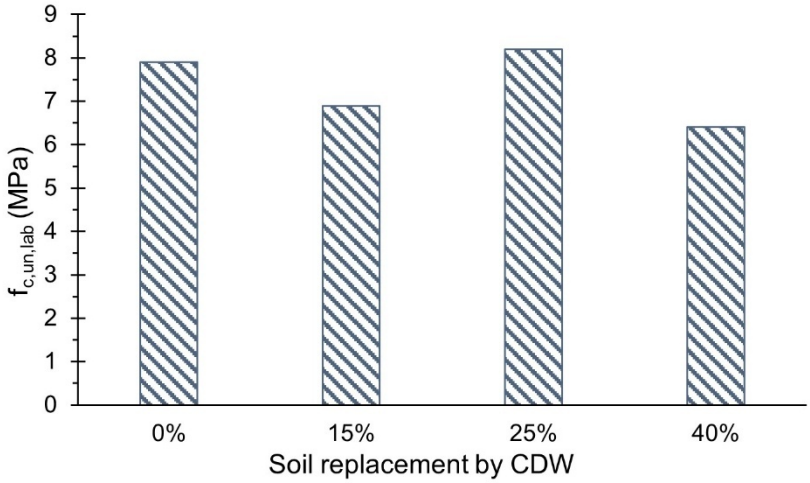

Figure 36 – Relationship between unconfined compressive strength ($f_{c,un,lab}$) and percentage of soil replacement by CDW.

4.3 Thermal characterisation - Transient Method

Table 13 to Table 15 presents the average results and standard deviations of the thermal characterization under different tested states, corresponding to the average value out of four points per block (two for each composition). The specific heat values (c) were calculated from the quotient between the volumetric heat capacity (cρ) and the dry bulk density of the specimen (ρ_{dry}). All tests were started at a minimum of 28 curing days, although the exact age of testing varied due to the large number of specimens tested.

Table 13 - Thermal properties of CEB in dry state, average values (AV) and standard deviations (SD).

Designation	$\lambda_{10^{\circ}C,dry}$ (W/(mK))		cρ (x10^6 J/(m^{3}K))		c (J/(kgK))		α (x10^{-6} m^2/s)	
	Av	SD	Av	SD	Av	SD	Av	SD
UCEB	0.78	0.059	1.34	0.008	668	1.5	0.59	0.042
UCEBCDW0	0.94	0.111	1.37	0.023	678	12.0	0.70	0.071
OPC4[a]	0.83	0.089	1.38	0.028	692	14.3	0.62	0.051
OPC8[a]	0.96	0.038	1.40	0.032	698	15.7	0.70	0.012
OPC8TH[a]	0.82	0.084	1.35	0.017	697	9.0	0.62	0.055
OPC8CDW0[a]	1.14	0.056	1.42	0.025	689	12.3	0.82	0.025
OPC8CDW15	1.00	0.053	1.43	0.042	712	21.1	0.72	0.022
OPC8CDW25	0.97	0.061	1.42	0.031	711	12.5	0.69	0.030
OPC8CDW40	0.79	0.087	1.37	0.029	687	15.6	0.59	0.053
OPC80RCP20[b]	0.96	0.033	1.40	0.015	710	4.8	0.71	0.031
OPC50RCP50[b]	0.83	0.06	1.38	0.024	704	12.2	0.62	0.031
OPC80RCC20[b]	0.81	0.098	1.36	0.028	691	15.4	0.61	0.061
OPC50RCC50[b]	0.81	0.016	1.37	0.007	699	5.5	0.61	0.013
PLC8	0.86	0.096	1.39	0.068	697	35.5	0.63	0.046
RCP8	0.79	0.069	1.38	0.044	723	23.4	0.59	0.037
RCP8CDW0	0.92	0.028	1.46	0.034	746	17.5	0.64	0.012
RCP4	0.67	0.078	1.34	0.023	698	12.0	0.51	0.050
RCC8	0.74	0.053	1.36	0.023	708	11.2	0.56	0.035

Legend: a - out of two measurements on one specimen; b - out of two measurements on two specimens (one each).

Table 14 - Thermal properties of CEB in equilibrium with lab environment, average values (AV) and standard deviations (SD).

Designation	$\lambda_{10^{\circ}C,lab}$ (W/(mK))		cρ (x10^6 J/(m^{3}K))		c (J/(kgK))		α (x10^{-6} m^2/s)	
	Av	SD	Av	SD	Av	SD	Av	SD
UCEB[b]	0.80	0.003	1.34	0.004	662	2.1	0.61	0.000
UCEBCDW0[c]	1.06	0.057	1.39	0.025	684	13.7	0.78	0.028
OPC4[a]	0.92	0.099	1.36	0.030	660	20.6	0.69	0.069
OPC8	1.03	0.141	1.38	0.038	669	16.2	0.76	0.085
OPC8TH[b]	1.03	0.038	-	-	-	-	0.72	0.002
OPC8CDW0[b]	1.32	0.078	1.42	0.027	666	12.5	0.95	0.038
OPC8CDW15	1.15	0.059	1.41	0.025	678	11.4	0.83	0.030
OPC8CDW25	1.13	0.064	1.41	0.027	677	8.0	0.82	0.032
OPC8CDW40	1.28	0.400	1.38	0.027	655	12.5	0.82	0.082
OPC80RCP20[c]	1.12	0.019	1.40	0.008	688	2.2	0.81	0.009
OPC50RCP50[b]	1.16	0.042	1.40	0.017	692	8.3	0.84	0.020
OPC80RCC20[c]	1.01	0.037	1.37	0.021	671	16.3	0.75	0.016
OPC50RCC50[c]	0.95	0.096	1.35	0.012	659	0.6	0.71	0.066
PLC8	0.98	0.045	1.36	0.015	657	9.2	0.74	0.025
RCP8[a]	0.83	0.195	1.35	0.046	667	26.0	0.62	0.126
RCP8CDW0	1.21	0.173	1.47	0.037	728	16.9	0.84	0.103
RCP4	0.84	0.135	1.35	0.031	672	15.7	0.63	0.087
RCC8	0.80	0.050	1.35	0.022	679	13.9	0.60	0.032

Legend: a - out of 3 measurements on two specimens; b - out of two measurements on one specimen; c - out of two measurements on two specimens (one per each).

Table 15 - Thermal properties of CEB saturated, average values (AV) and standard deviations (SD).

Designation	λ10˚C,sat (W/(mK))		cρ (x106 J/(m3K))		c (J/(kgK))		α (x10-6 m2/s)	
	Av	SD	Av	SD	Av	SD	Av	SD
OPC4	1.65	0.206	1.41	0.048	644	21.8	1.28	0.105
OPC8	1.93	0.057	1.50	0.070	681	33.8	1.31	0.046
OPC8TH	1.40	0.381	1.37	0.049	645	33.5	0.93	0.110
OPC8CDW0[a]	2.07	0.228	1.46	0.065	648	28.9	1.45	0.095
OPC8CDW15	1.90	0.124	1.47	0.048	661	21.7	1.32	0.044
OPC8CDW25	1.94	0.055	1.48	0.029	666	7.2	1.34	0.029
OPC8CDW40	1.68	0.200	1.42	0.038	641	17.5	1.20	0.113
OPC80RCP20[b]	1.78	0.033	1.44	0.003	665	0.7	1.25	0.020
OPC50RCP50[a]	1.70	0.110	1.42	0.039	655	18.1	1.22	0.045
OPC80RCC20[b]	1.65	0.036	1.40	1.396	638	9.3	1.21	0.064
OPC50RCC50[b]	1.70	0.020	1.40	0.002	642	3.1	1.24	0.013
PLC8	1.97	0.072	1.48	0.062	670	28.5	1.36	0.031
RCP8	1.41	0.472	1.42	0.057	663	27.7	1.00	0.297
RCP8CDW0	2.11	0.082	1.54	0.080	713	36.6	1.40	0.034
RCP4	1.41	0.322	1.37	0.041	635	19.7	1.04	0.209
RCC8	1.60	0.152	1.40	0.048	645	21.6	1.16	0.078

Legend: a - out of two measurements on one specimen; b - out of two measurements on two specimens (one each).

4.3.1 Thermal conductivity

To ensure the comparability of the data, it was necessary to convert the thermal conductivity values measured at various test temperatures to a reference value at 10°C. This conversion procedure follows the methodology established by the ISO 10456 (2007) standard, which is consistent with the reference values used in ITE 50 (2006), also based on a temperature of 10°C.

The ISO 10456 (2007) conversion method involves multiplying the thermal conductivity obtained from the test by three factors: age; moisture; temperature. The age factor was 1, reflecting the absence of significant variations in the age of the specimens throughout the testing period. The moisture factor was also set at 1, since the moisture content of the specimens remained constant during the tests. Finally, the temperature factor is calculated using expression 4.2, where F_T represents the temperature factor and T_m the average test temperature. An exponential function with a coefficient of 0.001 was adopted, which applies to materials such as fired clay. This final correction was performed using expression 4.3, adjusting the thermal conductivity values to reflect standard reference conditions. This allows for a concise and rigorous analysis of the data obtained.

$$F_T = e^{0{,}001(10-T_m)} \tag{4.2}$$

$$\lambda_2 = \lambda_1 F_T F_m F_a \tag{4.3}$$

Thermal conductivity varied widely, reflecting the broad range of CEB tested in this study, which differed in bulk density and compressive strength. (Table 13 to Table 15, Figure 37). The thermal conductivity in the dry state ranged from 0.67 W/(m·K) in RPC4 to 1.14 W/(m·K) in OPC8CDW0. Under

equilibrium with laboratory conditions, thermal conductivity varied between 0.80 W/(m·K), in UCEB and RCC8, to 1.32 W/(m·K) in OPC8CDW0. As discussed later, OPC8CDW0 standing out for having the highest thermal conductivity values observed in two of the studied states. As expected, the thermal conductivity increased in saturated conditions, ranging between 1.60 W/(m·K) in RCC8 and 2.11 W/(m·K) in RCP8CDW0.

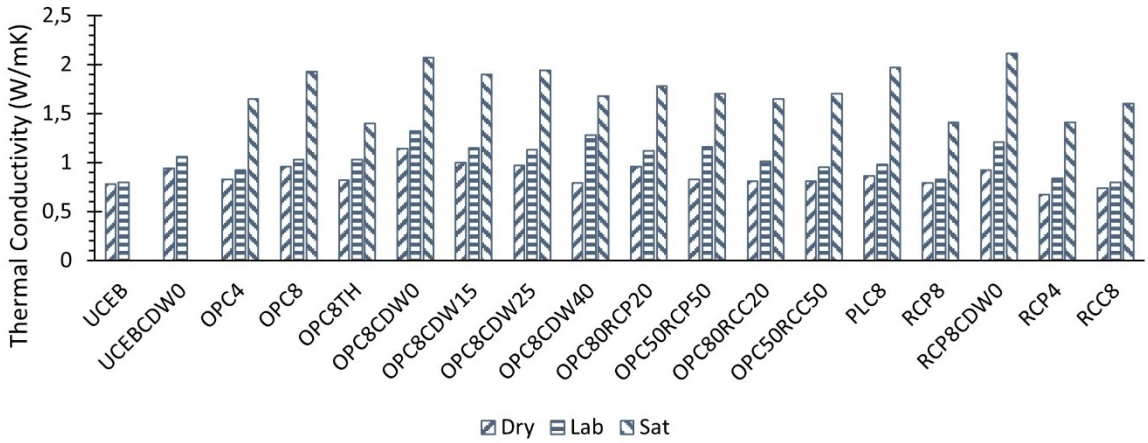

Figure 37 - Thermal conductivity (λ) for the analysed CEB compositions under different conditions.

The progressive increase of thermal conductivity with moisture content confirms the significant impact of water on the thermal properties of the materials (FIP, 1983; M. Hall and Allinson, 2009; Liuzzi et al., 2013). Considering that the thermal conductivity of water is approximately 25 times higher than that of air, the moisture content of the blocks becomes a crucial variable in this property, significantly enhancing their heat conduction capability (Real et al., 2016). On average, the thermal conductivity in the saturate state was about twice that in the dry state. This is within the range reported by other authors (Liuzzi et al., 2013; Real et al., 2024).

The thermal conductivity increase factor (Ks) was calculated, corresponding to the increase of thermal conductivity per 1% of moisture content. As shown in Figure 38, the Ks decreases with the increasing P_T, showing a strong correlation when CEB with different CDW contents are excluded. This trend can be explained by the fact that denser CEB correspond to a higher volume of water for a given weight-based water content. Small differences of Ks for a given PT are also affected by the porosity morphology (Real et al. 2024). As discussed in Real et al. (2024), CEB with varying amounts of CDW do not follow the same trend, because moisture within CDW has a different effect than within the surrounding earth.

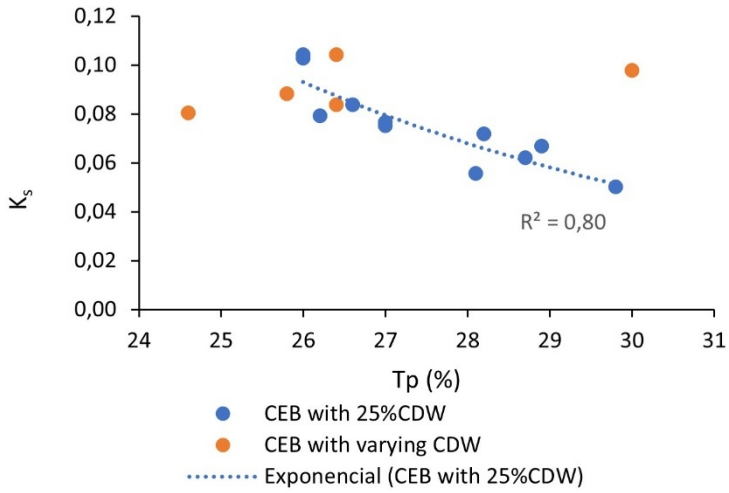

Figure 38 - Thermal conductivity increase factor (Ks) as a function of total porosity (Tp).

On average, the thermal conductivity increased 20% from dry state to the equilibrium with the laboratory environment. In fact, during a short drying period, the sample's relative humidity rapidly falls below 95%, releasing capillary free water, which significantly influences thermal conductivity. In Figure 37, the thermal conductivity results of each composition in the different tested states are presented, allowing a clear visualisation of the observed variations. The results of thermal conductivity obtained in this study align with those reported by other researchers (Figure 39), which follow an exponential relation with dry density (Adam and Jones, 1995; Bogas et al., 2019; Gomes et al., 2023; Real et al., 2016). In fact, thermal conductivity is primarily influenced by total porosity (Adam and Jones, 1995; Mansour et al., 2016), with composition playing a secondary role. However, within the limited range analysed in this study, the correlation between these properties was poor (Figure 38). In fact, despite only a small variation in dry density, thermal conductivity varied by as much as 30%. This indicates that the thermal conductivity of CEB is also influenced by other factors, such as composition, the mineralogical characteristics of the constituent materials, and the distribution of porosity (Gomes et al., 2023; Real et al., 2024). This is further discussed in 4.3.1.2.

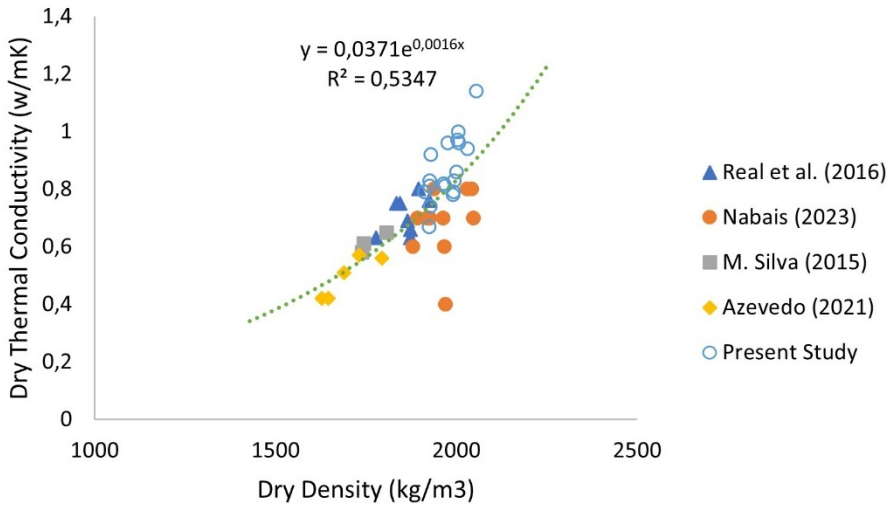

Figure 39 - Thermal conductivity (λ) of the dry CEB as a function of their dry density in this study and reported by other authors.

The thermal conductivity values obtained in this study were more than 30% higher than those reported in previous studies on CEB characterisation (Real et al., (2016), Nabais (2023), Azevedo (2021), M. Silva (2015)). This is essentially attributed to the greater compactness of the CEB produced in this study, achieved through the use of higher compaction pressures and an optimised mix design. Note that all indicated data in Figure 40 refer to measurements performed on the blocks in their dry state, ensuring a more reliable basis for comparison.

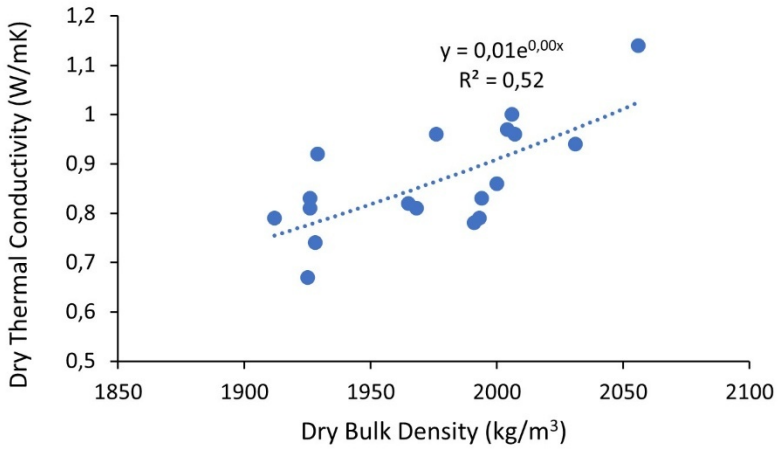

Figure 40 - Thermal conductivity (λ) for the analysed CEB as a function of their dry density.

4.3.1.1 Influence of the type and content of stabiliser

Figure 41 depicts the dry thermal conductivity of CEB, highlighting the influence of the type and amount of binder used, as well as total porosity. The unstabilised blocks, UCEB and UCEBCDW0, exhibited thermal conductivity values of 0.78 W/(m·K) and 0.94 W/(m·K), respectively, falling within the range of stabilised blocks (0.64-1.14 W/(m·K)).

As reported in other works, the thermal conductivity decreased with the replacement of PC with RC. On average, 19% reduction is observed when comparing OPC4, OPC8 and OPC8CDW0 with RCP4, RCP8, and RCP8CDW0, respectively. This decrease is explaining by both the lower dry density and higher total porosity of RC CEB.

The replacement of RCP with RCC led to small differences in thermal conductivity. However, despite its higher density, this property decreased 6% in RCC8 compared to RCP8. The same was observed in CEB with 20 to 50% OPC replaced with RCP or RCC.

The thermal conductivity increased with binder content, regardless of the stabiliser type. In PC CEB, the dry thermal conductivity increased from 0.78 W/(m·K) in UCEB to 0.83 W/(m·K) and 0.96 W/(m·K) in OPC4 and OPC8, respectively. Moreover, replacing 8% of PC with PLC, led to a slight reduction in thermal conductivity from 0.96 W/(m·K) to 0.86 W/(m·K), consistent with the reduction on dry density. In RC CEB, this property also increased from 0.67 W/(m·K) in RCP4 to 0.79 W/(m·K) in RCP8, respectively. However, density increased in the opposite direction, suggesting that other factors also play a significant role in thermal conductivity. In fact, Figure 41 to Figure 43 show that thermal conductivity does not correlate well with binder content or total porosity when all compositions are analysed together.

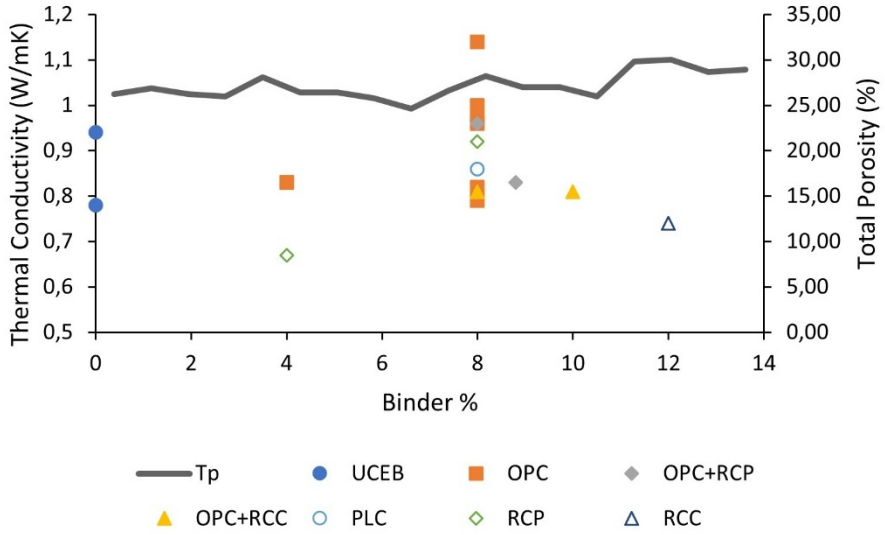

Figure 41 - Thermal conductivity (λ) of the dry CEB as a function of stabiliser percentage and total porosity (Tp).

However, the correlation coefficient between thermal conductivity and Tp increases when only mixtures with the same amount of CDW and identical content of stabiliser are considered (Figure 42). In this case, the thermal conductivity slightly increased with the incorporation of stabiliser.

Real et al. (2024) related the thermal conductivity to the microstructure of CEB produced with two types of earth and different types of stabilisers. For similar total porosity, the authors found that CEB with more refined porosity had slightly lower thermal conductivity. The authors concluded that porosity distribution may affect the contact between solids and respective heat flow path, altering the thermal insulation properties of CEB.

In a previous work, Cruz and Bogas (2024) characterised the microstructure of some of the CEB compositions tested in this study, namely the UCEB, PC8, PC8TH and RCP8. UCEB was characterised by a coarser macrostructure, while PC8TH and RCP8 presented finer mesoporosity. However, the stabilisation reduced the volume of very fine pores under 50 nm, regardless of the type of stabiliser. RC CEB developed a dual microstructure, where a coarser inter-porosity was filled with a more refined cementitious matrix than PC CEB. It was also concluded that a denser and less connected mesoporosity was formed in RC CEB than in PC CEB of equal w/c. As mentioned, in this study the thermal conductivity decreased in mixtures with coarser macroporosity, with less stabiliser content. PLC8 is in the same trendline of UCEB and CEB with 4% stabiliser, because the equivalent cement content is 5.6% (4.2).

Nevertheless, this study suggests that thermal conductivity is not significantly affected by the type of binder, provided the CEB is produced with similar total porosity.

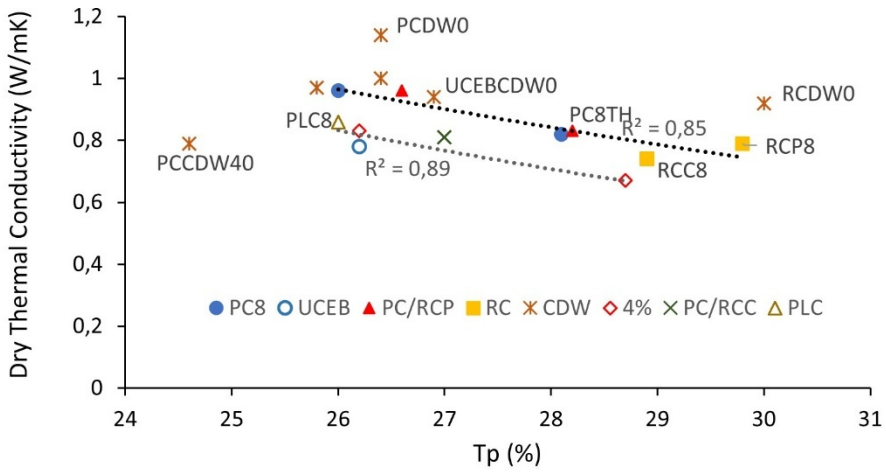

Figure 42 - Thermal conductivity in the dry state (λ) for the analysed CEB as a function of their total porosity.

When the thermal conductivity under laboratory conditions is analysed the trends of Figure 42 are significantly altered (Figure 43). On the one hand, total porosity does not fully reflect the water content in CEB, which, as discussed, has a significant impact on thermal conductivity. On the other hand, mixtures with a more open pore structure tend to dry more quickly, leading to lower relative thermal conductivity. The influence of CDW is discussed in 4.3.1.2.

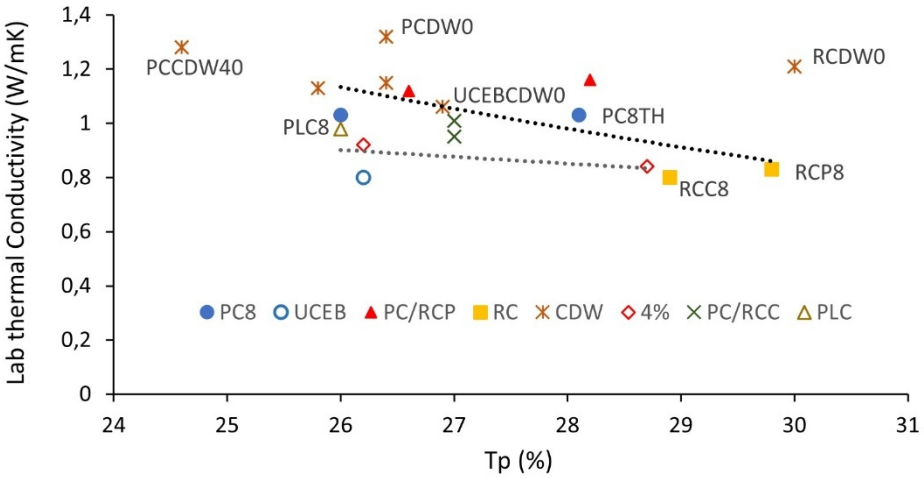

Figure 43 - Thermal conductivity (λ) in laboratory environment for the analysed CEB as a function of their total porosity

4.3.1.2 Influence of CDW

The thermal conductivity of CEB is influenced by the thermal properties of their constituent components, including the binder, the soil, and the CDW. Since CDW represents a significant percentage of the blocks' volume, changes in its intrinsic thermal conductivity, particle size distribution, or porosity can directly influence the heat transfer within the material. Specifically, more porous or less thermally conductive CDW particles can increase thermal resistance, thereby reducing the overall thermal conductivity of the CEB. On the other hand, replacing earth with CDW can enhance CEB compactness, as observed in the present study.

According to Real et al (2025) when dense earth particles are replaced with porous CDW, which has lower thermal conductivity than the surrounding earth matrix, heat flow tends to bypass the CDW particles. As a result, despite the higher density of the earth matrix, thermal insulation improves with increasing CDW content. The CDW disrupts the heat flow paths, making its presence more significant than simply causing a potential reduction in overall porosity.

Therefore, a progressive reduction in thermal conductivity was observed with increasing levels of soil replacement by CDW in OPC CEB (Figure 44a). This decrease was moderate, because, as mentioned, the changes in density among the mixtures were not significant. Similar outcomes Figure 44b) were found for the UCEB and RCP CEB, where adding up to 25% CDW decreased thermal conductivity by 17% and 14.1%, respectively. The direct replacement of soil by CDW, maintaining the same granulometric distribution, had little impact on porosity and thermal properties.

Figure 44a and Figure 44b show that CEB with CDW are differently affected by moisture content than other CEB. On the one hand, CEB with high amounts of CDW take longer to dry, which increases their thermal conductivity. On the other hand, in CEB with CDW, the heat flow travels through the porous earth matrix, which is more sensitive to moisture content (Real et al. 2024).

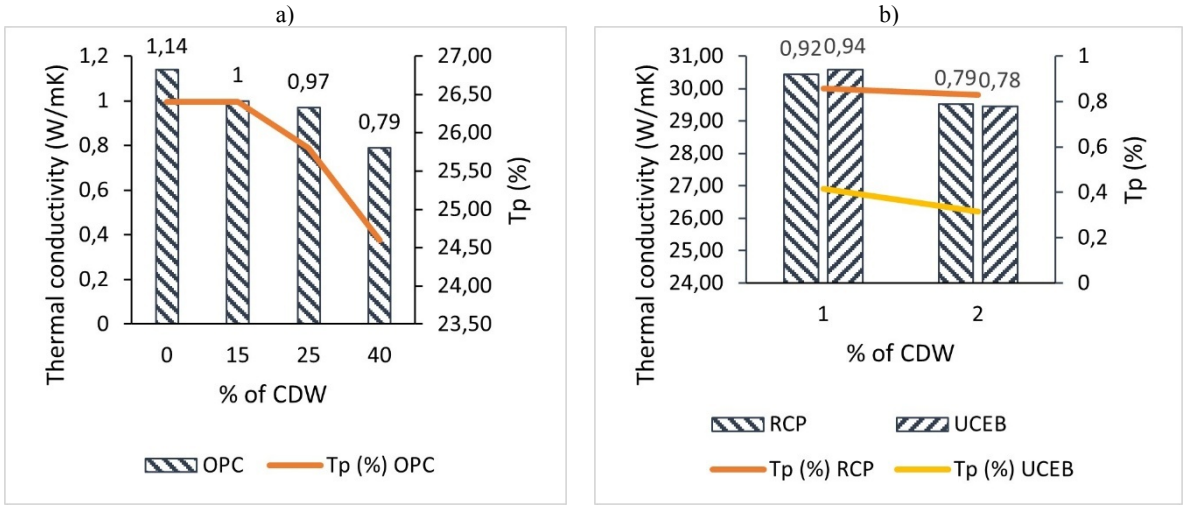

Figure 44 - Thermal conductivity (λ) of the dry CEB as a function of CDW percentage and total porosity (Tp).

4.3.2 Other thermal properties

The specific heat capacity in the dry state, cdry, ranged 668 - 746 J/(kg·K), as indicated in Table 13. UCEB had an average specific heat capacity of 673 J/(kg·K). The value of 698 J/(kg·K) was found for OPC stabilised blocks, while for the RCP CEB a higher value, equal to 722 J/(kg·K), was observed. CEB that combined two stabilisers, OPC and RCP or OPC and RCC, showed a specific heat capacity of 707 J/(kg·K) and 695 J/(kg·K), respectively.

Compared to PC8 CEB, the stabilisation with the same content of RCP and RCC slightly increased the specific heat capacity by 4% and 1%, respectively, essentially due to the increase in porosity. Indeed, as expected, the cdry tended to increase with the total porosity (Figure 45). The same trend is reported in literature (Gomes et al. 2023). Since denser CEB exhibit greater thermal conductivity, they require less energy to raise their temperature. However, despite this general trend, some deviations were observed, particularly in CEB with varying CDW content and in UCEB, as occurred in thermal conductivity.

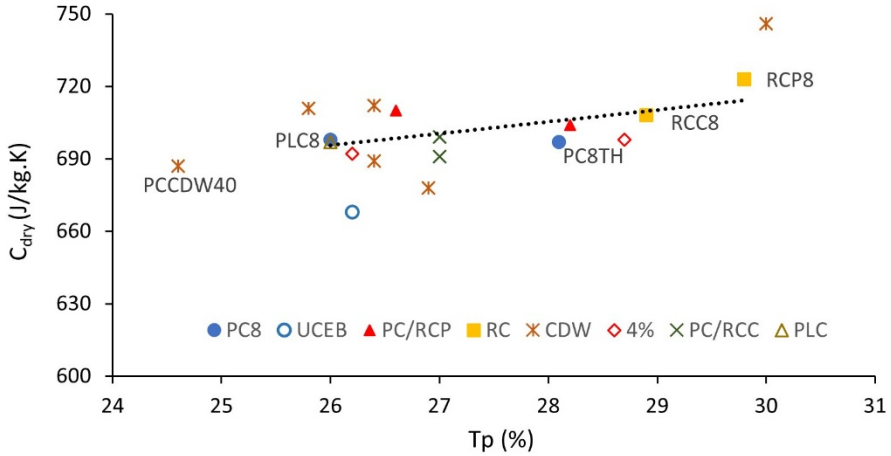

Figure 45 - Specific heat capacity of the dry CEB, c_{dry}, as a function of total porosity, Tp.

Thermal diffusivity is a property that, along with thermal conductivity (λ) and volumetric heat capacity (cρ), provides a better understanding of the thermal performance of materials and, by extension, of buildings. The thermal diffusivity, α, can be determined using expression 2.1, which depends on both the thermal conductivity (λ) and the volumetric heat capacity, cρ. This property describes how heat propagates through a material, offering a measure of the speed at which heat transfer occurs internally. This highlights the interdependence between the fundamental thermal properties, demonstrating how the composition and physical characteristics of the material affect its thermal response capacity.

The values of α are indicated in Table 13 and its relation with dry density is presented in Figure 47. As ldry increases with dry density and the volumetric heat capacity is little affected by this property, the thermal diffusivity (α) also increases with dry density. However, the coefficient of correlation was low (R^2 = 0.58), which suggests that density alone does not fully explain the thermal behaviour. This implies that other factors, such as the internal microstructure, may also play a role. This was already discussed in 4.2.1.1. As per thermal conductivity, α slightly decreased with increasing stabiliser content at a given density (Figure 46).

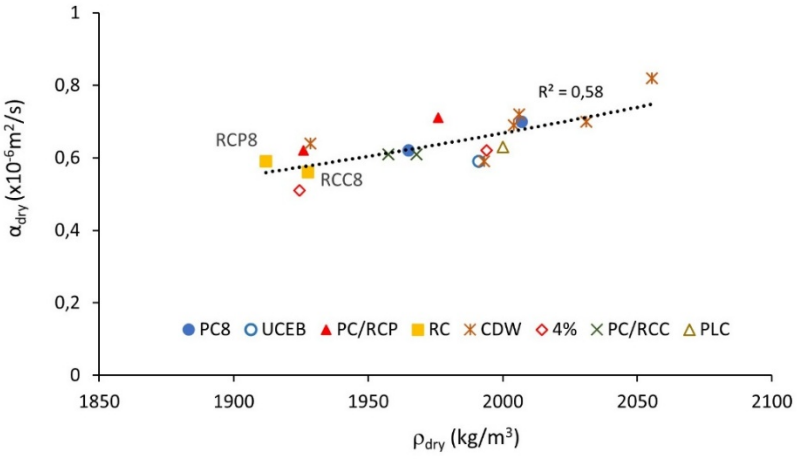

Figure 46 - Thermal diffusivity of the dry CEB as a function of dry density.

Thermal inertia (T_I) provides an indication of a material's ability to store energy and resist a given temperature variation. Materials with high thermal inertia are well-suited for locations with significant daily temperature fluctuations, as they help stabilise indoor temperatures by absorbing, storing, and gradually releasing heat, thereby enhancing thermal Comfort. This property can be determined according to Equation 4.4 and is directly proportional to the square root of thermal diffusivity, α. Materials with high thermal inertia are also characterised by their resistance to the establishment of steady-state thermal conditions. The average thermal inertia values of the CEB analysed under drying conditions in this study are summarised in Figure 47 andFigure 48.

$$T_I = \sqrt{..c} = .c\sqrt{\alpha} \ [J.m^{-2}.K^{-1}.s^{-\frac{1}{2}}] \quad (4.4)$$

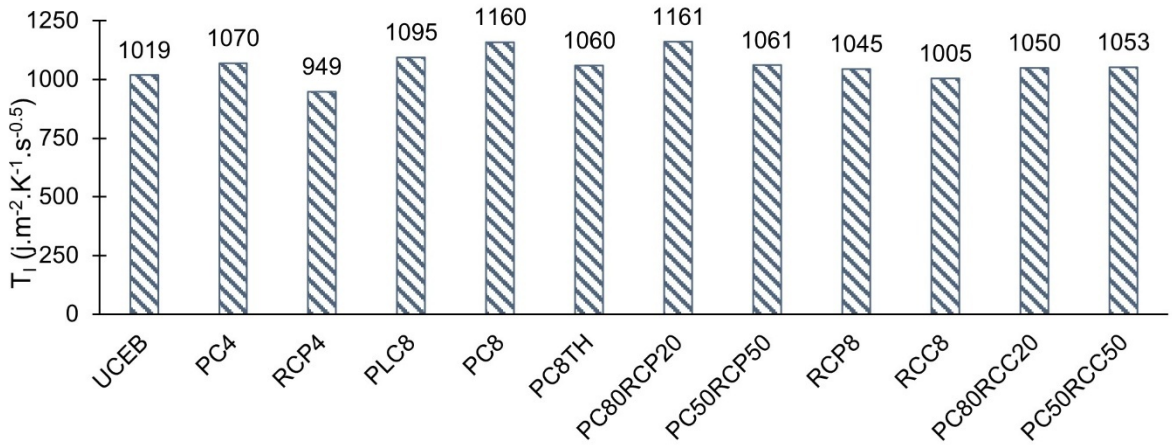

Figure 47 - Thermal inertia of dry CEB with 25% CDW.

The highest thermal inertia was found in OPC8 CEB, which also had the lowest total porosity. As expected, the thermal inertia decreased in CEB with RC of lower density and lower thermal diffusivity. The reduction in RCP8 was 10% compared to OPC8, but only 1.4% compared to OPC8TH. However, thermal inertia was not only affected by density. As observed with other properties, like thermal conductivity and diffusivity, thermal inertia increased with binder content when comparing samples of similar density. For example, with only a slight difference in density, the thermal inertia of PC8 was 14% higher than that of UCEB. In this context, stabilising CEB enhances their energy storage capacity, improving resistance to rapid temperature swings. The thermal inertia reduced with the incorporation of CDW, following a logic trend with density (Figure 49). The partial replacement of earth with 15 to 40% CDW led to 6 to 18% reduction in T_I, respectively.

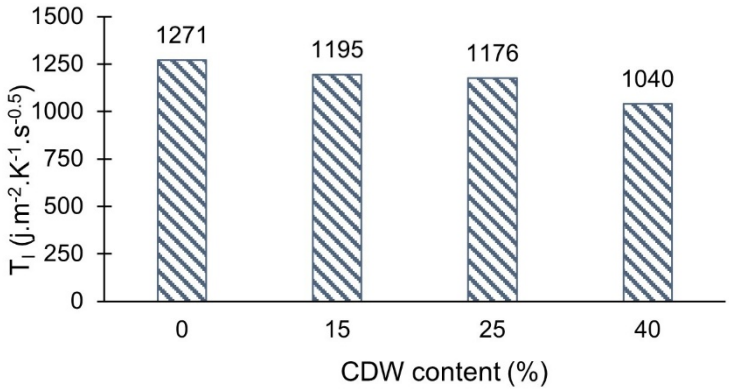

Figure 48 - Thermal inertia of dry PC CEB with 0-40% CDW.

In sum, compared to PC CEB, RC CEB is expected to offer greater thermal insulation capacity under both steady-state and transient conditions, due to their lower I and α. This is primarily attributed to their higher total porosity. For the same reason, thermal inertia tends to be lower. However, under identical porosity conditions, the thermal behaviour was not significantly affected by the type of stabiliser.

4.4 Thermal characterisation - Adapted Steady-State Method (climate chamber)

4.4.1 Temperature profiles

The results from the walls prototypes experiment are presented in Figure 49 and Figure 50. These figures illustrate the temperatures on the exterior and interior surfaces of the walls over time, as well as the heat fluxes through them. To make the visualisation easier, only the initial and final segments of the curves are shown in the main figures, while the complete curves are available in Appendix 1. Detailed information about the temperatures inside the walls is also provided in Appendix 1.

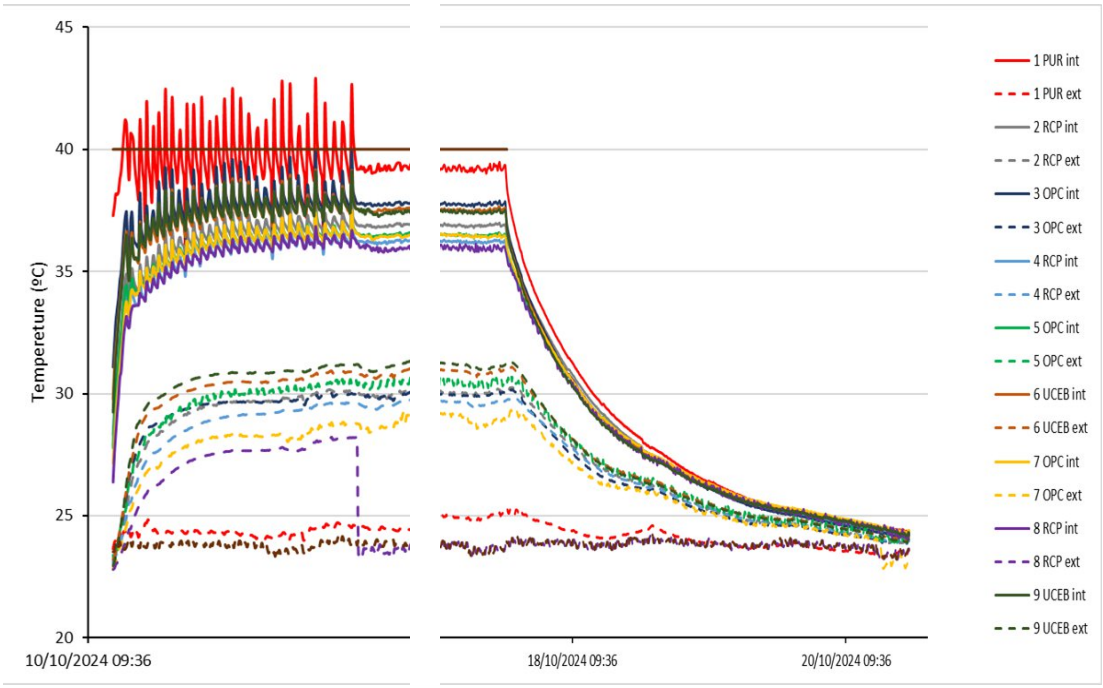

Figure 49 - Internal (continuous line) and external (dashed line) surface temperatures of the different CEB prototypes walls.

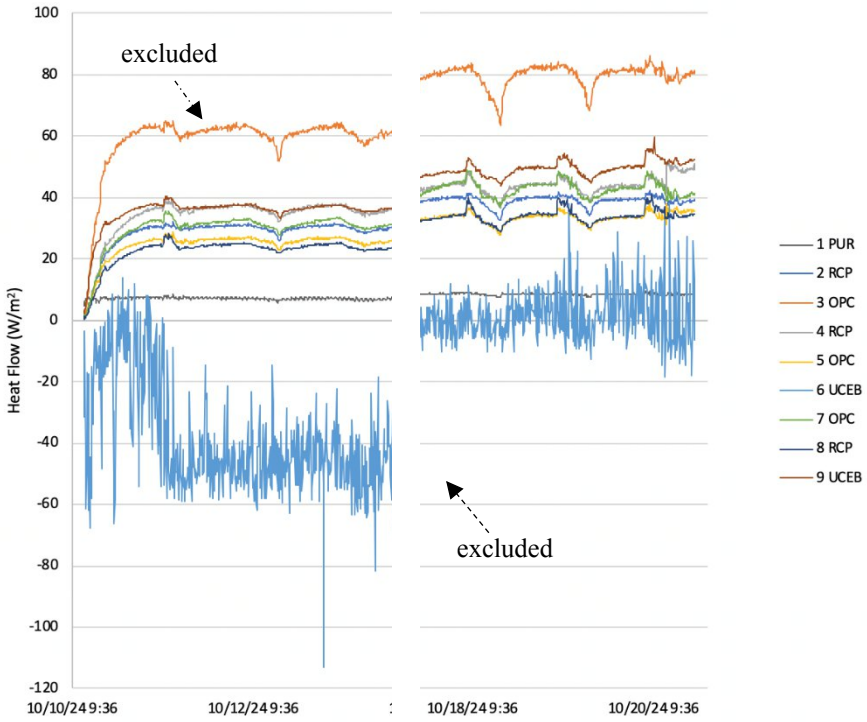

Figure 50 - Heat flow of different CEB walls prototypes.

In Figure 49, which presents temperature data, and in Figure 50, which details heat fluxes, some noise is observed in the initial values until they stabilise. It is important to highlight that in the mini-wall 8-RCP (position 8), there was a significant drop in the values of external surface temperature (dashed) due to the detachment of the thermocouple from the surface, which resulted in the monitoring of the air temperature from the laboratory instead of the surface values. Also note that data from positions 6 (UCEB) and 3 (OPC) were excluded due to significant discrepancies, likely caused by malfunctions in the data acquisition system. This was attributed to unstable sensor-to-surface contact and possible malfunction of the sensors itself.

Regular cycles associated with daily temperature oscillations in the laboratory environment are identified in Figure 49. Indeed, only the indoor temperature of the climate chamber was kept constant at 40 °C throughout the experimental period.

According to the thermal properties of the different mixes presented in Table 13, UCEB, RCP8 and OPC8TH have similar thermal performance, showing identical dry thermal conductivities. This may explain the overlap observed in the heat flow curves (Figure 51), where no clear distinction is evident between the performance of all tested specimens. Note that heat flow was influenced not only by the thermal properties of the blocks but also by the rendering mortars. As discussed later, the thermal conductivity of the unstabilised mortar was higher than that of the mortars used in RCP8 and OPC8TH systems. Moreover, the thermal behaviour of walls is affected by the joint mortars used between blocks, which apparently present higher thermal conductivity in UCEB. On the other hand, RCP CEB, which had lower bulk density and thermal conductivity on average, exhibited the lowest heat flow. Nevertheless, heat flows were very similar in RCP8 and OPC8TH, both produced with equal water content.

The rates of increase and decrease in heat flux (slope of the curves in the initial and final sections of the temperature profiles), as well as the rates of change in exterior surface temperature, appear quite similar among the different CEB compositions. This is supported by the similar thermal diffusivity values measured for the tested CEB, which ranged from 0.59 to 0.62×10^{-6} m²/s, as shown in Table 14. These small variations indicate a comparable rate of transient heat transfer across the different CEB. However, RCP8 with slightly lower thermal diffusivity than OPC8TH, exhibited slightly slower rates of change in both heat flux and surface temperature.

Regarding the time required for the small walls to reach equilibrium conditions, it was also found to be similar among the various mixes, including the unstabilised CEB. This can be attributed to the fact that the volumetric heat capacity of the tested CEB were nearly identical, indicating that they require approximately the same amount of time to reach thermal equilibrium.

According to the steady-state heat flux equation (Equation 2.4), it would be expected that, upon reaching thermal equilibrium, CEB with higher thermal conductivity would exhibit higher temperatures on their exterior surface and lower interior surface temperatures. However, this expectation was not confirmed. On the one hand, the thermal properties of all tested solutions were relatively similar. On the other hand, the interior surface temperatures were also influenced by airflow from the climate chamber's air conditioning system, which complicates the interpretation. In fact, although the steady-state heat flux equation assumes that the interior surface thermal resistance, R_{is}, is constant, variations in R_{is} can occur due to the airflow. Thus, R_{is} calculations were performed for each position (equation 4.5), with T_i the air temperature inside the chamber (ºC); T_{is} the interior surface temperature of the CEB (ºC); and q the heat flow per surface area (W/m^2). Values of interior surface thermal resistance ranged 0.06 - 0.12, being lower in positions 4 and 7, and higher in positions 3, 6, and 9. The same was reported by Real et al. (2016), considering similar tests, but involving normal weight and lightweight concretes. With the aid of a TAS hot-wire anemometer, these authors confirmed higher air velocities at positions 3, 6, and 9. Note that the current normative REH (2013), establishes the standard value of R_{is} at 0.13 (m²·ºC)/W.

$$R_{is} = \frac{T_i - T_{is}}{q} \tag{4.5}$$

As discussed in Chapter 3.5.4, the exterior temperature during the test corresponds to the air temperature of the Construction Laboratory, which operated under free-running conditions with natural ventilation. Consequently, even under thermal equilibrium, daily cyclic fluctuations in the exterior surface temperatures of the walls were observed. Compared to the exterior ambient temperature curve (Figure 49), the temperature evolution on the exterior surface of the reference polyurethane (PUR) small-wall closely followed the same pattern. However, the CEB small-walls exhibited more attenuated temperature peaks, particularly in systems with higher density (OPC8TH and UCEB). This was expected, as polyurethane, due to its low thermal inertia, is more responsive to temperature fluctuations. In contrast, CEB with higher bulk density and greater thermal inertia react more slowly to such changes, resulting in smaller thermal amplitude between daytime and night-time periods, as illustrated by the temperature variations in Figure 49 (see full cycle representation in Appendix 1). As shown in Figure 47 (Section 4.2.2), OPC8TH exhibited the highest thermal inertia, followed by RCP8 and UCEB. However, in these tests, UCEB demonstrated a performance similar to that of OPC8TH. Once again, the

differences between the mixtures were not substantial, likely due to the additional influence of the rendering mortars.

The temperatures inside blocks and mortars were also monitored for all the prototype walls tested. The temperature profiles across the thickness of each wall studied are presented in Figure 51 to Figure 53. In the case of 9-UCEB, the readings from two thermocouples were unavailable and are therefore missing from the temperature profile. The graphical representation of the temperatures is oriented from the interior to the exterior of the mini-walls, providing a clear view of the thermal behaviour of these materials. In Figure 54, the average temperature values are displayed according to the position of the different compositions.

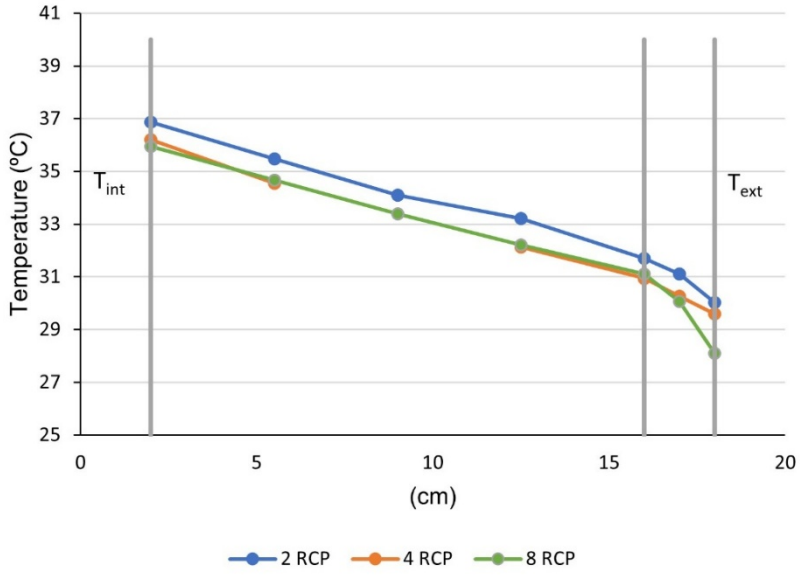

Figure 51 - Wall temperatures stabilised with RCP from inside to outside.

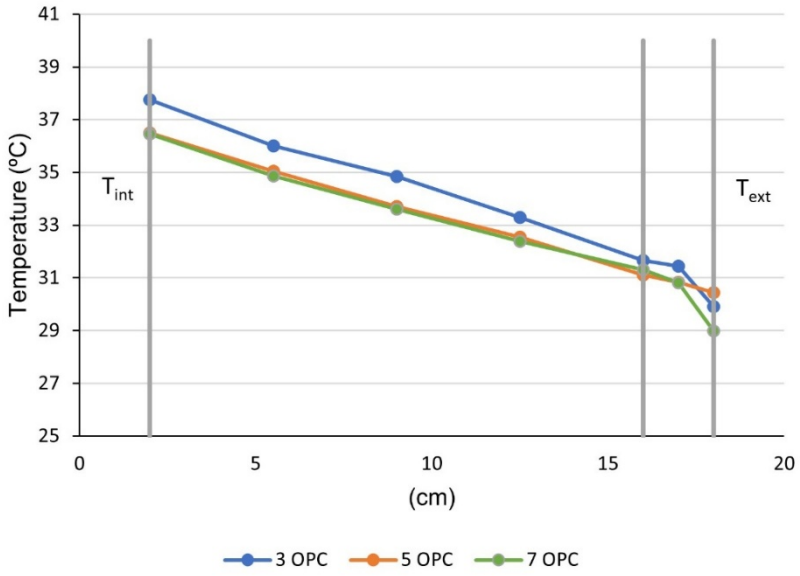

Figure 52 - Wall temperatures stabilised with OPC from inside to outside

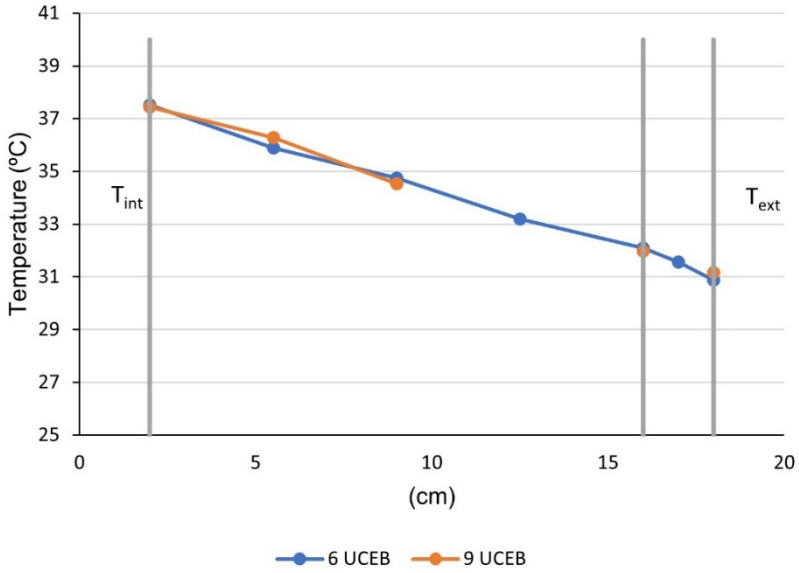

Figure 53 - Wall temperatures unstabilised from inside to outside

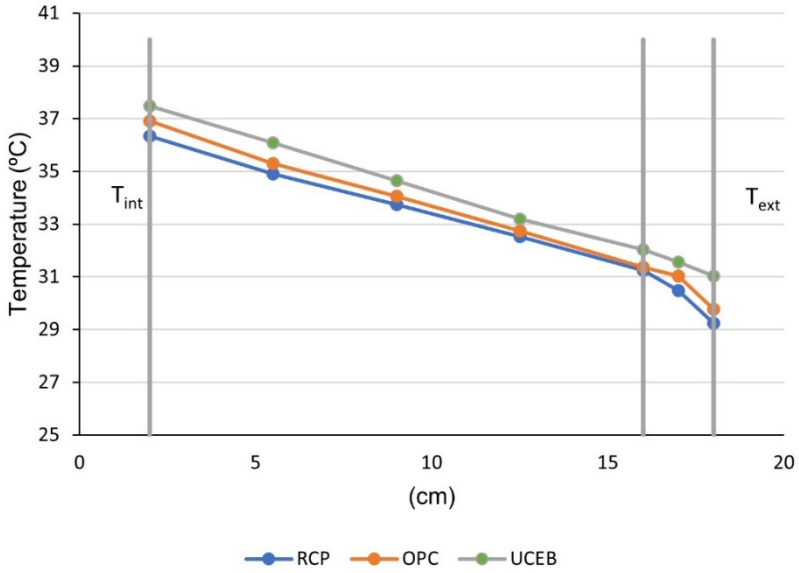

Figure 54 - Average wall temperatures of the different mixtures from inside to outside.

It was observed that the temperature of each wall decreased linearly along its thickness, suggesting that a nearly steady-state regime was achieved, where the heat flux remains approximately constant. Note that a decrease in temperature of approximately 1.2 ºC was observed within the exterior render layers of RCP and OPC prototype walls, while the temperature drop was significantly smaller (~0.5ºC) in UCEB.

The overall temperature drop between the interior and exterior surfaces was approximately 6.9 °C for RCP, 7.2 °C for OPC, and 6.5 °C for UCEB. These variations reflect the distinct thermal behaviour of each composition, with the PC wall exhibiting the highest gradient. This would not be expected, since OPC8TH and OPC8 are associated with slightly higher thermal conductivity. As

mentioned, the results were very similar across mixtures, with differences falling within the tests' natural variability range.

The different slope of the curves of CEB and mortars, indicates less heat transfer through the mortars, suggesting lower thermal conductivity of the rendering mortars compared with the blocks. This was expected, given that renders were produced with a higher water-to-cement ratio and without compaction.

Although there are differences in initial surface temperatures, probably due to non-homogeneous interior conditions inside the chamber caused by airflow, the temperature profiles across the thickness of flthe CEB remain consistently linear. Therefore, it is still possible to analyse the general behaviour of each mixture by comparing the slope and shape of the curves, as previously discussed.

However, as also noted in previous studies (A. Silva 2015), blocks with higher thermal inertia tend to present greater sensitivity to external factors such as airflow inside the testing chamber, particularly during the initial heating period. This behaviour can introduce higher uncertainty in the determination of thermal conductivity, especially when steady-state conditions are not fully achieved. To minimise this source of error, the progressive mean method, as described in chapter 3.5.4.2, was applied, reducing the influence of short-term fluctuations and improving the stability and reliability of the thermal conductivity results.

4.4.2 Thermal conductivity

The average thermal conductivity results of the walls, obtained using the quasi-static method (QSM), l_{QSM}, are presented in Table 16. As previously described, the values of thermal conductivity were adjusted to a reference temperature of 10 ºC. As mentioned, due to significant discrepancies in results and problems with the equipment, the thermal conductivity values from position 3 (OPC8TH) and position 6 (UCEB) were excluded from data analysis. Moreover, thermal conductivity data was available from only one UCEB prototype wall, located in position 9. For comparison purposes, the results obtained from the application of the transient method (Isomet 2114), l_{isomet}, are also presented in Table 16.

Table 16 - Thermal conductivity of the compositions.

CEB	TP (%)	r_{dry} (Kg/m^3)	$l_{10ºC}$ Heat flux meter			$l_{10ºC}$ Isomet 2114
			Wall	Block	Plaster	Block
RCP CEB	29.8	1912	0.72	0.78	0.45	0.79
OPC CEB	28.1	1965	0.76	0.82	0.50	0.82
UCEB	26.2	1991	0.83	0.83	0.78	0.78

Gomes et al. (2023) considering similar tests on concretes with different bulk densities (1440–2340 kg/m³) and thermal conductivities between 0.88 and 2.37 W/(mºC), reports differences between l_{QSM} and l_{Isomet} of less than about 5%, for $\lambda < 1.6$ W/(m.K). In this study, only small variations on thermal conductivity measurements were obtained between different methods (Table 16). The greatest variation was observed for the UCEB mini-wall, which can be partly attributed to the fact that the heat flux meter readings were based on a single wall only (the one in position 6 was excluded from calculation). Moreover, l_{Isomet} measurements are also affected by sample surfaces, thickness, boundary effect, sample homogeneity, and environmental conditions (Yüksel 2016). Indeed, the values obtained

with Isomet 2114 were very similar to those reported in 4.2.1, under the dry state, and those from the quasi-stationary method, except for UCEB.

As observed in Figure 55, it is confirmed a general increase trend of thermal conductivity with density, with only the lQSM from UCEB as an outlier. In general, the differences between methods were within the error tolerance declared by the Isomet 2114 manufacturer, which specifies a measurement error of ±5% plus 0.001 W/(m·K) for values between 0.015 and 0.7 W/(m·K), and ±10% for values between 0.7 and 6 W/(m·K). Based on this, the calculated acceptable deviation would be approximately 0.039 W/(m·K) for RCP, 0.041 W/(m·K) for OPC, and 0.0415 W/(m·K) for UCEB, all falling within the lower range. The exception occurs for UCEB, with a variation of 6% between lIsomet and lQSM. Differences between results are also within the standard deviations indicated in Table 13 to Table 15 (0.04-0.08 w/m.K). Also note that blocks were also tested with different moisture content. Moreover, as mentioned, results can be affected by the presence of mortar joints.

The thermal conductivity was little affected by the incorporation and type of stabiliser. Nonetheless, it is confirmed the slightly lower insulation properties of PC CEB, of higher density and finer porosity (4.2.1).

Rendering mortars were produced without compaction and with higher w/c, presenting lower density and higher total porosity than corresponding blocks. The dry densities of mortars were 1567 kg/m^3, 1589 kg/m^3 and 1703 kg/m^3, for RC12, OPC12TH and unstabilised mortar (UM), respectively. Taking into account the curve presented in Figure 40, it would be expected higher values of l for the mortars, over 0.4 w/(mºC). Aluma (2023) characterised the thermal conductivity of various plasters produced with different additives, namely straw, sand, cow dung, sheep wool and pine-needles. The author reported thermal conductivities in the range of about 0.4-0.6 w/(mºC) for densities between about 1300 and 1750 kg/m^3. Santos et al. (2017) reported a thermal conductivity of 0.85 w/(mºC) for an unstabilised mortar produced with 20% water and 1777 kg/m^3 of dry density.

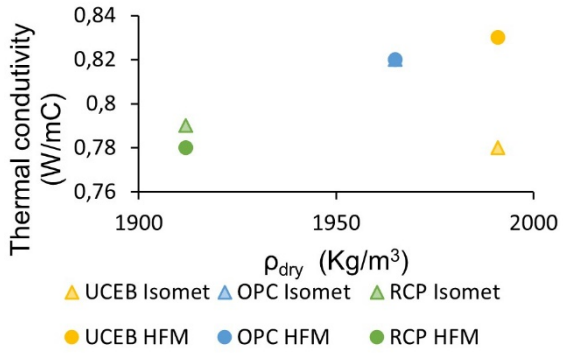

Figure 55 - Thermal conductivity as a function of CEB dry bulk density by transient and stationary method.

The thermal conductivity obtained with the Isomet plane probe on the prototype walls surface ranges 0.64-0.78 W/(m·K), presenting values lower than those of the blocks. This was expected, as the mortars showed only about 35.5% of the thermal conductivity of the blocks. As such, the measured value represents an equivalent thermal conductivity of the combined mortar and block layers, with the mortar's lower conductivity having a substantial influence on the result.

4.4.3 Building envelope solutions

Following the analysis of the thermal properties of the different CEBs unstabilised (UCEB) and stabilised with OPC, RCP, it is important to understand their performance when applied in real construction elements. This section, therefore, examines the thermal behaviour of these elements, based on the previously studied compositions, assessing their compliance with the regulatory requirements in flat thermal bridge zones, as defined by the Energy Performance Regulation for Residential Buildings (REH 2013).

The reference solution adopted corresponds to a double-leaf wall made of hollow ceramic brick, with an air cavity and internal thermal insulation (XPS), as shown in Figure 57. The characteristics remain consistent with those used in previous analyses. The structural elements under assessment consist of walls made with different compositions (RCP, OPC and UCEB), complemented by an external render layer.

The primary objective of this analysis is to determine the minimum thickness of thermal insulation required for CEB-based structural solutions to comply with the REH (2013) requirements in flat thermal bridge zones. Two insulation alternatives are considered: extruded polystyrene (XPS) boards and a commercial thermal plaster (Isodur), for which the technical datasheet is provided in Appendix 2 (7.2).

According to REH (2013), the thermal transmittance coefficient (U) in flat thermal bridge zones must be lower than the maximum value allowed for the climatic zone under study and lower than twice the U-value of the reference wall (current zone). For this analysis, the location considered was Lisbon, which, according to Ordinance No 138-I/2021, is classified within climatic zone I1 with the maximum permissible thermal transmittance for this zone being 0.50 W/(m²·ºC). However, for construction solutions based on rammed earth or similar traditional techniques, the same ordinance establishes a higher permissible threshold, with a maximum U-value of 1.30 W/(m²·ºC).

The thermal transmittance coefficient values calculated for the RCP, OPC, and UCEB compositions are presented in Table 17, alongside the corresponding thermal resistance values (R). These were determined based on the thermal conductivities and thicknesses of the plaster and CEB blocks used in each solution, including the surface resistances defined by standard norms.

Table 17 - Thermal resistance and thermal transmittance coefficient of RCP, OPC and UCEB.

Composition	R (m²·k)/W			U (W/(m²·k))
	Block	Plaster	$R_{total} + R_{si} + R_{se}$	
RCP	0.178	0.045	0.393	2.54
OPC	0.171	0.040	0.381	2.62
UCEB	0.168	0.026	0.364	2.75

As an initial approach, and in order to allow a direct comparison with the construction of the studied solutions, the configuration presented in Table 18 is analysed. This corresponds to a simplified wall system (Figure 56) of the reference zone, composed of 15 cm perforated clay brick masonry and a 2 cm external render layer. This configuration represents a common construction practice and serves as a thermal performance reference. The thermal transmittance coefficient (U) obtained for this solution

is 1.72 W/(m²·K), which is significantly lower than the values calculated for the stabilised earth block wall solutions, namely, 2.54 W/(m²·K) for the RCP composition, 2.62 W/(m²·K) for OPC, and 2.75 W/(m²·K) for UCEB. These differences correspond to increases of approximately 48%, 52%, and 60% in thermal transmittance, respectively, when compared with the clay brick solution, highlighting the less favourable thermal performance of CEB walls without additional insulation.

Table 18 - Composition and thermal performance of a simplified exterior wall.

Exterior wall construction system	e (m)	l W/(m·k)	R (m²·k)/W	Reference
1 - Render	0.02	1.3	0.015	p. I.7 ITE50 LNEC
2 - Perforated clay brick masonry	0.15	-	0.390	p. I.12 ITE50 LNEC
Total	0.17		0.405	

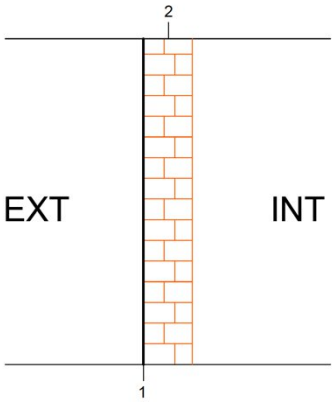

Surface Thermal Resistance	
R_{se}	0.04
R_{si}	0.13
R_{total}	0.58
U (W/(m²·k))	1.72

Figure 56 - Layer arrangement of the single-wall construction.

In Table 19, the characteristics of the layers that make up the reference wall section (Figure 58) are presented, along with the corresponding calculations of the thermal transmittance coefficient.

Table 19 - Current zone characteristics.

Exterior wall construction system	e (m)	l W/(m·k)	R (m²·k)/W	Reference
1 - Render	0.02	1.300	0.015	p. I.7 ITE50 LNEC
2 - Perforated clay brick masonry	0.15	-	0.390	p. I.12 ITE50 LNEC
3 – Air cavity	0.03	-	0.090	-
4 – XPS thermal insulation	0.04	0.037	1.081	p. I.3 ITE50 LNEC
5 - Perforated clay brick masonry	0.15	-	0.390	p. I.12 ITE50 LNEC
6 – Sprayed plaster	0.02	0.180	0.111	p. I.6 ITE50 LNEC
Total	0.41		2.077	

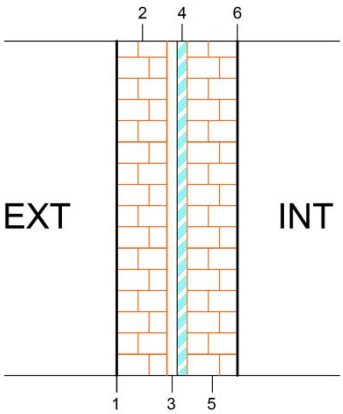

Figure 57 - Layer arrangement of the double-wall construction (reference).

Surface Thermal Resistance	
R_{se}	0.04
R_{si}	0.13
R_{total}	2.25
U (W/(m²·k))	0.44

Once the various layers and their properties had been defined, Table 20 presents the results for the required thermal insulation thicknesses to be applied to walls composed of the different CEB compositions studied, to meet the requirements set out in REH (2013). The thermal conductivity values of the mixtures were based on the results obtained using the Adapted Steady-State Method.

Table 20 - Minimum thickness of thermal insulation required to meet regulatory limits.

Composition	R (m²·k)/W	U (W/(m²·k))	U_c	$2U_c$	U_{max} (l_1)	Min ($2U_c$, U_{max})	e_{min} (cm) XPS	e_{min} (cm) Thermal Plaster
RCP	0.393	2.54	0.44	0.88	1.30	0.88	2.75	5.20
OPC	0.381	2.62					2.80	5.29
UCEB	0.364	2.75					2.86	5.41

The results presented in Table 20 clearly demonstrate that the application of thermal insulation is essential to ensure compliance with the thermal transmittance requirements defined in the REH (2013). Among the compositions analysed, the UCEB exhibited the highest U-value, thus requiring a greater thickness of insulation to meet the regulatory limits. In contrast, the RCP composition showed relatively better thermal performance, although still insufficient to meet the requirements without additional insulation.

It is important to note that the mixtures used for this comparison only include an external render layer, which significantly reduces their thermal insulation capacity, leading to an increase in the thickness of insulation required to comply with the regulations.

Nevertheless, these results highlight the inferior thermal performance of stabilised earth blocks (with or without recycled cement), when compared to conventional ceramic masonry solutions, reinforcing the necessity of integrating thermal insulation layers in structural solutions composed of CEBs.

In addition to assessing the thermal performance of the CEB compositions and their corresponding insulation requirements, a complementary analysis was carried out with the aim of establishing a basis for comparison with conventional structural solutions made from a single material. As such, the required thicknesses of conventional concrete (assuming a thermal conductivity value of $\lambda = 1.65$ W/(m·K)) that would yield the same thermal transmittance coefficient (U-value) as the different CEB compositions under study were determined.

This approach provides a clearer understanding of the thermal impact of CEB solutions in comparison to conventional structural concrete, offering a direct reference in terms of the material's intrinsic thermal performance without the inclusion of additional insulation. The equivalent concrete thicknesses required to achieve the same U-values as those of the RCP, OPC and UCEB compositions are presented in Table 21.

Table 21 - Concrete thickness for U-value equivalent to CEB compositions.

Composition	Thickness of concrete for equivalent U-value (cm)
RCP	0.65
OPC	0.63
UCEB	0.60

5 Conclusions

This dissertation aimed to characterise the thermal properties of CEB stabilised with recycled cement, exploring the theme through two distinct methods of analysis: the transient method and the adapted stationary method. The choice of these methods allowed a comprehensive evaluation of the thermal properties of CEB, providing an in-depth understanding of how recycled cement influences the thermal conductivity, diffusivity, and volumetric heat capacity of these materials. These methods were selected for their relevance and accuracy in obtaining data that reflects the real behaviour of materials under conditions close to operational, and it can be stated that the initially outlined objectives were fully achieved.

In the following subchapter, the general conclusions of this work will be presented. Special attention will be given to the comparative analysis between CEB stabilised with Portland cement and recycled cement, also focusing on the two testing methods and the interpretation of the collected data, with an emphasis on the influence of the physical characteristics of CEB, such as porosity and density, on their thermal performance. The practical implications of the obtained results will also be discussed, with the goal of contributing to the advancement of sustainable construction practices. Finally, future research directions will be suggested that may deepen the understanding of the thermal properties of CEB stabilised with recycled cement and explore new applications of this type of material in the construction sector.

5.1 General conclusions

In this dissertation, for the thermal characterisation of CEB stabilised with recycled cement, two distinct types of soil, FA and TV, the latter being richer in clay, were used. Additionally, CDW was incorporated in the production of the blocks, emphasising an ecological production approach and promoting the circularity of materials. This addition did not significantly alter the granulometric curve, which remained identical to that presented by FA, demonstrating the compatibility of CDW with the CEB production process. Furthermore, a finer granulometry CDW was used in the production of the plaster.

For the chemical stabilisation of the blocks, two types of Portland cement were used, CEM I 42.5 R (OPC) and CEM II/B-L 32.5 (PLC), with a greater focus on CEM I 42.5 R. The RC used was obtained from hydrated cement pastes and concrete specimens over three months old. The fresh bulk density values of the CEB varied between 2097 kg/m³ and 2195 kg/m³, while the dry bulk density was between 1912 kg/m³ and 2056 kg/m³, with total porosities between 24.6% and 30%. These values, slightly lower than those reported by other authors, reflect the optimisation of the mixes for block production.

The porous nature of RC resulted in a higher water demand and consequently in higher porosity. Thus, CEB stabilised with RCC and RCP showed higher total porosity values, due to the higher water content in the mix, which reduced block compaction.

Compressive strength varied between 1.8 MPa and 8.2 MPa, noting that RCC stabilised CEB required the incorporation of 12 wt% RCC, to compensate for impurities present in RC, achieving compressive strength values similar to those of RCP. Compared with unstabilised blocks, any

stabilisation shows a significant improvement in mechanical properties. It was also found that partial substitution of PC with RC, promoted higher mechanical strengths than its complete substitution.

Regarding thermal conductivity, dry stabilised CEB showed values between 0.67 W/(m·K) and 1.14 W/(m·K), and UCEB between 0.78 W/(m·K) and 0.94 W/(m·K). Results generally indicate a reduction in thermal conductivity of stabilised CEB compared to unstabilised ones, with variations depending on porosity and dry bulk density. It was observed that mechanical strength and bulk density vary inversely proportional to thermal conductivity.

It is concluded that thermal conductivity is influenced not only by bulk density and porosity but also by the characteristics of the different materials selected for different compositions. For instance, the partial earth substitution with CDW, have a considerable impact on thermal conductivity, showing an improvement in thermal behaviour due to CDW lower density and higher porosity compared to FA.

Specific heat values varied from 668 to 746 J/(kg·K), with RCP CEB presenting, on average, higher results (722 J/(kg·K)). Additionally, the thermal conductivity of the CEB was characterised based on an adapted stationary method using a climatic chamber, ensuring as much as possible, a uniform distribution of temperatures and constant heat flow in the wall areas. The differences observed between the stationary and transient methods are generally less than 5%, except for the unstabilised CEB (6%) due to data acquisition issues.

In summary, this study confirmed that it is possible to achieve solutions that improve the thermal behaviour of CEB with RCP stabilisation compared to UCEB and PC CEB, despite a slight decrease in their mechanical strength. The choice of the best solution should be determined based on the intended purpose for the construction, highlighting the potential of CEB stabilised with RC when bulk density and thermal performance are critical factors.

5.2 Future research directions

This study deepened the understanding of the thermal properties of CEB stabilised with recycled cement from pastes and concrete. While the research has significantly enriched our understanding/knowledge of these materials, it is essential to continue the research to optimise and validate the hypotheses presented, thereby promoting sustainable and conscious construction aligned with the principles of a circular economy in construction. As a follow-up to this work, several suggestions for future developments are proposed herein, to further enrich the knowledge in this area and expand its application domain.

- A study on the economic feasibility of the developed solution, both in terms of reducing the amount of additional insulation and the costs of production, transportation, and application, compared to current solutions.
- A study on the environmental impact of the analysed solutions, quantifying the embodied energy and the operational energy requirements (and savings) for dwellings made of UCEB, OPC CEB and RC CEB.
- A study on the coupled effect of hygroscopic and thermal behaviour, considering the highly hygroscopic nature of earth-based materials.
- Extend the study on mortars stabilised with recycled cement.

- Conduct further testing in the climatic chamber using a sinusoidal temperature variation, simulating more realistic daily thermal cycles and better assess the dynamic thermal behaviour of the CEBs.
- Perform more $testing methods with the aim of finding more expedient, cost-effective, and simple methods to conduct.
- Assess the acoustic properties of UCEB, OPC CEB and RC CEB.

References

Abdulsalam, Mutahar, Malek Abdulkarem, Esho Emmanuel Olumide, and Farzad Hejazi. 2018. “Effect of Addition of Silica Fume and Oil Palm Fiber on the Engineering Properties of Compressed Earth Block.” *Civil Engineering Research Journal* 6(2): 1–7. doi:10.19080/CERJ.2018.06.555684.

Adam, E. A., and P. J. Jones. 1995. “Thermophysical Properties of Stabilised Soil Building Blocks.” *Building and Environment* 30(2): 245–53. doi:10.1016/0360-1323(94)00041-P.

Allinson, David, and Matthew Hall. 2010. “Hygrothermal Analysis of a Stabilised Rammed Earth Test Building in the UK.” *Energy and Buildings - ENERG BLDG* 42: 845–52. doi:10.1016/j.enbuild.2009.12.005.

Aluma, Bernad. 2023. “DETERMINING THE THERMAL CONDUCTIVITY OF EARTH PLASTER SAMPLES WITH MORTAR MIXES SUITABLE FOR AFRICAN ARCHITECTURE.” MIDDLE EAST TECHNICAL UNIVERSITY.

Applied Precision. 2023. “Thermal Properties Analyzer User’s Guide.” www.appliedp.com (May 28, 2025).

ASTM C177-19. 2019. *Standard Test Method for Steady-State Heat Flux Measurements and Thermal Transmission Properties by Means of the Guarded-Hot-Plate Apparatus*.

ASTM C518-21. 2021. *Standard Test Method for Steady-State Thermal Transmission Properties by Means of the Heat Flow Meter Apparatus*.

ASTM D 698 - 12. 2021. *Compaction Characteristics of Soil Using Standard Effort*.

ASTM D2497-11. 2011. *Standard Practice for Classification of Soils for Engineering Purposes (Unified Soil Classification System)1*.

Ávila, Fernando, Esther Puertas, and Rafael Gallego. 2022. “Mechanical Characterization of Lime-Stabilized Rammed Earth: Lime Content and Strength Development.” *Construction and Building Materials* 350: 128871. doi:10.1016/J.CONBUILDMAT.2022.128871.

Azevedo, Bruno. 2021. *Blocos de Terra Comprimida Estabilizados Com Cimento Reciclado Engenharia Civil Orientadores*.

Bandeira, José. 2020. “Caracterização Mecânica e Retração Em Argamassas Produzidas Com Cimento Reciclado.” Instituto Superior Técnico - Universidade Lisboa.

Bogas, J. A., A. Carriço, and M. F.C. Pereira. 2019. “Mechanical Characterization of Thermal Activated Low-Carbon Recycled Cement Mortars.” *Journal of Cleaner Production* 218: 377–89. doi:10.1016/J.JCLEPRO.2019.01.325.

Bogas, J Alexandre, Miguel Silva, and M Glória Gomes. 2019. “Unstabilized and Stabilized Compressed Earth Blocks with Partial Incorporation of Recycled Aggregates.” *International Journal of Architectural Heritage* 13(4): 569–84. doi:10.1080/15583058.2018.1442891.

Bogas, J, Miguel Silva, and M Gomes. 2018. “Unstabilized and Stabilized Compressed Earth Blocks with Partial Incorporation of Recycled Aggregates.” *International Journal of Architectural Heritage* 13: 1–16. doi:10.1080/15583058.2018.1442891.

Bogas, José Alexandre, Ana Carriço, and Antonio José Tenza-Abril. 2020. “Microstructure of Thermoactivated Recycled Cement Pastes.” *Cement and Concrete Research* 138: 106226. doi:10.1016/J.CEMCONRES.2020.106226.

Bogas, José Alexandre, Sofia Real, Ana Carriço, J. C.C. Abrantes, and Mafalda Guedes. 2022. “Hydration and Phase Development of Recycled Cement.” *Cement and Concrete Composites* 127: 104405. doi:10.1016/J.CEMCONCOMP.2022.104405.

Bogas, José Alexandre, Sofia Real, Ricardo Cruz, and Bruno Azevedo. 2023. “Mechanical Performance and Shrinkage of Compressed Earth Blocks Stabilised with Thermoactivated Recycled Cement.” *Journal of Building Engineering* 79. doi:10.1016/j.jobe.2023.107892.

C. Sekhar, Darshan, and Sitaram Nayak. 2018. “Utilization of Granulated Blast Furnace Slag and Cement in the Manufacture of Compressed Stabilized Earth Blocks.” *Construction and Building Materials* 166: 531–36. doi:10.1016/J.CONBUILDMAT.2018.01.125.

Cabrera, Santiago, Yolanda Aranda-Jiménez, Edgardo Suarez-Dominguez, Rodolfo Rotondaro, and Yolanda Guadalupe. 2021. “COMPRESSED EARTH BLOCKS (CEB) STABILIZED WITH LIME AND CEMENT. EVALUATION OF BOTH THEIR ENVIRONMENTAL IMPACT AND COMPRESSIVE STRENGTH.” *Revista Hábitat Sustentable* 10: 70. doi:10.22320/07190700.2020.10.02.05.

Carriço, Ana, José Alexandre Bogas, and Mafalda Guedes. 2020. “Thermoactivated Cementitious Materials – A Review.” *Construction and Building Materials* 250: 118873. doi:10.1016/J.CONBUILDMAT.2020.118873.

Carriço, Ana, José Alexandre Bogas, Susana Hu, Sofia Real, and Manuel Francisco Costa Pereira. 2021. “Novel Separation Process for Obtaining Recycled Cement and High-Quality Recycled Sand from Waste Hardened Concrete.” *Journal of Cleaner Production* 309: 127375. doi:10.1016/J.JCLEPRO.2021.127375.

Carriço, Ana, José Alexandre Bogas, Sofia Real, and Manuel Francisco Costa Pereira. 2022. “Shrinkage and Sorptivity of Mortars with Thermoactivated Recycled Cement.” *Construction and Building Materials* 333: 127392. doi:10.1016/J.CONBUILDMAT.2022.127392.

Carriço, Ana, Sofia Real, José Alexandre Bogas, and Manuel Francisco Costa Pereira. 2020. “Mortars with Thermo Activated Recycled Cement: Fresh and Mechanical Characterisation.” *Construction and Building Materials* 256: 119502. doi:10.1016/J.CONBUILDMAT.2020.119502.

Cavanaugh, Kevin. 2002. *Guide to Thermal Properties of Concrete and Masonry Systems - Reported by ACI Committee 122*.

CEMBUREAU Activity Report. 2023. “ACTIVITY REPORT 2 0 2 3.” www.cembureau.eu (December 19, 2024).

Cruz, Ricardo, and José Alexandre Bogas. 2024a. “Durability of Compressed Earth Blocks Stabilised with Recycled Cement from Concrete Waste and Incorporating Construction and Demolition Waste.” *Construction and Building Materials* 450: 138673. doi:10.1016/J.CONBUILDMAT.2024.138673.

Cruz, Ricardo, and José Alexandre Bogas. 2024b. “Durability of Compressed Earth Blocks Stabilised with Recycled Cement from Concrete Waste and Incorporating Construction and Demolition Waste.” *Construction and Building Materials* 450: 138673. doi:10.1016/J.CONBUILDMAT.2024.138673.

Cruz, Ricardo, José Alexandre Bogas, Andrea Balboa, and Paulina Faria. 2024. “Water Resistance of Compressed Earth Blocks Stabilised with Thermoactivated Recycled Cement.” *Materials* 17(22). doi:10.3390/ma17225617.

Egenti, C., J. Khatib, and D. Oloke. 2013. “High Carbon Fly Ash and Soil in Shelled Compressed Earth

Masonry Units." https://www.researchgate.net/publication/320357381_High_Carbon_Fly_ash_and_Soil_in_Shelled_Compressed_Earth_Masonry_Units (January 16, 2025).

EN 772-1. 2011. *Methods of Test for Masonry Units - Part 1: Determination of Compressive Strength*.

EN 772-3. 1998. *Methods of Test for Masonry Units - Part 3: Determination of Net Volume and Percentage of Voids of Clay Masonry Units by Hydrostatic Weighing*.

EN 772-13. 2000. *Methods of Test for Masonry Units - Part 13: Determination of Net and Gross Dry Density of Masonry Units (except for Natural Stone)*.

Exelbirt, Joseph. 2011. "Characterizing Compressed Earth Bricks Based on Hygrothermal Aging and Wind-Driven Rain Erosion." UNIVERSITY OF FLORIDA.

F. Pacheco-Torgal. 2011. "Earth Construction: Lessons from the Past for Future Eco-Efficient Construction." https://core.ac.uk/reader/55617620 (September 25, 2024).

Fernandes, Luís, and Francisco Leitão. 2023. "The Portuguese Roadmap for Carbon Neutrality. A Perspective for Buildings Construction and Rehabilitation."

Fernandes, Pedro Miguel de Oliveira. 2014. "Caracterização Térmica de Painéis Sanduíche Em Polímero Reforçado Com Fibra de Vidro (GFRP)." Instituto Superior Técnico.

Fidalgo, Alexandra, Jose Paulo Farinha, José Martinho, and Laura Ilharco. 2013. "Flexible Hybrid Aerogels Prepared under Subcritical Conditions." *J. Mater. Chem. A* 1. doi:10.1039/C3TA12431B.

FIP. 1983. *FIP "Manual of Lightweight Aggregate Concrete."* 2ª. ed. Fédération internationale de la Précontrainte. Surrey University press.

Franco, Alessandro. 2007. "An Apparatus for the Routine Measurement of Thermal Conductivity of Materials for Building Application Based on a Transient Hot-Wire Method." *Applied Thermal Engineering* 27(14–15): 2495–2504. doi:10.1016/J.APPLTHERMALENG.2007.02.008.

Gomes, Maria da Glória, José Alexandre Bogas, Sofia Real, António Moret Rodrigues, and Rita Machete. 2023. "Thermal Performance Assessment of Lightweight Aggregate Concrete by Different Test Methods." *Sustainability* 15(14). doi:10.3390/su151411105.

Gomes, Nuno. 2015. "Caracterização de Blocos de Terra Para Construção de alvenarias Ecoeficientes." Faculdade de Ciências e Tecnologia - Universidade Nova de Lisboa.

Gonçalves, Diogo. 2023. *Estabilização de Blocos de Terra Com Ligantes Recuperados a Partir Da Fração Cimentícia de Resíduos de Betão-Caracterização Mecânica e Retração Engenharia Civil*.

Goodhew, Steve, R Griffiths, D Short, and L Watson. 2000. *Some Preliminary Studies of the Thermal Properties of Devon Cob Walls, Terra 2000, 8th International Conference on the Study and Conservation of Earthen Architecture*.

Hall, Matthew, and David Allinson. 2009. "Analysis of the Hygrothermal Functional Properties of Stabilised Rammed Earth Materials." *Building and Environment* 44(9): 1935–42. doi:10.1016/J.BUILDENV.2009.01.007.

Hall, Matthew R., K. B. Najim, and P. Keikhaei Dehdezi. 2012. "Soil Stabilisation and Earth Construction: Materials, Properties and Techniques." *Modern Earth Buildings: Materials, Engineering, Constructions and Applications*: 222–55. doi:10.1533/9780857096166.2.222.

HB 195. 2002. *The Australian Earth Building Handbook*.

Holm, Thomas A., and Theodore W. Bremner. 2000. *State-of-the-Art Report on High-Strength, High-Durability Structural Low-Density Concrete for Applications in Severe Marine Environments.* Washington, DC.

Hu, Susana. 2019. “Separação de Constituintes Do Betão Visando a Obtenção de Cimentos Reciclados.” Instituto Superior Técnico .

Islam, Mohammad Shariful, Tausif E. Elahi, Azmayeen Rafat Shahriar, and Nashid Mumtaz. 2020. “Effectiveness of Fly Ash and Cement for Compressed Stabilized Earth Block Construction.” *Construction and Building Materials* 255: 119392. doi:10.1016/J.CONBUILDMAT.2020.119392.

ISO 8301. 2010. *Thermal Insulation – Determination of Steady-State Thermal Resistance and Related Properties – Heat Flow Meter Apparatus*.

ISO 8302. 1991. *Thermal Insulation — Determination of Steady-State Thermal Resistance and Related Properties — Guarded Hot Plate Apparatus*.

ISO 10456. 2007. *Building Materials and Products – Hygrothermal Properties – Tabulated Design Values and Procedures for Determining Declared and Design Thermal Values*. Switzerland.

ITE 50. 2006. *Coeficientes de Transmissão Térmica de Elementos Da Envolvente Dos Edificios*.

Jorge, F.; Fernandes, M.; Correia, M. 2006. *Arquitectura de Terra Em Portugal*. 1ª. Lisboa.

Kerali, Anthony. 2001. “Durability of Compressed and Cement-Stabilised Building Blocks.” University of Warwick.

Krosnowski, A. 2011. “A Proposed Best Practice Method of Defining a Standard of Care for Stabilized Compressed Earthen Block Production.” University of Colorado.

Little, Becky, and Tom Morton. 2001. *BUILDING WITH EARTH IN SCOTLAND: INNOVATIVE DESIGN AND SUSTAINABILITY*.

Liuzzi, S., M. R. Hall, P. Stefanizzi, and S. P. Casey. 2013. “Hygrothermal Behaviour and Relative Humidity Buffering of Unfired and Hydrated Lime-Stabilised Clay Composites in a Mediterranean Climate.” *Building and Environment* 61: 82–92. doi:10.1016/J.BUILDENV.2012.12.006.

LNEC E-195. 1966. *Preparação Por via Seca de Amostras (Reparação Por via Seca de Amostras Para Ensaios de Identificação)*. Lisboa.

Lourenço, Patrícia. 2002. “Construção Em Terra.” Instituto Superior Técnico - Universidade Lisboa.

Lourenço, Patrícia, Jorge De Brito, and Fernando Branco. 2002. *The Use of Compacted Earth Blocks (BTC) in Modern Construction*.

Ma, Jiaming, Ahmed Abdelaal, Hongru Zhang, Annan Zhou, Yang Fu, and Yi Min Xie. 2024. “Ultra-Compressed Earth Block Stabilized by Bio-Binder for Sustainable Building Construction.” *Case Studies in Construction Materials* 21: e03523. doi:10.1016/J.CSCM.2024.E03523.

Malkanthi, S. N., W. G.S. Wickramasinghe, and A. A.D.A.J. Perera. 2021. “Use of Construction Waste to Modify Soil Grading for Compressed Stabilized Earth Blocks (CSEB) Production.” *Case Studies in Construction Materials* 15: e00717. doi:10.1016/J.CSCM.2021.E00717.

Mansour, Mohamed Ben, Ahmed Jelidi, Amel Soukaina Cherif, and Sadok Ben Jabrallah. 2016. “Optimizing Thermal and Mechanical Performance of Compressed Earth Blocks (CEB).” *Construction and Building Materials* 104: 44–51. doi:10.1016/j.conbuildmat.2015.12.024.

Marsh, Alastair T M, and Yask and Kulshreshtha. 2022. “The State of Earthen Housing Worldwide: How

Development Affects Attitudes and Adoption." *Building Research & Information* 50(5): 485–501. doi:10.1080/09613218.2021.1953369.

Mendonça, Amanda, Paula V Morais, Ana Cecília Pires, Ana Paula Chung, and Paulo Venda Oliveira. 2021. "A Review on the Importance of Microbial Biopolymers Such as Xanthan Gum to Improve Soil Properties." *Applied Sciences* 11(1). doi:10.3390/app11010170.

Meneses, Tiago, R. Vicente, A. Costa, A. Figueiredo, H. Varum, and N. Soares. 2011. *Comportamento Térmico de Construções Em Alvenaria de Adobe: Ensaios Experimentais Sobre Três Células de Teste à Escala 1:4, Construcción Com Tierra. Tecnologia y Arquitectura. Congresos de Arquitectura de Tierra En Cuenca de Campos. Valladolid: Cátedra Joan de Villanueva. Universidad de Valladolid*.

Minke, Gernot. 2005. *Building with Earth: Design and Technology of a Sustainable Architecture*. Basel-Berlin-Boston: Birkhäuser – Publishers for Architecture;

Morel, Jean Claude, Abalo Pkla, and Peter Walker. 2007. "Compressive Strength Testing of Compressed Earth Blocks." *Construction and Building Materials* 21(2): 303–9. doi:10.1016/J.CONBUILDMAT.2005.08.021.

Nabais, Martim. 2023. *Caraterização Mecânica de Blocos de Terra Comprimida Com Incorporação de Agregado e Cimento Reciclado Engenharia Civil*.

NBR 8492. 1984. *Tijolo Maciço de Solo Cimento Determinação Da Resistência a Compressão e Da Absorção de Água*.

NBR 10833. 1989. *Fabricação de Tijolo Maciço e Bloco Vazado de Solo-Cimento Com Utilização de Prensa Hidráulica*.

Neves, Mariana. 2019. "Proposta de Procedimentos Normativos Para a Caracterização Mecânica de Blocos de Terra Compactada Estabilizados Com Cimento." Instituto Superior Técnico - Universidade de Lisboa.

Neville, A. M. 1995. *Properties of Concrete*. 4ª. ed. Longman Group. UK Limited.

NP EN 933-1. 2012. *Tests for Geometrical Properties of Aggregates - Part 1: Determination of Particle Size Distribution - Sieving Method*.

NP EN 933-11. 2011. *Ensaios Das Propriedades Geométricas Dos Agregados : Parte 11 : Ensaio Para Classificação Dos Constituintes de Agregados Grossos Reciclados*.

NP EN 1097-6. 2016. *Ensaios Das Propriedades Mecânicas e Físicas Dos Agregados. Parte 6: Determinação Da Massa Volúmica e Da Absorção de Água*.

NP EN 1097-7. 2012. *Ensaios Das Propriedades Mecânicas e Físicas Dos Agregados : Parte 7 : Determinação Da Massa Volúmica Do Fíler : Método Do Picnómetro*.

NP EN 12667. 2012. *Desempenho Térmico de Materiais e Produtos Da Construção --- Determinação Da Resistência Térmica Pelos Métodos de Placa Quente e Fluxometria de Calor --- Produtos de Resistência Térmica Elevada e Media*. Monte da Caparica.

NP-143. 1969. *Solos: Determinação Dos Limites de Consistência*.

Ouedraogo, Kouka Amed Jeremy, Jean Emmanuel Aubert, Christelle Tribout, and Gilles Escadeillas. 2020. "Is Stabilization of Earth Bricks Using Low Cement or Lime Contents Relevant?" *Construction and Building Materials* 236: 117578. doi:10.1016/J.CONBUILDMAT.2019.117578.

Ranesi, Alessandra, Paulina Faria, and Maria do Rosário Veiga. 2021. "Traditional and Modern Plasters for

Built Heritage: Suitability and Contribution for Passive Relative Humidity Regulation." *Heritage* 4(3): 2337–55. doi:10.3390/heritage4030132.

Real, Sofia. 2019. *Durabilidade e Desempenho Térmico de Betões Estruturais de Agregados Leves Produzidos Com Diferentes Tipos de Materiais Cimentícios*.

Real, Sofia, José Alexandre Bogas, Ricardo Cruz, Maria Glória Gomes, and Martim Nabais. 2024. "Thermal Performance of Compressed Earth Blocks Stabilised with Thermoactivated Recycled Cement." *Energy and Buildings* 314: 114288. doi:10.1016/J.ENBUILD.2024.114288.

Real, Sofia, José Alexandre Bogas, Gomes M. Glória, and Beatriz Ferrer. 2016. "Thermal Conductivity of Structural Lightweight Aggregate Concrete." *https://doi.org/10.1680/jmacr.15.00424* 68(15): 798–808. doi:10.1680/JMACR.15.00424.

REH. 2013. "Regulamento de Desempenho Energético Dos Edifícios de Habitação."

Ren, Qifan, João Pacheco, Jorge de Brito, and Jianhua Hu. 2024. "Analysis of the Influence of the Attached Mortar's Geometry on the Mechanical Behaviour of Recycled Aggregate Concrete through Mesoscale Modelling." *Engineering Fracture Mechanics* 297: 109876. doi:10.1016/J.ENGFRACMECH.2024.109876.

Rigassi, V, and CRATerre-EAG. 1985. 1 *Compressed Earth Blocks : Manual of Production*. Deutsches Zentrum für Entwicklungstechnologien - GATE.

Riza, Fetra, Ismail Abdul Rahman, and Ahmad Zaidi. 2011. CSSR 2010 - 2010 International Conference on Science and Social Research *A Brief Review of Compressed Stabilized Earth Brick (CSEB)*. doi:10.1109/CSSR.2010.5773936.

Rodrigues, José. 2024. *Estabilização de Blocos de Terra Com Ligantes Recuperados a Partir Da Fração Cimentícia de Resíduos de Betão-Durabilidade Engenharia Civil Orientador*.

Sampaio, Sofia, M. Glória Gomes, J. Alexandre Bogas, and António Abel. 2014. "Thermal Conductivity of Compressed Earth Blocks (CEB) with Different Insulating Materials." In *9th International Masonry Conference 2014 in Guimarães*, , 1–12.

Santos, Tânia, Lina Nunes, and Paulina Faria. 2017. "Production of Eco-Efficient Earth-Based Plasters: Influence of Composition on Physical Performance and Bio-Susceptibility." *Journal of Cleaner Production* 167: 55–67. doi:10.1016/J.JCLEPRO.2017.08.131.

Shui, Zhonghe, Dongxing Xuan, Wei Chen, Rui Yu, and Rui Zhang. 2009. "Cementitious Characteristics of Hydrated Cement Paste Subjected to Various Dehydration Temperatures." *Construction and Building Materials* 23(1): 531–37. doi:10.1016/J.CONBUILDMAT.2007.10.016.

Silva, Alexandre. 2015. "CARACTERÍSTICAS DE ISOLAMENTO TÉRMICO DE BETÕES LEVES E DE MASSA VOLÚMICA NORMAL PRODUZIDOS COM DIFERENTES TIPOS DE AGREGADOS Engenharia Civil." Instituto Superior Técnico - Universidade Lisboa.

Silva, Filipa. 2017. "CONDUTIBILIDADE TÉRMICA DE ARGAMASSAS TÉRMICAS COM EPS E AEROGEL DE SÍLICA." Instituto Superior Técnico - Universidade Lisboa .

Silva, Filipe Jorge. 2005. *Arquitectura de Terra Em Portugal*. 1ª. Lisboa: Argumentum.

Silva, Miguel. 2015. "Blocos de Terra Compactada Com e Sem Materiais Cimenticios." Instituto Superior Técnico - Universidade Lisboa.

Silva, Rui A., Daniel V. Oliveira, Tiago Miranda, Nuno Cristelo, Maria C. Escobar, and Edgar Soares. 2013.

"Rammed Earth Construction with Granitic Residual Soils: The Case Study of Northern Portugal." *Construction and Building Materials* 47. doi:10.1016/j.conbuildmat.2013.05.047.

Silveira, Dora, Humberto Varum, Aníbal Costa, Tiago Martins, Henrique Pereira, and João Almeida. 2012. "Mechanical Properties of Adobe Bricks in Ancient Constructions." *Construction and Building Materials* 28(1): 36–44. doi:10.1016/j.conbuildmat.2011.08.046.

Soebarto, Veronica. 2009. "Analysis of Indoor Performance of Houses Using Rammed Earth Walls." *IBPSA 2009 - International Building Performance Simulation Association 2009*.

Sousa, Vitor, José Alexandre Bogas, Sofia Real, Inês Meireles, and Ana Carriço. 2023. "Recycled Cement Production Energy Consumption Optimization." *Sustainable Chemistry and Pharmacy* 32: 101010. doi:10.1016/J.SCP.2023.101010.

Taylor, P., and M. B. Luther. 2004. "Evaluating Rammed Earth Walls: A Case Study." *Solar Energy* 76(1–3): 79–84. doi:10.1016/J.SOLENER.2003.08.026.

Tchouateu Kamwa, Rolande Aurelie, Sylvain Tome, Judicael Chongouang, Idriss Eguekeng, Alex Spieß, Markus N.A. Fetzer, Kamseu Elie, Christoph Janiak, and Marie Annie Etoh. 2022. "Stabilization of Compressed Earth Blocks (CEB) by Pozzolana Based Phosphate Geopolymer Binder: Physico-Mechanical and Microstructural Investigations." *Cleaner Materials* 4: 100062. doi:10.1016/J.CLEMA.2022.100062.

Turco, Chiara, Mohammadmahdi Abedi, Elisabete Teixeira, and Ricardo Mateus. 2024. "Thermophysical Properties of Compressed Earth Blocks Incorporating Natural Materials." *Energies* 17(9). doi:10.3390/en17092070.

Turco, Chiara, Adilson C. Paula Junior, Elisabete R. Teixeira, and Ricardo Mateus. 2021. "Optimisation of Compressed Earth Blocks (CEBs) Using Natural Origin Materials: A Systematic Literature Review." *Construction and Building Materials* 309: 125140. doi:10.1016/J.CONBUILDMAT.2021.125140.

UNEP. 2021. "UN Environment Programme." https://www.unep.org/ (February 6, 2025).

Uzoegbo, H. C. 2020. "Dry-Stack and Compressed Stabilized Earth-Block Construction." *Nonconventional and Vernacular Construction Materials: Characterisation, Properties and Applications*: 305–50. doi:10.1016/B978-0-08-102704-2.00012-3.

Venkatarama Reddy, B. V. 2012. "Stabilised Soil Blocks for Structural Masonry in Earth Construction." *Modern Earth Buildings: Materials, Engineering, Constructions and Applications*: 324–63. doi:10.1533/9780857096166.3.324.

WBCSD & IEA. 2009. "Cement Technology Roadmap 2009. Carbon Emissions Reductions up to 2050." *World Business Council for Sustainable Development (WBCSD) and International Energy Agency (IEA)*.

WD-ARS 1333. 2018. *Compressed Stabilized Earth Blocks – Requirements, Production and Construction*.

XP P13 - 901. 2001. *Compressed Earth Blocks for Walls and Partitions: Definitions-Specifications-Testing Methods-Acceptance Conditions*.

XP P13-901. 2001. *Compressed Earth Blocks for Walls and Partitions: Definitions Specifications—Test Methods—Acceptance Conditions*.

XP P94-047. 1998. *Sols : Reconnaissance et Essais - Détermination de La Teneur Pondérale En Matières Organiques d'un Matériau - Méthode Par Calcination*.

Yogananth, Youganathan, Thanushan Kirupairaja, Pooraneswaran Sangeeth, Juthathatheu Coonghe, and Navaratnarajah Sathiparan. 2019. “Comparison of Strength and Durability Properties between Earth-Cement Blocks and Cement–Sand Blocks.” *Innovative Infrastructure Solutions* 4. doi:10.1007/s41062-019-0238-8.

Yu, Rui, and Zhonghe Shui. 2014. “Efficient Reuse of the Recycled Construction Waste Cementitious Materials.” *Journal of Cleaner Production* 78: 202–7. doi:10.1016/J.JCLEPRO.2014.05.003.

Yüksel, Numan. 2016. “The Review of Some Commonly Used Methods and Techniques to Measure the Thermal Conductivity of Insulation Materials.” doi:10.5772/64157.

Zhang, Youchao, Shuangli Jiang, Dengzhou Quan, Kun Fang, Bo Wang, and Zhiming Ma. 2024. “Properties of Sustainable Earth Construction Materials: A State-of-the-Art Review.” *Sustainability (Switzerland)* 16(2). doi:10.3390/su16020670.

Appendices

Appendix 1 - Stationary test

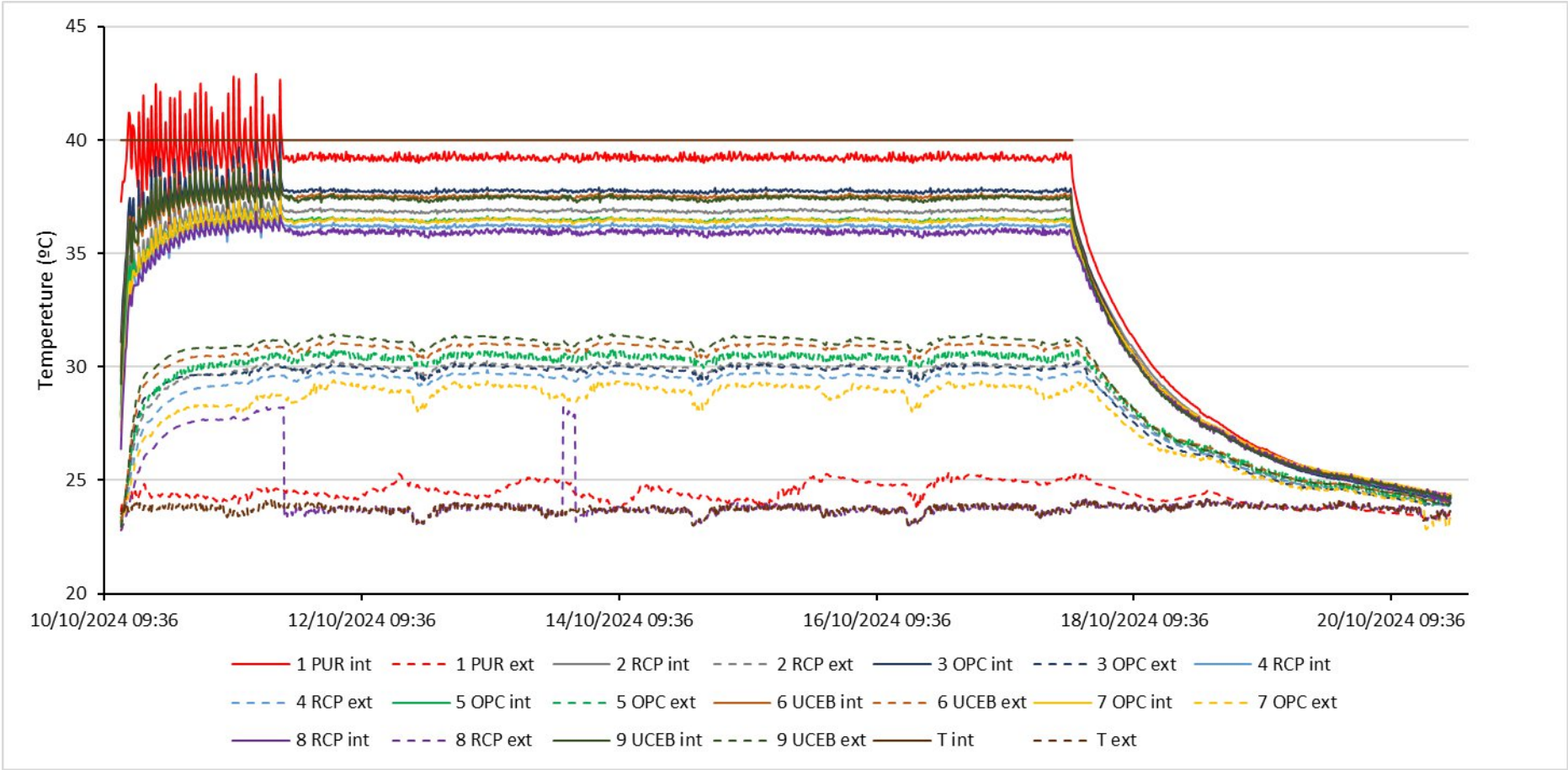

Figure A 1 - Interior and exterior surface temperatures of the different walls.

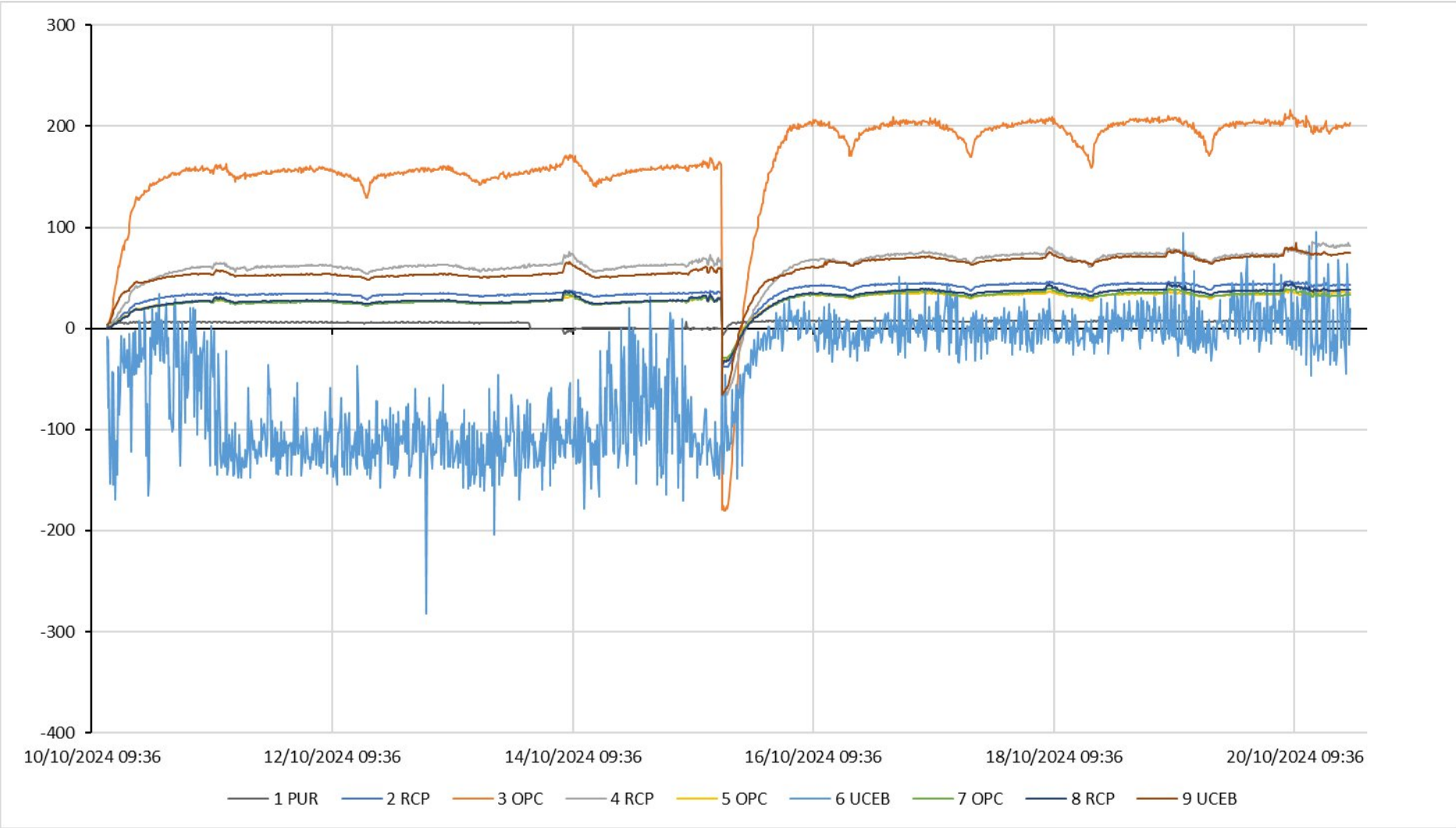

Figure A 2 - Heat Fluxes of the walls.

The graphs detailing the temperatures of each wall use the following nomenclature to describe the positions of the measurement points, from the interior to the exterior of the climatic chamber: I - Interior face of the block; Ii - Interior intermediate; M - Center of the block; Ei - Exterior intermediate; E - Exterior face of the block; MR - Center of the plaster; R - Face of the plaster.

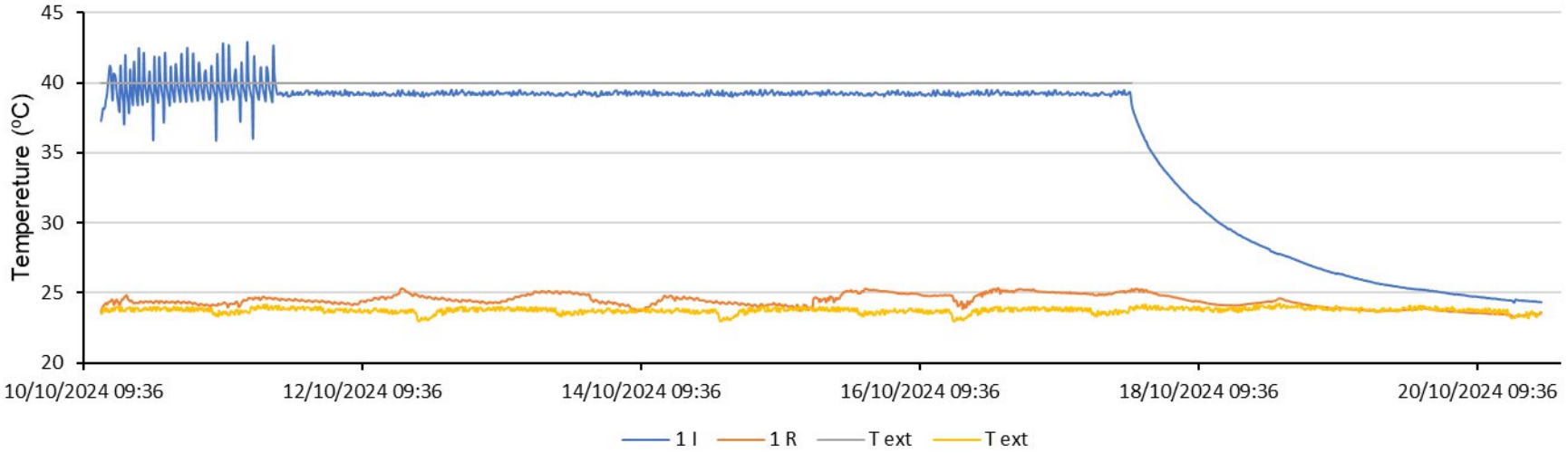

Figure A 3 - Temperatures from position 1 (PUR).

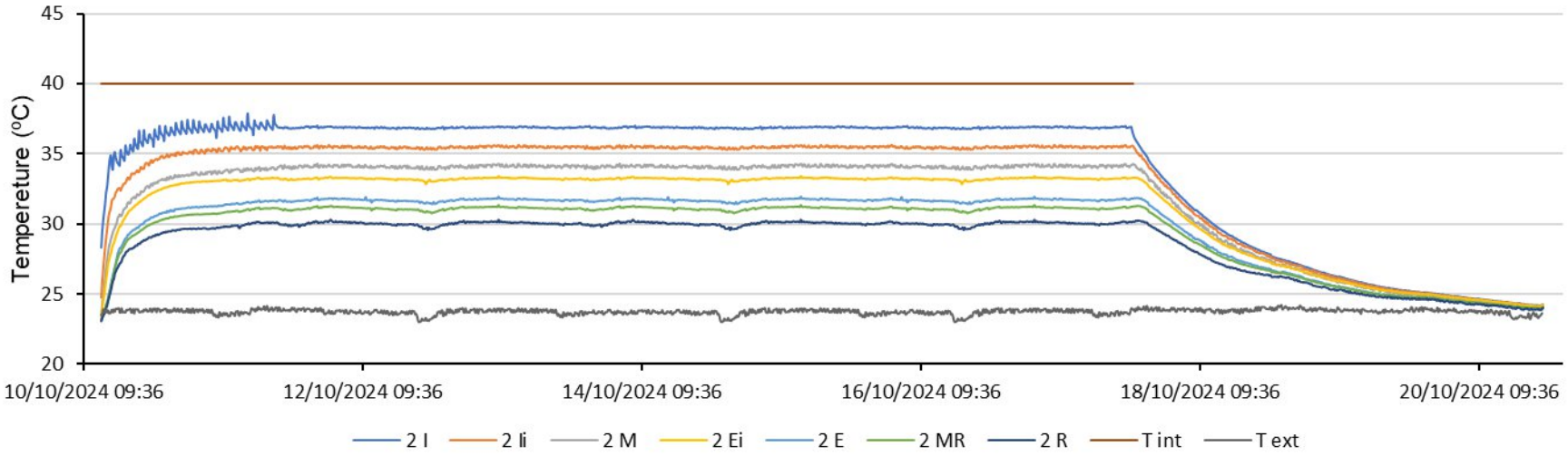

Figure A 4 - Temperatures from position 2 (RCP).

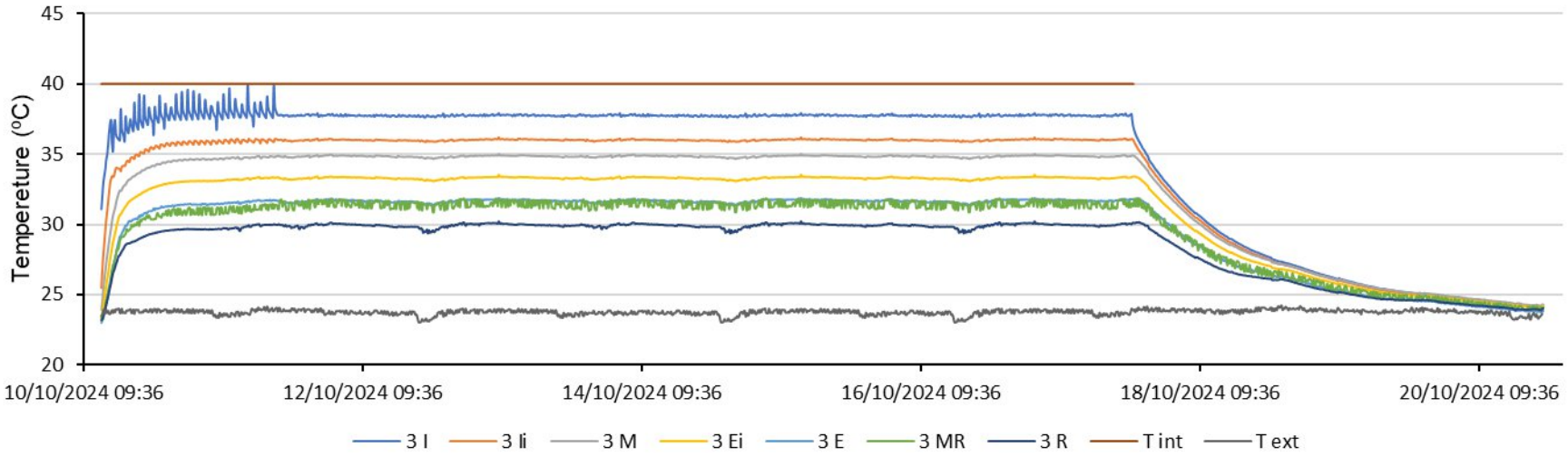

Figure A 5 - Temperatures from position 3 (OPC).

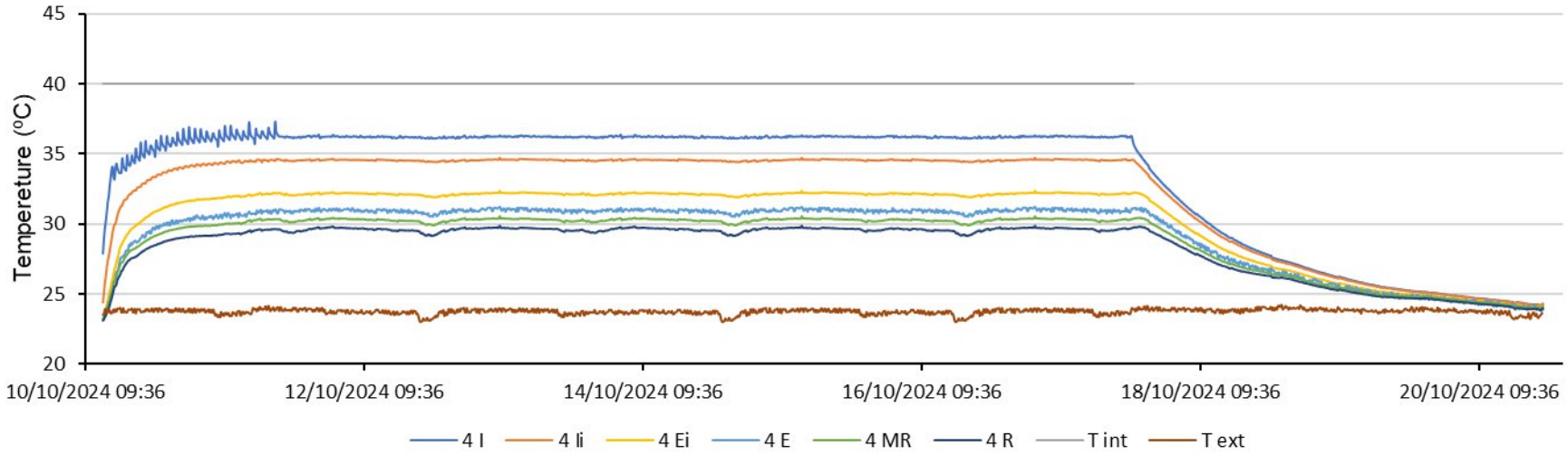

Figure A 6 - Temperatures from position 4 (RCP).

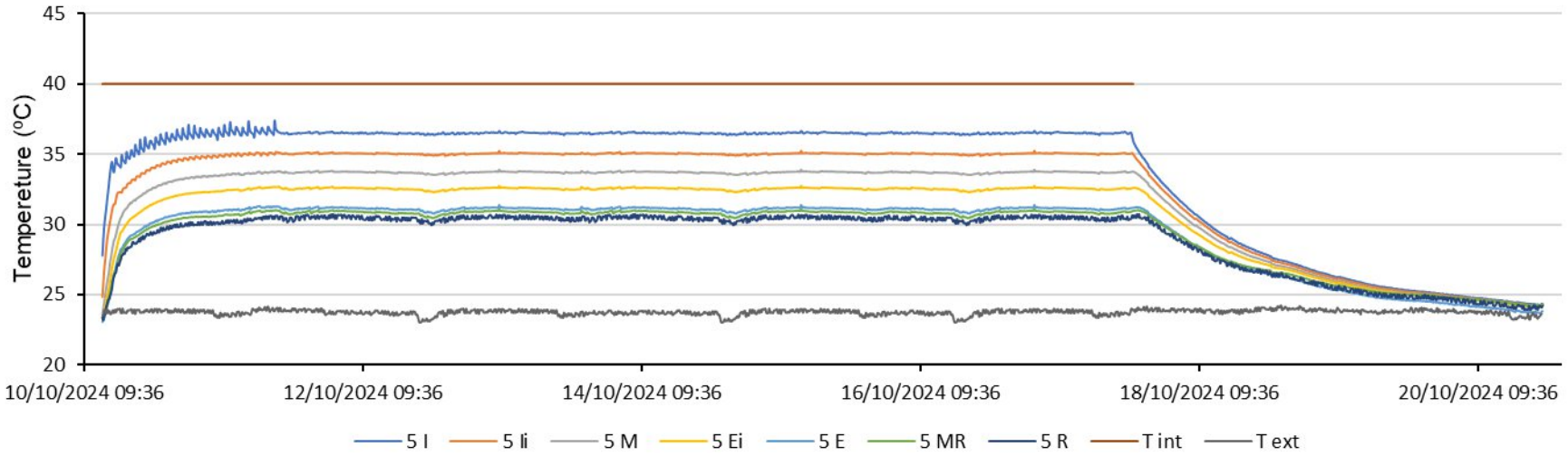

Figure A 7 - Temperatures from position 5 (OPC).

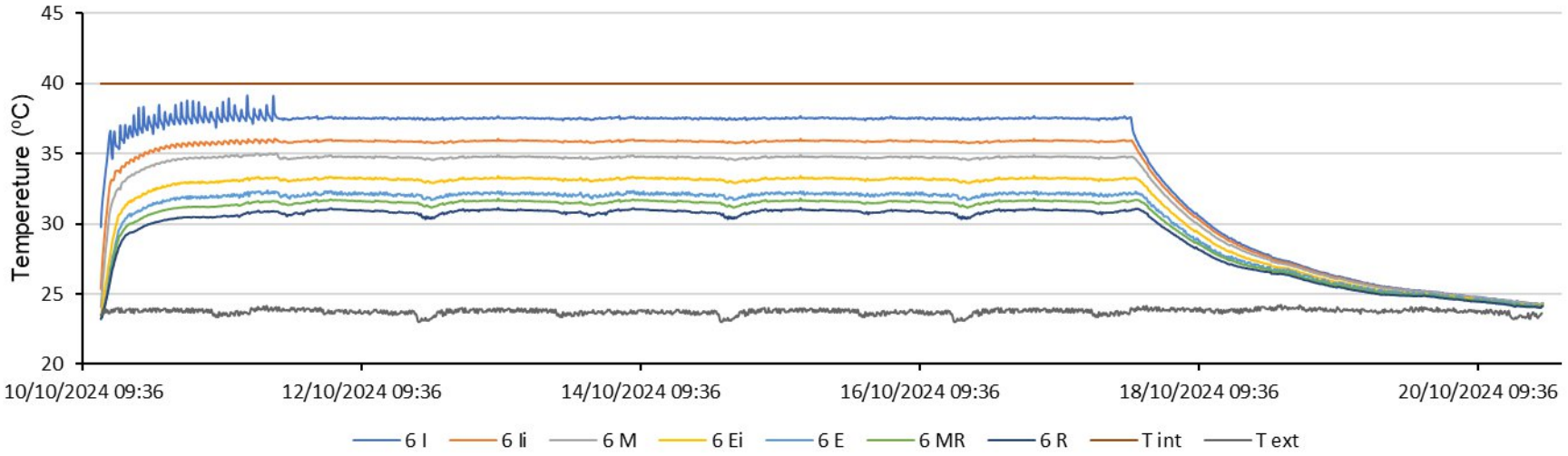

Figure A 8 - Temperatures from position 6 (UCEB).

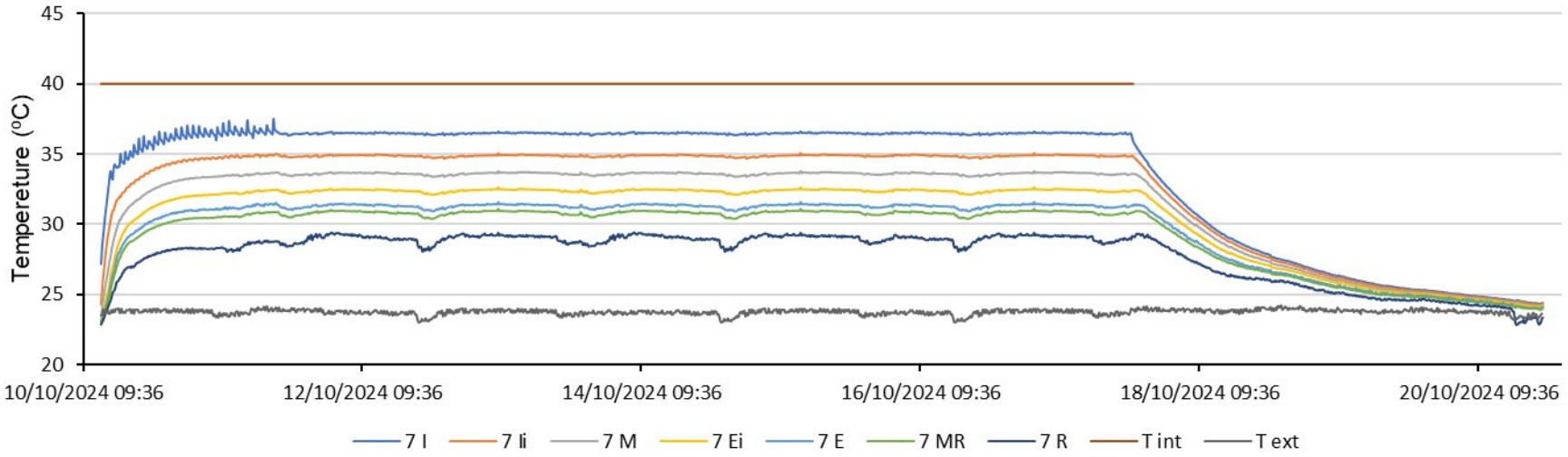

Figure A 9 - Temperatures from position 7 (OPC).

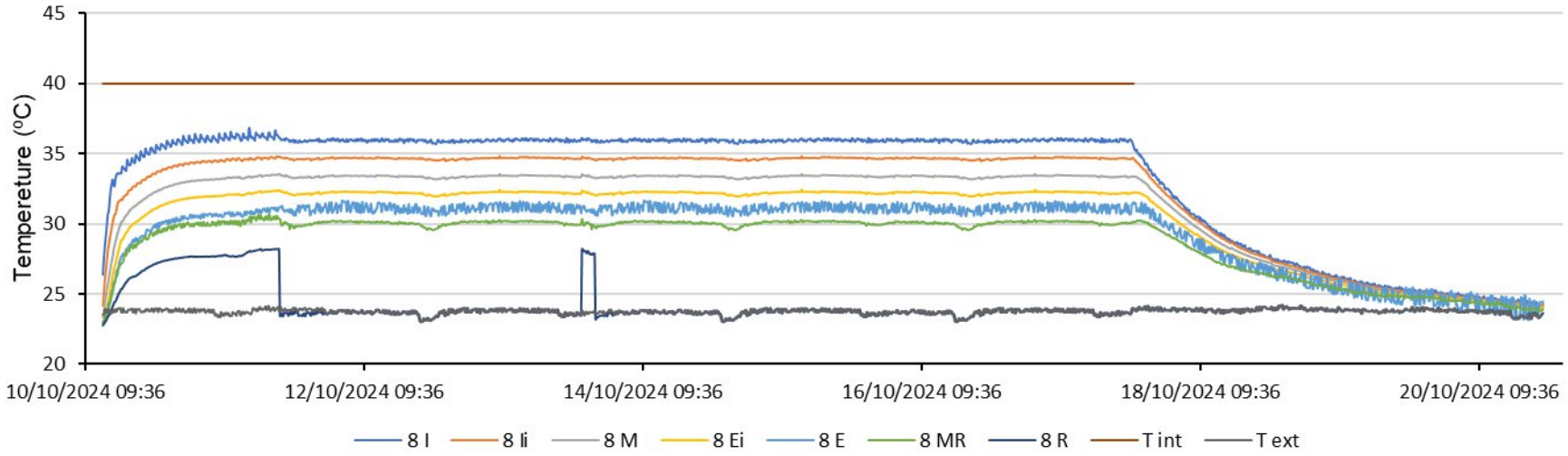

Figure A 10 - Temperatures from position 8 (RCP).

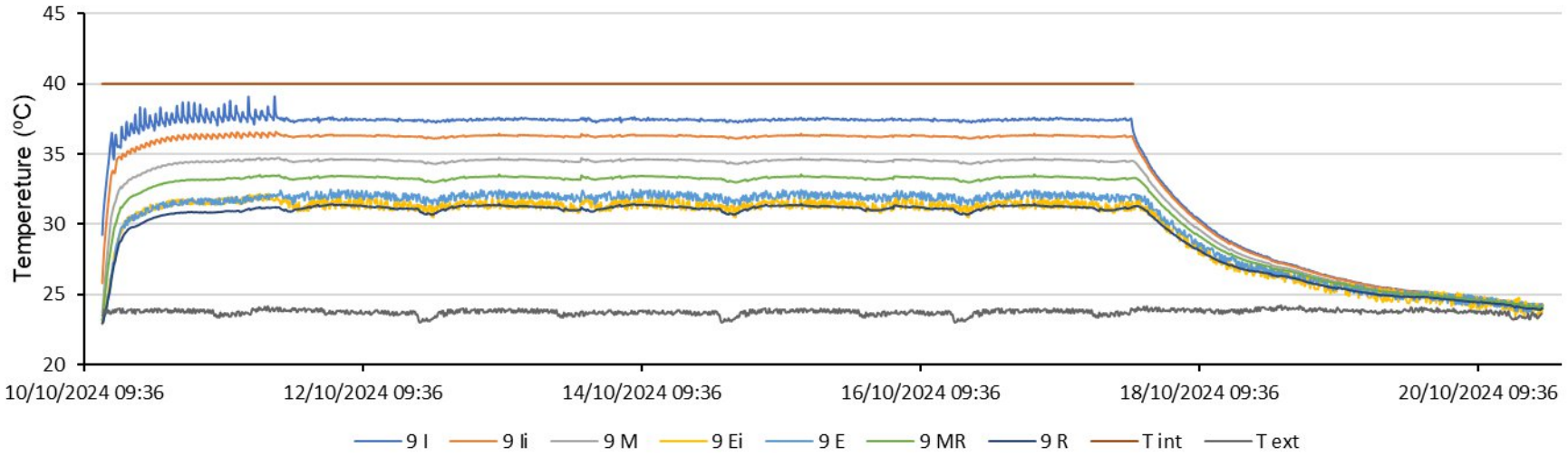

Figure A 11 - Temperatures from position 9 (UCEB).

Appendix 2 – ISODUR thermal plaster – Technical datasheet

ISODUR

REBOCO TÉRMICO PROJECTADO

TC.E.068.4

1. DESCRIÇÃO

O *ISODUR* é uma argamassa seca, formulada a partir de ligantes mistos, agregados especiais de muito baixa densidade (Poliestireno Expandido - EPS) e adições, destinada à execução de rebocos exteriores e interiores de isolamento térmico.

É um produto vocacionado para aplicação projectada.

2. DOMÍNIO DE UTILIZAÇÃO

O *ISODUR* é utilizado como reboco de isolamento térmico, aplicado sobre suportes em alvenaria de tijolo, blocos de cimento ou betão, sendo constituinte do sistema de revestimento isolante que promove o tratamento térmico das paredes envolventes utilizando pano simples e/ou duplo.

Utilizado em intervenções de renovação de edifícios, a aplicação de *ISODUR* constitui um método prático e eficiente para incrementar o desempenho térmico daquelas construções, quer se trate de paredes de pano duplo quer de monolíticas.

O sistema do revestimento isolante que integra o *ISODUR* foi desenvolvido para fazer face às exigências regulamentares. O sistema aplicado de forma contínua nas superfícies da envolvente promove o tratamento eficaz das pontes térmicas, contribuindo de forma decisiva para a prevenção de patologias na construção.

O *ISODUR* pode ainda ser utilizado como betonilha aligeirada para o enchimento de pavimentos.

3.CARACTERÍSTICAS DO PRODUTO

PRODUTO EM PÓ	VALOR	NORMA
Cor	Branco	-
Granulometria	< 1,5 mm	EN 1015-1

PRODUTO EM PASTA	VALOR	NORMA
Água de amassadura	80,0 ± 5,0 %	-
Massa volúmica	400 ± 50 kg/m^3	EN 1015-6
Consumo teórico	3,1 kg/m^2/cm	-

PRODUTO ENDURECIDO	VALOR	NORMA
Resistência à compressão	Classe CS I	EN 1015-11
Aderência ao tijolo e bloco / Modo de fractura	0,1 MPa / B	EN 1015-12
Massa volúmica	250 ± 50 kg/m^3	EN 1015-10
Módulo de elasticidade	500 N/mm^2	BS 1881-5
Capilaridade	Classe W2	EN 1015-18
Permeabilidade ao vapor de água μ	< 5	EN 1015-19
Reacção ao fogo	Classe B s1 d0	EN 988-1
Condutibilidade térmica	0,07 W.(m/K)	EN 12664
Índice de redução sonora*	44 dB	-

* Indice de redução sonora a sons aéreos (Rw) - (parede de tijolo cerâmico de 22 cm com 1 cm de RHP Plus interior e 4 cm de ISODUR revestido com 3 mm de FLEXDUR no exterior)

4. APLICAÇÃO

Preparação de suportes

Os suportes devem estar isentos de poeiras, descofrantes, matérias desagregadas ou instáveis, eflorescências, bem como, de qualquer tipo de material que afecte as normais condições de aderência.

Em tempo quente ou seco o suporte deve ser saturado com água iniciando-se a sua aplicação quando este se mostrar seco.

Secil Argamassas

Secil Martingança, S.A.
Apoio ao Cliente: Apartado 2 | 2406 – 909 – Maceira – LRA – Portugal
Tel: +351 244 770 220 | Fax: +351 244 777 997 | E-mail: comercial@secilargamassas.pt

www.secilargamassas.pt